Stony Brook University

Biochemical and Dynamic Analysis of Promyelocytic Leukemia Nuclear Bodies

A Dissertation Presented

by

Yi-Chun Maria Chen

to

The Graduate School

in Partial Fulfillment of the

Requirements

for the Degree of

Doctor of Philosophy

in

Molecular and Cellular Biology

(Biochemistry and Molecular Biology)

Stony Brook University

August 2007

Stony Brook University

The Graduate School

Yi-Chun Maria Chen

We, the dissertation committee for the above candidate for the
Doctor of Philosophy degree, hereby recommend
acceptance of this dissertation

Dr. David L. Spector – Dissertation Advisor
Professor, Director of Research,
Cold Spring Harbor Laboratory

Dr. Patrick Hearing - Chairperson of Defense
Professor, Department of Molecular Genetics and Microbiology,
Stony Brook University

Dr. Dafna Bar-Sagi
Professor, Department of Molecular Genetics and Microbiology,
Stony Brook University

Dr. Katherine L.B. Borden
Professor, Department of Pathology and Cell Biology Investigator,
Institute for Research in Immunology and Cancer,
University of Montreal

This dissertation is accepted by the Graduate School

Lawrence Martin
Dean of the Graduate School

Abstract of the Dissertation

Biochemical and Dynamic Analysis of

Promyelocytic Leukemia Nuclear Bodies

by

Yi-Chun Maria Chen

Doctor of Philosophy

in

Molecular and Cellular Biology

(Biochemistry and Molecular Biology)

Stony Brook University

2007

Promyelocytic leukemia nuclear bodies (PML NBs) are dynamic nuclear organelles suggested to be involved in tumor suppression, viral defense, DNA repair, and transcriptional regulation. However, their precise role in one or more of these processes is still largely unknown. In order to gain additional insights into their potential functions, I performed biochemical and dynamic analysis of PML NBs in this study. I have developed a fractionation protocol that successfully enriched structurally intact PML NBs from the immunoprecipitation eluate of mouse tissues. The protein constituents in the eluate were further identified by mass spectrometry. The presence of many nuclear matrix proteins that were co-immunoprecepitated with PML protein support the idea that PML NBs may have a direct association with the nuclear matrix. To analyze the dynamics of PML NBs upon entry into and exit from mitosis, I developed a U2OS cell line stably expressing two different marker proteins that localize to PML NBs, PML-ECFP and EYFP-Sp100. Three dimensional time lapse live cell imaging revealed that PML NBs exhibit a higher percentage of rapid directed movement when cells progressed from prophase to pro-metaphase as compared to their

interphase dynamics. This window of increased dynamic movement occurred upon nuclear entry of Cyclin B1 but prior to nuclear membrane breakdown. The PML NBs moved within the interchromatin space and fused to form fewer mitotic PML NBs which contain lower levels of Sp100 and Daxx protein as compared to interphase PML NBs. Upon exit from mitosis, Sp100 and Daxx entered the daughter nuclei after a functional nuclear membrane was reformed. However, the formation of PML NBs was dependent upon the presence of PML protein. My data suggest that entry into prophase results in a loss of tethering between regions of chromatin and PML NBs thereby resulting in their increased dynamics. Upon exit from mitosis, PML NB formation is initiated by PML protein. Overall, by using biochemical and cell biological approaches, my study suggests that PML NBs have a close association with nuclear matrix proteins and chromatin which likely influences their nuclear organization and function.

This work is dedicated to my parents, Wen-tao Chen and Chun-ping Liu

Table of Contents

List of Figures and Tables

List of Abbreviations

Ad5	Adenovirus type 5
APC	Anaphase-promoting complex
APL	Acute promyelocytic leukemia
AR	Androgen receptor
AS	Ammonium sulfate
atRA	all-*trans*-retinoic acid
ATRX	α-thalassemia/ mental retardation syndrome protein
BHK	Baby hamster kidney
BHK-S	BHK suspension
CA	Calyculin A
CBP	CREB binding protein
CBs	Cajal bodies
Cdk1	Cyclin dependent kinase 1
ChIP	Chromatin immunoprecipitation
cPML	Cytoplasmic PML
CT	Chromosome territories
DAPI	4',6-diamidino-2-phenylindole
Daxx	Death-domain-associated protein
DFCs	Dense fibrillar components
DIC	Differential interference contrast
ECFP	Enhanced cyan fluorescent protein
eIF4E	Eukaryotic translation initiation factor 4E
ES	Embryonic stem
FACS	Fluorescent activated cell sorting
FCs	Fibrillar centers
FISH	Fluorescence in situ hybridization
FSC	Forward scattered
GCs	Granular components
GFP	Green fluorescent protein
HAUSP	Herpes-associated ubiquitin-specific protease
HDM2	Human homolog of MDM2
hnRNPs	Heterogeneous nuclear ribonuclear proteins

Hp1α	Heterochromatin protein 1α
HSV-1	Herpes simple virus
IB	Immunoblotting
IBB	Importin-β binding domain
IF	Immunofluorescent
IGCs	Interchromatin granule clusters
ImmunoEM	Immuno-electron microscopy
IP	Immunoprecipitation
LRCIs	Long-range chromosomal interactions
LSP	Low speed pellet
LSS	Low speed supernatant
MAPPs	Mitotic accumulations of PML protein
MARs	Matrix attachment regions
MCBs	Mitotic CB remnants
MDM2	Murine double minute 2
MEFs	Mouse embryonic fibroblasts
MIGs	Mitotic interchromatin granules
MPF	M-phase-promoting factor
MSD	Mean square displacement
NcoR	Nuclear co-repressor
ND10	Nuclear domain 10
NDFs	Nucleolus-derived foci
NEBD	Nuclear envelope breakdown
NEM	N-ethylmaleimide
NLS	Nuclear localization signal
NORs	Nucleolar organizing regions
NuMA1	Nuclear mitotic apparatus protein 1
OA	Okadaic acid
Orf3	Open reading frame 3 protein product
p14ARF	p14 alternate reading frame
PCC	Premature chromosome condensation
PEG	Polyethylene glycol
PIASy	Protein inhibitor of activated STAT1
Plks	Polo-like kinases
PML NBs	Promyelocytic leukemia nuclear bodies
PODs	PML oncogenic domains

PP1	Type 1 protein phosphatase
PP2A	Type 2A protein phosphatase
pre-rRNAs	Pre-ribosomal RNAs
RAR	Retinoic acid receptor
RBCC	RING, B-boxes, and coiled-coil domain
SAF-B2	Scaffold attachment factor B2
SARA	Smad anchor of receptor activation
SATB1	Special AT-rich sequence binding protein 1
SIM	SUMO-interacting motif
snoRNPs	Small nucleolar RNPs
snRNA	Small nuclear RNA
snRNPs	Small nuclear ribonucleoprotein complexes
SRC-1	Steroid receptor coactivator-1
SSC	Side scattered
SUMO	Small ubiquitin-like modifier,
TGFβ	Transforming growth factor β
USP7	Ubiquitin-specific protease 7
VLPs	Virus-like particles

Acknowledgments

I am extremely grateful to my advisor, Dr. David L. Spector, for all of his invaluable advice throughout the course of my study. Being my role model, he showed me how to pursue scientific questions with passion and patience, and most importantly, how to be a true scientist with integrity. I would also like to acknowledge my collaborators, Scott Patterson, Mike Davis, and Paul Auger from Amgen, Inc. for mass spectrometry analysis, as well as Roland Eils and Constantin Kappel from German Cancer Research Center for image analysis. I thank Stephen Hearn for helping me verify the PML NB integrity by electron microscopy. I am also grateful for being able to work with a group of excellent colleagues in the Spector lab, who supported me with experimental reagents and valuable discussions on a daily basis. I especially thank Jonathan S. Kui for extensive proofreading of my manuscripts. I would like to thank all of my committee members for staying with me and providing insightful advice for my project for the past five years. Last but not least, I want to thank my friends and my family. Thank them for their love and friendship to help me go through difficult times as well as enjoy my life during the course of my PhD study.

Chapter 1: Introduction

I. The Cell Nucleus: A History of Discovery Paralleled by Developments in Technology

Since Robert Brown (1773-1858) described the existence of a cellular structure which he named “nucleus” in 1831, tremendous advances have been made in our understanding of this important cellular organelle. In the early nineteenth century, the nucleus was first recognized as a cellular compartment containing granular structures within it. At about the same time, the first description of what we now refer to as the “nucleolus” was published in 1835 by Rudolph Wagner (1805-1864). He identified “a yellowish refractile, dark spot” in the cell nucleus of the Graafian follicle of the sheep. Gabriel Gustav Valentin (1810-1883) identified the same structure in nerve cells in 1836 and first introduced the word “nucleolus” in 1839. However, due to the optical limitations of the light microscopes that were available at that time, it was not possible to further study the structural details of this cellular organelle, let alone its functional analysis.

It was not until the late nineteenth century, when the clear delineation of chromosomes was drawn during cell division, that the nucleus was bestowed a more functional role in the cell. In 1876, Edouard-Gérard Balbiani (1825-1899) first provided a more comprehensive explanation of how nuclear division occurs by showing all stages of mitosis and the dissolving of the mitotic nucleus into “narrow little rods,” which were unequal in size and split into two during later stages of division. Many scientists published similar results both in plant and animal cells during this time period. It was Edouard van Beneden (1846-1910), however, who first provided the details of nuclear division as it occurred during fertilization with amazingly accurate drawings to precisely describe the process that two identical “secondary loops” generated from the “primary loops” went into the two primary blastomeres, respectively. Van Beneden was the first to imply that the identity of structure may reflect the identity of function.

The hereditary nature of the nucleus was first suggested by Ernst Haeckel (1834-1919) in 1866. However, without definitive experiments to support this idea, it was debated for another two decades until Eduard Strasburger (1844-1912)

provided decisive experimental evidence when investigating the fertilization of orchids in 1884. He showed that when the pollen tube reached the embryo sac, the nucleus was pushed out into the sac and the cytoplasm was left behind. This implied that it was the nucleus that carried the hereditary material into the next generation. Subsequently, Theodor Boveri (1862-1915) proved in 1888 that chromosomes are separate entities and that the sperm and egg contribute an equal number of chromosomes to the zygote. He turned his observations into two famous principles, “the Continuity and the Individuality of Chromosomes” indicating that chromosomes are the units of heredity. Nevertheless, it was not until the famous Hershey and Chase experiment in 1952, using a radioactively labeled bacteriophage, that DNA was finally ascertained to be the cellular determinant of heredity.

With the improvement in microscopic technologies, in particular the invention and commercialization of the electron microscope in the early twentieth century, more structural details of the nucleus were revealed. The double nuclear membrane and its interruption by nuclear pores, the ultrastructure of the nucleolus, and chromosomes were all described in both plant and animal cells (Bernhard *et al.*, 1952; Afzelius, 1955; Grasse *et al.*, 1956; De, 1957). The nucleus was no longer thought of as a hollow space in the cell, but as an organized organelle. In 1960, a very interesting class of nuclear inclusions was first reported by G. de Thé and referred to as nuclear bodies (de The,1960). Several morphological studies performed in the 1960’s attempted to classify these bodies by their ultrastructure (Bouteille *et al.*, 1967; Krishan *et al.*, 1967). They were described roughly as single, compound, or coiled bodies with different granular and fibrillar features (Busch, 1974). These nuclear bodies were often observed in cancer cells at a higher frequency and were larger in size, and therefore correlated to different pathological conditions. However, the functions or composition of these nuclear bodies remained a mystery at that time. It was not until the 1980’s, when modern immunocytochemistry techniques and molecular biology were practically matured, that nuclear bodies could be more precisely categorized according to their composition and potential functions. For example, autoimmune sera were largely used to label distinct types of nuclear bodies by immunofluorescence microscopy or immunoelectron microscopy (Spector *et al.*, 1983; Bernstein *et al.*, 1984; Szostecki *et al.*, 1990; Andrade *et al.*, 1991). The genes for the component proteins were subsequently cloned and analyzed for their correlation to the function of the respective nuclear bodies.

From the 1980's to 1990's, two major technological advances again brought the field of nuclear organization to another level. The first innovation was fluorescence in situ hybridization (FISH) which made the visualization of DNA and RNA possible (Langer *et al.*, 1981). Detailed organization of specific DNA regions was precisely mapped (Manuelidis *et al.*, 1982). The procedure for whole-chromosome painting also suggested that individual chromosome occupied specific territories in the nucleus (Lichter *et al.*, 1988). The analysis of the whole chromosome to detect deletions and duplications also led to great advances in cytogenetic studies (for review see Trask, 2002). Moreover, visualization of single copy gene transcripts provided pivotal insight into how mRNAs were distributed after they were transcribed (Singer and Ward, 1982; Lawrence *et al.*, 1989). The second technological development of extreme importance during the late twentieth century was the use of live cell imaging, i.e. green fluorescent protein (GFP) (Chalfie *et al.*, 1994) and its enhanced colorful variants (for review see Lippincott-Schwartz and Patterson, 2003; Shu *et al.*, 2006). They provide an extremely powerful tool for *in vivo* dynamic studies by showing not only where, but also when and how a certain fluorescent-tagged protein interacts with its cellular environment and potential substrate(s). The functions of many nuclear domains, which were often implied by compositional or structural studies, surprisingly took an unexpected turn after they were analyzed by real time live cell imaging. The best known example is in the case of interchromatin granule clusters (IGCs), which are also known as nuclear speckles. They are mainly composed of an array of pre-mRNA splicing factors and other components of the splicing machinery; however, the actual splicing event does not occur within these nuclear structures, instead pre-mRNA splicing factors are recruited from nuclear speckles to transcription sites (Misteli *et al.*, 1997). Therefore, in addition to the traditional compositional and structural approaches, it is crucial to obtain dynamic information in order to fully comprehend the function of nuclear organelles.

II. Nuclear Domains

Today, the twenty-first century perception of the nucleus has leaped from a simple structural sketch to the most complex and colorful painting of the cell. As shown in Fig. 1, the mammalian cell nucleus is packed with distinct domains which are defined regions of concentrated proteins or nucleic acid that are held together without being surrounded by lipid membranes (for review see Spector, 2001). Beside chromosome territories, another twelve distinct nuclear domains are generally observed in mammalian nuclei. Some of the domains were discovered a hundred years ago and have a long history of research focused on them. The other domains were discovered quite recently and therefore are less well characterized. What the function(s) of these domains are and how they interact with each other have been the two most interesting areas of research in the nuclear field during the past decade. Here, I focus on a few major nuclear domains that are well characterized, and I summarize what we know about their structure and dynamic nature today.

i. Chromatin and chromosome territories

The majority of space in the nucleus is taken up by chromatin. It occupies discrete regions, namely chromosome territories (CT), and is highly organized and dynamic (for review see Cremer *et al.*, 2006). The chromatin compaction and localization usually correlate to the expression states of the genes in the region. In an interphase nucleus, chromatin is classified as heterochromatin or euchromatin depending on its condensational state. Heterochromatin, condensed and transcriptionally inactive, can be visualized by heterochromatin protein 1α (Hp1α) and appears in patches in the nucleus (James *et al.*, 1989). It is generally clustered at the periphery of the nucleus and at adjacent regions of the nucleolus. Euchromatin, on the contrary, spreads through out the nucleoplasm and carries active genes. The differences between heterochromatin and euchromatin are controlled by the modifications on both DNA and its associate proteins (Biessmann *et al.*, 2005). Heterochromatin can be further divided into constitutive and facultative forms. For example, centromeres and telomeres, which contain long stretches of repetitive DNA sequences, are flanked by constitutive heterochromatin (for review see Dunleavy *et al.*, 2005). On the other hand, facultative heterochromatin can be formed at normal euchromatin regions when

the genes are inactivated during certain developmental stages. By introducing repetitive elements, euchromatin can be converted into heterochromatin reversibly by changing the transcriptional state (Janicki *et al.*, 2004). The molecular details of formation and maintenance of heterochromatin are still controversial. The most popular hypothesis is the “histone code” theory purposed by C. David Allis (Jenuwein and Allis, 2001). By post-translational modification on the amino-termini of the histone molecules, i.e. methylation, acetylation, phosphorylation, etc., the chromatin structure can be changed into euchromatin or heterochromatin accordingly to activate or silence genes. However, due to the complexity as well as the inconsistency of the histone modifications, it is still open for debate whether a “code” really exists or it is merely a reflection of some other higher order of regulation.

In addition to regulation of gene activity due to changes in the compaction of chromatin, the nuclear position of a gene can also affect its expression. In the studies of a more global scale of radial CT positioning, CT containing low gene density tend to locate at the periphery of the nucleus, while gene-rich CT usually localize at the interior of the nucleus (Kurz *et al.*, 1996; Croft *et al.*, 1999). Upon inhibition of transcription, chromosomes containing the active genes moved from the interior of the nucleus towards the periphery. More localized CT rearrangements are best exemplified by position effect variegation (Csink *et al.*, 1994; Dernburg *et al.*, 1996). The genes positioned to the region immediately flanking the heterochromatin are usually silenced. Moreover, the position effect works not only at the intrachromatin level, but also at the interchromatin level. Detailed cell-by-cell mapping of known genes affected by position effect variegation was reported by John Sedat’s group (Harmon and Sedat, 2005). They found that the long-range chromosomal interactions (LRCIs) between specific gene loci and the heterochromatin region from either the same chromosome or from the adjacent chromosome were strongly correlated with gene silencing. However, there are studies indicated that instead of a functional accountability of chromosome positioning, the position of a CT may be determined by the gene complexity and/or, simply, by size (for review see Cremer *et al.*, 2006). Though the precise 3D-mappying of CT may still be open for debate, positioning of CTs provides to some extend an additional layer of gene regulation.

ii. Nucleolus

The nucleolus is another major domain in the nucleus that has been intensively studied. It is formed around the ribosomal gene (rDNA) clusters which contain about 100 to 400 copies of a 140Kb rDNA repeat, depending on species, from 5 different chromosomes. These gene clusters are known to be responsible for the structural organization of the nucleolus, and thus are also known as the nucleolar organizing regions (NORs) (McClintock, B., 1934). The substructures within the nucleolus were defined by the ultrastructural observations in early EM studies and were later correlated to its biological functions (for review see Lam *et al.*, 2005). From inside out, a nucleolus can be divided into fibrillar centers (FCs) surrounded by dense fibrillar components (DFCs) and then coated by granular components (GCs) which comprise the major part of the nucleolus. The main function of the nucleolus is ribosome biogenesis (for review see Scheer and Hock, 1999; Carmo-Fonseca *et al.*, 2000). Active rDNA genes are transcribed by RNA polymerase I at the periphery of FCs, and the elongating and the full-length primary transcripts of rDNA are transiently accumulated in DFCs. These pre-ribosomal RNAs (pre-rRNAs) are also posttranscriptionally modified within the DFC regions. At the end, assembly and maturation of ribosomal components occur in the GCs (for review see Hernandez-Verdun, 2006). During mitosis, nucleolar disassembly began with the loss of RNA polymerase I subunits from the FCs before the initiation of nuclear envelope breakdown (NEBD) (Leung *et al.*, 2004). The dissociation of other components, such as fibrillarin and B23, occurred later, which coincided with the process of NEBD. The reformation pathway also follows a defined temporal sequence, which FCs reform before DFCs and the assembly of GCs occurs last. Interestingly, a recent study showed that highly condensed ribosomal gene loci during mitosis were still accessible to transcription factors and chromatin proteins, and these factors were rapidly exchanged at rDNA clusters, especially during anaphase and telophase (Chen *et al.*, 2005). This supports an emerging model of replication independent core histone replacement.

iii. Nuclear speckles

Nuclear speckles were first observed by Hewson Swift in a detailed, EM ultrastructural study of the nucleus (Swift, 1959). He identified a new type of

nuclear structure and named it interchromatin granule cluster (IGC). Independently, Beck in 1961 discovered “speckle” patterns in rat liver nuclei after labeling with autoimmune sera (Beck, 1961). It was only realized later that these two structures were actually the same domain in the nucleus (Spector *et al.*, 1983). It is known now that IGCs are the storage and processing centers of the components of splicing machineries surrounding by the nascent transcripts (Fakan and Nobis, 1978; Lamond and Spector, 2003). A typical mammalian nucleus contains 20 to 50 IGCs. The biochemical purification followed by proteomic analysis of IGCs showed that they are enriched in pre-mRNA splicing factors plus some splicing specific regulatory kinases and phosphatases, transcription factors, and RNA processing factors (Monneron and Bernhard, 1969). Even though there is no DNA within IGCs and no active transcription or active splicing occurs within these structures, they are often found in the vicinity of an active transcription site (Fakan and Nobis, 1978). When RNA polymerase II transcription is inhibited, IGCs round up and lose their typical “speckle” shape indicating that their organization is tightly correlated with their functions. Live cell imaging studies showed that splicing factors were dynamically recruited from IGCs to the active transcription sites (Mintz *et al.*, 1999; Saitoh *et al.*, 2004). It is believed that the phosphorylation status of these splicing factors regulates their trafficking between IGCs and transcription/splicing sites (Bubulya *et al.*, 2004). Upon entry of mitosis, IGC components are disassembled and diffused into the cytoplasm after NEBD. They are later recruited into mitotic interchromatin granules (MIGs), the structural equivalents of interphase IGCs, as the cell progresses through mitosis (Ferreira *et al.*, 1994; Prasanth *et al.*, 2003). In telophase, pre-mRNA splicing factors are recycled into daughter nuclei concurrent with the disappearance of MIGs, and reassemble into IGCs in G1.

iv. Cajal bodies

Cajal bodies (CBs), previously known as coiled bodies, were renamed after their discoverer, Santiago Ramon y Cajal, who first described these spherical structures in the sensory neuron in 1903 and called them nucleolar accessory bodies (for review see Gall, 2000). There are typically 2 to 8 CBs per human cell nucleus and their size range from 0.1μm to 1.0μm. Besides coilin, which is the marker protein of CBs, small nuclear ribonucleoprotein complexes (snRNPs) involved in pre-mRNA splicing and small nucleolar RNPs (snoRNPs) involved in

rRNA processing are also found in CBs. However, even though the biochemical purification of these nuclear bodies has been attempted, but the complete proteomic analysis has not been reported (Lam *et al.*, 2002). CBs were also known to associate with histone and small nuclear RNA (snRNA) gene loci (Smith and Lawrence, 2000; Frey and Matera, 2001; Shopland *et al.*, 2001). As shown in live cell studies using fluorescent-tagged CB component proteins, CBs are highly mobile and their movements can be described and categorized by anomalous diffusion into three types: simple diffusion, constrained diffusion, and diffusion with flow (Platani *et al.*, 2000; Platani *et al.*, 2002). They exhibit fusion and fission motions among themselves, as well as association and disassociation events with dense regions of chromatin and nucleoli. Interestingly, their association with chromatin requires ATP and active transcription since CBs increases their dynamics after ATP depletion and transcriptional inhibition (Platani *et al.*, 2002). The major function of CB appears to be the maturation of nuclear RNP complexes including snRNP and snoRNPs (for review see Filipowicz and Pogacic, 2002). During mitosis, CBs broke down into a small number of mitotic CB remnants (MCBs), which consisted of coilin and snRNP proteins. A similar phenomenon was also observed in mitotic breakdown of the nucleolus, which became the nucleolus-derived foci (NDFs) and functioned as a site for mitotic preservation of rRNA processing complexes (Sleeman *et al.*, 2003). Therefore, MCBs may also play the same role during mitosis to partially preserve the RNA processing complexes. The close relationship between CBs and nucleoli became apparent in the studies showing the similarity of their molecular composition (for review see Gall, 2000). They may potentially have cooperative functions in the processing of many RNA species.

III. Promyelocytic Leukemia Nuclear Bodies

Promyelocytic leukemia nuclear bodies (PML NBs), also known as nuclear domain 10 (ND10), Kremer (Kr) bodies, or PML oncogenic domains (PODs), were first characterized using human autoimmune antibodies and have been correlated to human disease since the very beginning of their discovery (Ascoli and Maul, 1991; Stuurman *et al.*, 1992). During this time period, the PML gene locus was discovered in 1990 when Hugues de Thé characterized a t(15;17) chromosomal translocation in acute promyelocytic leukemia (APL) cells (de The *et al.*, 1990). Not until 1994 was it realized that the ND10s described earlier were the same structure as PODs and now known as PML NBs (Dyck *et al.*, 1994; Koken *et al.*, 1994; Weis *et al.*, 1994).

i. Morphology of PML NBs

PML protein is the hallmark of PML NBs which are observed in all known mammalian cells. A typical nucleus contains about 10 to 30 PML NBs and the size of the bodies ranges from 0.2 μm to 1 μm (Weis *et al.*, 1994). As shown in Fig. 2, PML NBs appear as elliptical or spherical in shape with various sizes when examined using immunofluorescent (IF) labeling. Analysis by immuno-electron microscopy (immunoEM) on thin sections revealed that the ultrastructure of PML NBs is generally a ring or doughnut shape with PML protein outlining the dense border that defines the PML NBs. The inner cores can sometimes be filled with electron-dense materials, or additional layers of PML protein (Koken *et al.*, 1994). Unlike other nuclear domains, the morphology of PML NBs may vary under different physiological conditions. For example, upon interferon treatment, PML NBs increase both in size and in number per cell nucleus by enhancing the expression level of PML protein (Chelbi-Alix *et al.*, 1995). PML NBs can also incorporate satellite DNA into a highly organized DNA-protein structure and may function as chromatin remodeling factories for late-replicated satellite DNA during G2 phase (Luciani *et al.*, 2006). Moreover, as PML NBs show no association with the nucleolus in the transformed cell lines typically used for previous PML NB studies, it was recently reported that in the embryonic stem (ES) cells and senescent cells, they formed a sphere or an open barrel structure adjacent to the nucleolus and encircled or engulfed part of the nucleolar components. When rRNA synthesis was shut off, PML NBs reorganized and completely surrounded

the segregated nucleolus (Janderova-Rossmeislova *et al.*, 2007). It has been proposed that the basic structure of PML NBs containing an outer shell plus an inner core can be used as interaction surface and a potential storage space, respectively. The morphological heterogeneity of these nuclear domains may indicate the uniqueness of how they function in the nucleus.

ii. Structural integrity of PML NBs

The first line of evidence indicating a correlation of PML NB structural integrity to their functions came from studies focused on acute promyelocytic leukemia (APL). In 98% of APL patients, a translocation between the *myl* locus and the retinoic acid receptor (RAR) α gene was found to be responsible for the onset of the leukemia (for review see Melnick and Licht, 1999). This translocation resulted in the production of a PML-RARα fusion protein acting as a dominant negative oncogen (de The *et al.*, 1991). The fusion protein bound firmly to DNA and induced the disruption of PML NBs into a micro-speckled pattern through PML/PML-RARα heterodimerization and recruitment of the PML partners onto chromatin (Daniel *et al.*, 1993). The fusion protein also caused the repression of RARα responsive genes therefore myeloid differentiation was inhibited (Daniel *et al.*, 1993). Interestingly, all-*trans*-retinoic acid (atRA) or arsenic trioxide (As_2O_3) treatments can reverse the process and, at the same time, lead to complete tumor remission (Warrell *et al.*, 1993; Soignet *et al.*, 1998). This is the first indication that PML protein may function as a tumor suppressor and that the integrity of PML NBs may play a role in their functions (Dyck et al 1994 and Weis et al 1994).

The mechanisms of how these two therapeutic agents induced terminal differentiation and/or apoptosis of APL cells are distinct and yet, similar in strategies (for review see Zhu *et al.*, 2001). Both drugs cause degradation and cleavage of the PML-RARα fusion protein by targeting of different moieties. Binding of atRA to the AF2 transactivation domain of RARα reactivates the transcription of differentiation genes (Zhu *et al.*, 1999). This later leads to the degradation or cleavage of the fusion protein by catabolism coupled with transcriptional activation or by caspase activation which occurs upon differentiation of the hematopoietic cells (Nervi *et al.*, 1998). Since the PML protein remains in a micro-speckle pattern when RA-induced degradation is inhibited, the reformation of PML NBs is not the cause but the result of RA therapeutic effects. On the contrary, unlike RA, arsenic can actually induce

remission by enhancing the reformation of PML NBs (Lallemand-Breitenbach *et al.*, 2001). First, it increased the SUMOylation on PML and PML-RARα proteins and forced the formation of mature PML NBs from the primary PML protein aggregates. PML component proteins were then correctly recruited into the NBs including the proteasome 11S complex which was responsible for the degradation of PML as well as fusion protein.

Other lines of evidence came from studies of viruses. Very early on, it was known that the family of interferon proteins can induce PML protein expression and result in an increased number and larger PML NBs in the infected nucleus (de The *et al.*, 1990). This indicated that PML NBs may play a role in viral defense pathway. The first direct evidence for the involvement of PML NBs came later and was reported by Gerd Maul in 1993. Before ND10 and PODs were known to be the same nuclear domains, he discovered that PML NBs were rapidly disrupted upon herpes simple virus (HSV-1) infections when the viral immediate-early regulatory protein, ICP0, was targeted to PML NBs (Maul *et al.*, 1993). ICP0 specifically disrupted PML NBs by inducing proteasome-mediated degradation of PML and Sp100, particularly the SUMOylated forms (Everett *et al.*, 1998). Many other types of viruses also affect the composition and/or organization of PML NBs; however, the strategies used by each virus vary from type to type. For example, in the case of adenovirus type 5 (Ad5) virus, one of the viral effectors, open reading frame 3 protein product (Orf3) of E4 gene, disrupted PML NBs during the early phase of Ad5 infection (Carvalho *et al.*, 1995). Instead of degrading the PML protein, Ad5 Orf3 altered the PML protein localization into “track-like” structures. Orf3 plays a crucial role in multiple steps of the Ad5 life cycle and its tight association with PML NBs further indicates that the structural integrity of PML NBs is important for viral propagation.

Lastly, upon exposure of cells to sublethal environmental stresses, e.g. heat shock or $CdCl_2$ treatment, the structure and composition of PML NBs undergo reorganization (Eskiw *et al.*, 2003; Nefkens *et al.*, 2003). Upon introducing cellular stress, PML NBs partially disassembled to form micro-speckles and released some of the component proteins. The mechanisms have not been fully understood yet, but there are some indications that heat shock and Cd^{2+} exposure both altered the post-translational modifications of the proteins in PML NBs through different pathways (Nefkens *et al.*, 2003). While the dispersal of PML NBs caused by cadmium can be blocked by the inhibitors of p38 MAPK or ERK1/2, the deSUMOylation of PML protein induced by heat shock can be rescued by SUMO

overexpression. Together, these studies indicate that structural integrity of PML NBs plays an important role in their functions.

iii. Elucidation of PML NB Functions via Composition

The composition of PML NBs is heterogeneous. Until now, the functions of PML NBs were mostly elucidated by studying their partner proteins presuming that the pathways those factors involved may also engage PML NBs as one of their components. Thus far, more than 50 proteins known to be involved in transcriptional regulation, apoptosis, premature senescence, DNA replication, DNA repair, or antiviral defense have been reported to be localized to PML NBs. This suggests that these nuclear bodies may play important roles in a variety of cellular processes (for review see Borden, 2002). However, how the different roles are integrated in PML NBs and their involvement in the molecular and biochemical mechanisms in these various processes still remain largely unknown. One major difficulty of partner protein studies is that its use of transient transfection in elucidating associations is often unreliable in the case of PML NBs. Some groups have detected localization of foreign proteins in PML NBs when they were ectopically overexpressed in the cell nucleus (Tsukamoto *et al.*, 2000). In addition, live cell tracking of the virus-like particles (VLPs) which delivered the plasmid DNA into cell nuclei without normal viral effector proteins showed that the episomal transgene is regulated by nuclear spatial positioning and PML NBs(Bishop *et al.*, 2006). The author also showed that PML NBs were recruited to the sites of integration when the transgene was transcriptionally active. This association between PML NBs and transcriptionally active loci is not sufficient for transcriptional repression of the transgene, but it is necessary for type I interferon-mediated inhibition of transgene expression. These data suggest that PML NBs may function as a nuclear sensor to retain misfolded, aggregated foreign proteins, or viral genomes within the NBs (Bishop *et al.*, 2006). Therefore, it is important to establish that these interactions occur not only at overexpressed levels, but also at endogenous levels (for review see Borden, 2002). Several proteins, such as PML, Sp100, Daxx, and SUMO, are ubiquitously present at PML NBs. SUMOylation of PML protein is required for the recruitment of component proteins into PML NBs; however, while often SUMOylated, many of the proteins do not require their SUMOylation to enter PML NBs (Ishov *et al.*, 1999).

PML - When knocking out PML protein by exon 2 deletion of the PML gene, PML protein expression was abolished by non-sense mediated decay of the PML mRNA. PML NBs were no longer present in the *pml*$^{-/-}$ mouse nuclei and all the other resident proteins were dispersed in the nucleoplasm (Wang *et al.*, 1998a). Upon restoring the expression of PML protein in *pml*$^{-/-}$ mouse embryonic fibroblasts (MEFs), PML NBs reformed and all the components relocalized back to PML NBs. The *pml*$^{-/-}$ mice had no apparent developmental phenotype, but under stress, they were more susceptible to viral infection and tumorigenesis. This indicates that among PML NB component proteins, PML is the major structural component and may play a major role in the functions of PML NBs.

The domain structure of PML protein, as shown in Fig. 3, contains a RBCC or TRIM motif, which consists of one RING, two B-boxes, and one coiled-coil domain (for review see Jensen *et al.*, 2001). RING and B-box domains are rich in cysteine residues and are responsible for protein-protein and/or DNA-protein interactions while the coiled-coil domain may function as homo- or heterodimerization site. Alternative splicing generates 7 major PML isoforms by different usage of 3' exons, i.e. exon 7, 8, and 9. Therefore, each isoform consists of a conserved amino (N)-terminal RBCC motif and a distinct carboxyl (C)-terminus. All of the isoforms were expressed in cell lines or primary cells that have been tested (Condemine *et al.*, 2006). Isoform I to VI are conserved in the usage of exon 1 to exon 6 and all include the nuclear localization signal (NLS) from exon 6. They are localized in the nucleus and present in every PML NB, but with different endogenous expression levels. Stable expression of individual PML isoforms in the *pml*$^{-/-}$ MEF cells showed distinct nuclear patterns and PML isoforms always colocalized together when expressed simultaneously (Condemine *et al.*, 2006). Moreover, two recent studies indicated that specific PML isoforms were preferentially targeted by viral proteins to induce the disruption of PML NBs upon viral infection (Guccione *et al.*, 2004; Hoppe *et al.*, 2006). This suggests that the C-terminal domains of PML proteins have unique interaction with specific cellular structures. PML-I and PML-II are the major isoforms expressed in the cell (Condemine *et al.*, 2006). However, most of the early studies primarily utilized PML-IV when investigating the interactions or localizations of PML NBs in cell growth control pathways. As a result, a reevaluation is needed to determine if some of the functional correlations are merely due to the overexpression of PML-IV.

Interestingly, PML-VII is the only cytoplasmic isoform which only includes

the usage of exon 1 to exon 4 plus partial exon 7, thus containing no NLS. Unexpectedly, it plays a major role in transforming growth factor β (TGFβ) signaling pathway shown by Pier Paolo Pandolfi's group (Lin *et al.*, 2004). They first discovered that *pml*$^{-/-}$ primary cells were resistant to TGFβ-dependent tumor suppression signaling as those cells contained mislocalized TGFβ signaling molecules. Therefore, the induction of TGFβ target genes was failed in those cells. Cytoplasmic PML (cPML) was shown to physically interact with TGFβ signaling proteins, Smad2/3 and SARA (for Smad Anchor of Receptor Activation) (Lin *et al.*, 2004). It is required for the Smad2/3 and SARA association and also for the targeting of SARA and TGFβ receptor in the early endosome. They further confirmed that the TGFβ signaling pathway was also impaired in APL cells showing the similar defects observed in *pml*$^{-/-}$ cells. These data indicated that cPML plays a crucial role in cancer pathogenesis through regulating the TGFβ pathway.

Sp100 - Sp100 was the first component protein of PML NBs identified through autoimmune sera from primary biliary cirrhosis patients during the early 1980s (Bernstein, et al, 1984). It forms nuclear speckles, now known as PML NBs, and has an anomalous electrophoretic mobility of 100kD, hence the name Sp100, speckle protein of 100 kDa. In contrast to PML protein, Sp100 is not essential for NB formation since human embryonic ND2 cells, which do not express Sp100, still contain PML NBs (Ishov *et al.*, 1999). Like PML, Sp100 also has several splice variants, Sp100A, Sp100B, Sp100-HMG, and Sp100C (Seeler *et al.*, 2001). They all are covalently modified by SUMO at lysine297 residue, but this modification is not required for its localization to the core of PML NBs (Sternsdorf *et al.*, 1999). The expression level of Sp100 variants, besides Sp100A, is usually undetectable by immunoblotting unless they are induced by interferon treatment. This suggests that Sp100 variants may also play specific roles in viral defense. The potential function of Sp100 is often overlooked due to its close association with PML NBs. However, recent studies showed that it may be involved in transcriptional regulation via direct interaction with HP1 and ETS-1 (Seeler *et al.*, 1998; Wasylyk *et al.*, 2002). Further, upon HSV-1 infection, Sp100 isoforms B, C, and HMG, but not Sp100A, were responsible for the suppression of the ICP0 and ICP4 early expression (Negorev *et al.*, 2006). These data suggest Sp100 may carry some independent functions in PML NBs in collaboration with PML protein.

Daxx - The death-domain-associated protein (Daxx) was first cloned from its interaction with a transmembrane death receptor, FAS (CD95) (Yang *et al.*, 1997). It bound to the death domain of FAS in the cytoplasm and potentiated FAS-induced apoptosis. However, the majority of Daxx protein is nuclear and often colocalizes within PML NBs. In different cell lines or under different physiological conditions, Daxx also associates with other nuclear domains. For example, in S phase or in *pml*$^{-/-}$ cells, Daxx is localized at the α-thalassemia/ mental retardation syndrome protein (ATRX)-positive heterochromatic region and may involve in chromatin remodeling (Ishov *et al.*, 2004). The pro-apoptotic function of Daxx is established by its interaction with different signaling molecules of the apoptotic pathways. Besides FAS, Daxx can also sensitize cells to apoptosis induced by TGFβ, IFNγ, and arsenic trioxide where the localization to PML NBs and the interaction with PML protein is necessary for Daxx pro-apoptotic function (Kawai *et al.*, 2003). These studies suggest the involvement of PML NBs in the apoptotic pathway.

eIF4E - Recently, eukaryotic translation initiation factor 4E (eIF4E) has been shown to directly interact with the PML RING domain to form a tight complex (Cohen *et al.*, 2001). The binding between PML and eIF4E induced a conformational change in eIF4E and reduced the eIF4E affinity to its substrate, the m^{7}G capped mRNA. This indicates that PML serves as a negative regulator for eIF4E-dependent mRNA export, including cyclin D1 mRNA, and therefore, suppresses eIF4E-mediated transformation (Topisirovic *et al.*, 2002). Intriguingly, unlike other PML NB associated proteins, eIF4E can form distinct nuclear bodies in the absence of PML protein, and the restoration of PML protein expression in the *pml*$^{-/-}$ cells leads to its colocalization with eIF4E nuclear bodies (Cohen *et al.*, 2001). Moreover, m^{7}GpppG cap analogue treatment not only disrupts eIF4E bodies, but also PML NBs and its components such as SP100, which indicates that at least part of PML NB forming mechanism depends on eIF4E (for review see Strudwick and Borden, 2002). The association of PML and eIF4E suggests that PML NBs may have a role in regulation of mRNA export.

iv. PML NB Formation in Molecular Details

Post-translational modification of PML protein by SUMO plays a crucial role in PML NB assembly and disassembly. SUMO is a small ubiquitin-like modifier,

which was first reported to be a PML interacting protein in yeast two-hybrid studies (Boddy et al 1996). Three lysines of PML have been identified to be SUMOylated: K65 at RING domain, K160 at first B-box domain, and K490 at the NLS sequence, which is at C-terminus of the coiled-coil domain. PML protein with three lysine mutations is mislocalized in the nucleus and all known component proteins also leave PML NBs (Muller et al 1998, Kamitani et al 1998, and Zhong et al 2000). However, SUMOylation is not required for PML protein to form primary aggregates in vivo, but is necessary for proper recruitments of its associated proteins to form mature PML NBs (Lallemand-Breitenbach et al 2001). The primary aggregates of PML protein may be developed through the self-assembly properties of the RING domain since it has been demonstrated that RING domain alone can form spherical structures in vitro (Kentsis *et al.*, 2002).

Two recent studies elegantly revealed the molecular details of PML NB formation and proposed a model of how PML NBs regulate the function of their component proteins through SUMOylation (Lin *et al.*, 2006; Shen *et al.*, 2006). They identified that in the exon 7 of PML protein, there is a SUMO-interacting motif (SIM) with the consensus sequence (VVVI) which was shared by various proteins as reported earlier (Song *et al.*, 2004). They demonstrated that even though the RING domain was crucial for PML SUMOylation and aggregation, the SIM motif is necessary for PML NB maturation (Shen *et al.*, 2006). Therefore, the authors proposed a 3-step maturation process of PML NBs. The primary assembly of PML protein using its RBCC domain is SUMOylated first. A PML-network is then built up through the interaction between two PML molecules by the binding of their SIM motifs to their SUMOylated sites. The last step is the recruitment of PML NB components. SUMOylated proteins can be recruited to PML NBs by PML SIM motif while proteins with a SIM motif can bind to SUMOylated PML. Therefore, this non-covalent interaction between SIM motif and SUMO moiety is crucial for PML NB formation. It also provides a potential mechanism for PML NB function. By changing the SUMOylation of certain binding partners, SIM containing proteins, such as Daxx, can shuffle between PML NBs and their target genes in the nucleoplasm (Lin *et al.*, 2006). This suggests a plausible mechanism for PML NBs to integrate their involvement in different cellular processes by simply regulating the localization of different proteins.

v. The Dynamics of PML NBs

PML NB composition and morphology are highly dynamic. Many of the PML NB components, such as p53 and NDHII, have been shown to dynamically associate or disassociate with these bodies. They can be sequestered or activated in PML NBs under certain physiological conditions (for review see Jensen *et al.*, 2001). For example, ubiquitin-specific protease 7 (USP7) was recruited to PML NBs shortly after cells were stimulated by Herpes simplex virus infection (Everett *et al.*, 1997). There, it was activated to deSUMOylate PML protein and caused the disruption of PML NBs. On the contrary, steroid receptor coactivator-1 (SRC-1) was originally sequestered in PML NBs (Rivera *et al.*, 2003). Upon its agonist-mediated activation, SRC-1 relocated from PML NBs into nuclear speckles through the interaction with androgen receptor (AR).

In addition, besides changing the composition, several PML NB resident proteins, e.g. PML, Sp100, and CBP, have also been shown to exhibit high turnover rates by FRAP and FLIP analysis (Wiesmeijer *et al.*, 2002). The dynamic movements of PML NBs have also been previously characterized in interphase BHK cells (Muratani *et al.*, 2002). PML NBs were categorized into three populations according to their dynamics: stationary (25%), limited localized movement (63%), and rapid movement (12%). The stationary and localized movements, similar to the motions of Cajal bodies (Platani *et al.*, 2002), were shown to be independent of the size of PML NBs. However, the rapid moving PML NBs, which are usually small in size and typically represent one to two PML NBs per nucleus, were not found in HeLa cells (Eskiw *et al.*, 2003). This may be due to the heterogeneity of PML NBs in different cell types of differences in imaging protocols. Nevertheless, the movement of this group of PML NBs depends upon metabolic-energy, but not transcription. This data suggests that PML NBs may carry out part of their function(s) by being actively transported within the nucleoplasm.

vi. Mitotic accumulations of PML protein (MAPPs)

The most dramatic changes of PML NBs occur at mitosis, during which time PML NBs are partially disassembled and the formation of large PML NBs (PML patches) occurs at the cell periphery (Everett *et al.*, 1999b). The authors also demonstrated that PML NBs reform to their normal size and number at early G1

phase, but a small amount of PML protein remains outside the newly formed daughter nuclei and becomes cytoplasmic bodies. Biochemical and immunocytochemical studies have shown that many resident components of PML NBs, such as Sp100 and Daxx, leave the bodies while PML protein still accumulated in mitotic PML NBs (Everett *et al.*, 1999b). Analysis of a metaphase cell extract showed that the PML protein lost its SUMOylation and became phosphorylated (Everett *et al.*, 1999b). A recent study, using two dimensional time lapse imaging, showed that PML NBs aggregated into mitotic accumulations of PML protein (MAPPs) and became mobile during mitosis (Dellaire *et al.*, 2006). In addition, FRAP analysis showed that there was very little exchange of PML protein in those structures. A subset of MAPPs remained associated with chromosomes and was suggested to contribute to the reformation of interphase PML NBs in early G1 nuclei as no new PML protein is synthesized during mitosis. Nevertheless, how PML NBs change their dynamic behavior in early prophase and how they reassemble their component proteins into daughter nuclei in early G1 phase is still unclear.

Figure 1: Nuclear domains in a mammalian cell nucleus

The cartoon diagram shows a typical mammalian cell nucleus containing a large number of different nuclear domains that have been identified. (Modified from Spector, 2003)

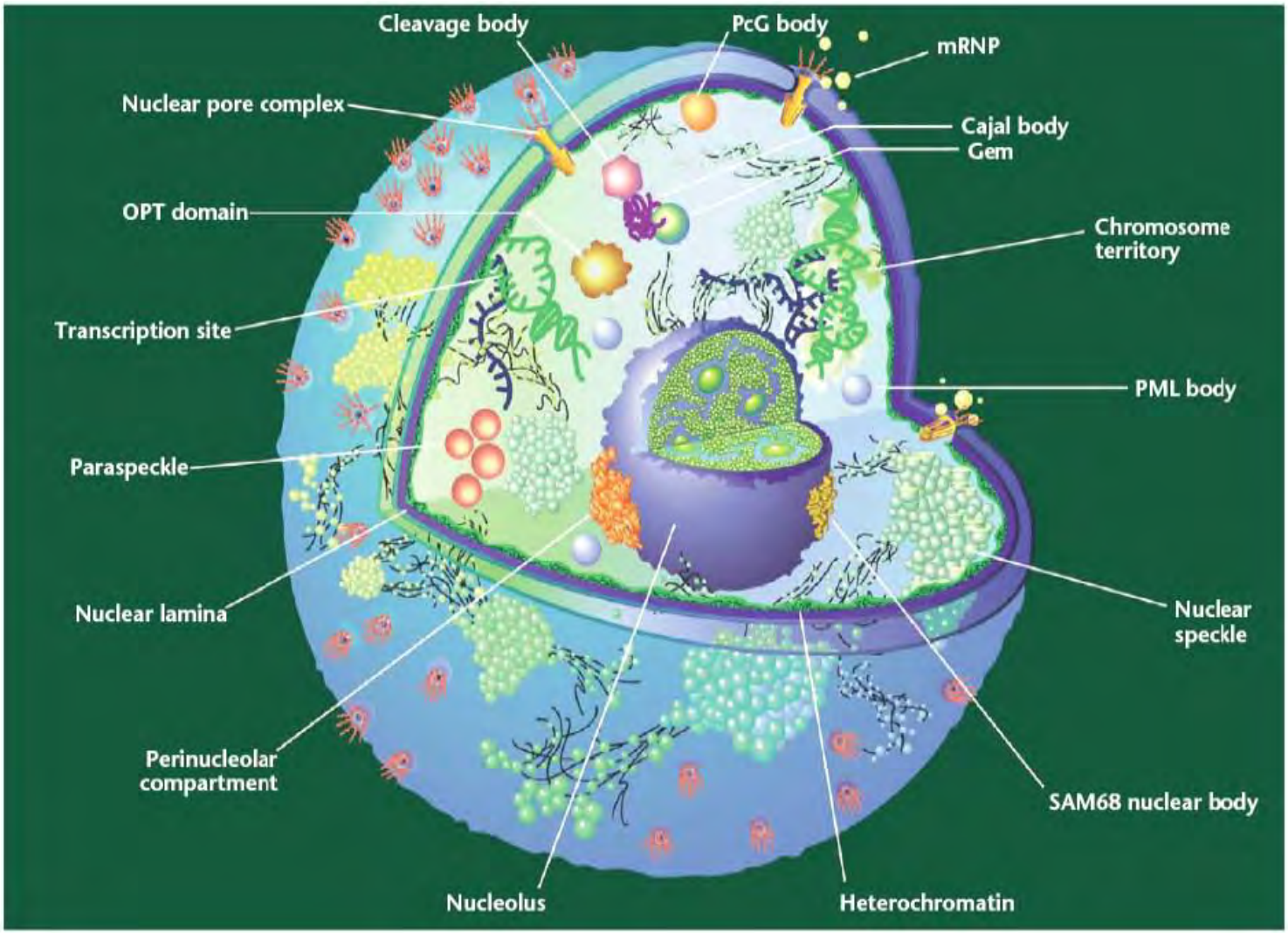
Cleavage body
PcG body
mRNP
Nuclear pore complex
Cajal body
Gem
OPT domain
Chromosome territory
Transcription site
PML body
Paraspeckle
Nuclear lamina
Nuclear speckle
Perinucleolar compartment
SAM68 nuclear body
Nucleolus
Heterochromatin

Figure 2: Morphology of PML NBs in BHK cells

(A) Immunofluorescent (IF) labeling of endogenous PML NBs. BHK cells were fixed and permeablized according to previously published procedures (Spector *et al*., 1998). Cells were then labeled with anti-PML antibodies (mAb 5E10) followed by FITC conjugated goat anti-mouse secondary antibodies. The image shows a single Z section.
(B) Ultrastructure of an endogenous PML NB. The thin section of a BHK cell nucleus is immunogold-labeled with anti-PML antibodies (mAb PML37) showing the localization of PML protein (5nm immunogold particles) is concentrated at the periphery of the PML NB. Courtesy of Stephen Hearn, Microscopy Shared Resource, Cold Spring Harbor Laboratory, New York, USA.

A

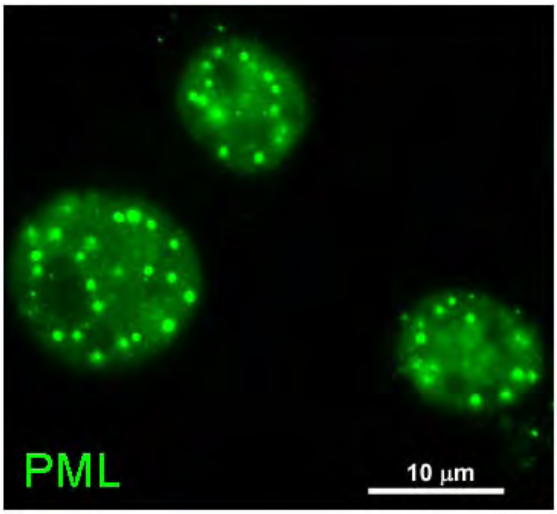

B

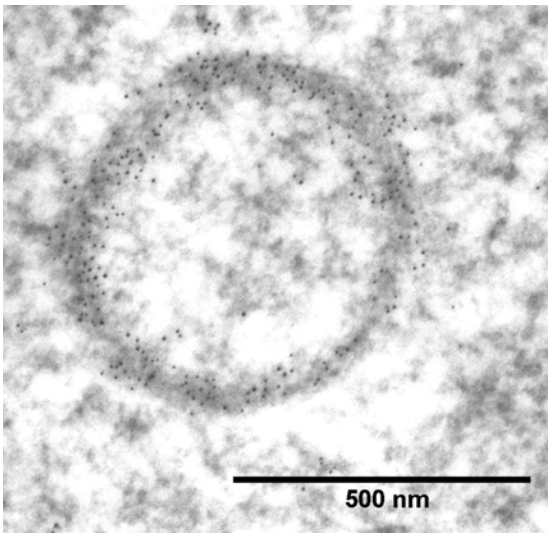

Figure 3: PML protein domain structure and PML isoforms

Diagram of PML protein domain assembly and isoforms. Exons 1 to 6 are conserved in isoform I to isoform VI while Isoform VII contains only exon 1 to 4. The different C-terminal region of each isoform is generated by using alternative 3' exons. The different length of PML isoforms is listed on the right. There are two common breakpoints associated with the chromosomal translocations in APL patients as indicated by the arrows. Three SUMOylation sites at amino acid positions 65, 160, and 490 are also illustrated as encircled S. R, Ring domain. B1 and B2, B-box domain 1 and B-box domain 2. CC, coiled-coil domain. NLS, nuclear localization sequence. (Adapted from Jensen *et al.*, 2001)

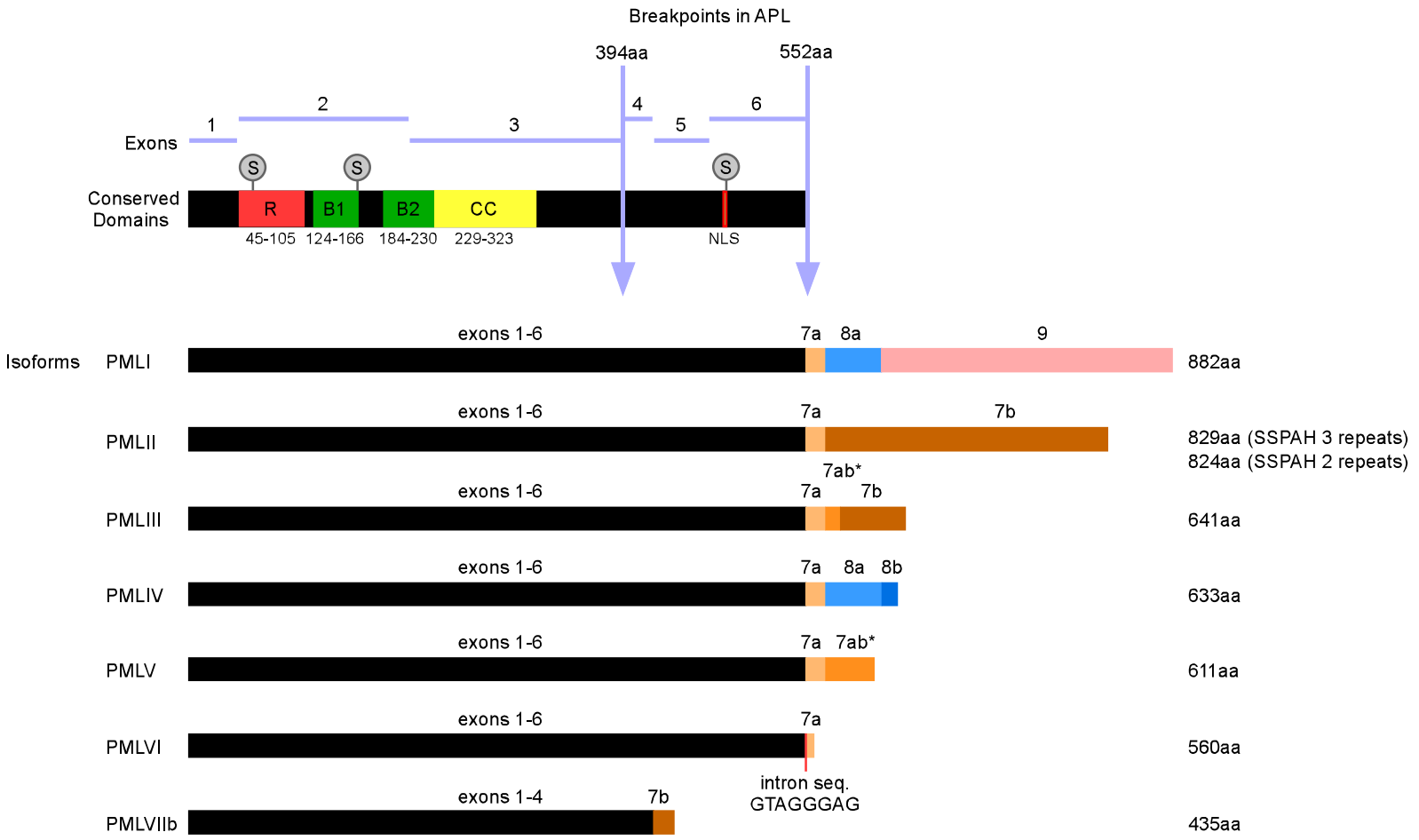
Breakpoints in APL
394aa
552aa
Exons
1
2
3
4
5
6
Conserved Domains
S
S
S
R
B1
B2
CC
45-105
124-166
184-230
229-323
NLS
Isoforms
PMLI
exons 1-6
7a
8a
9
882aa
PMLII
exons 1-6
7a
7b
829aa (SSPAH 3 repeats)
824aa (SSPAH 2 repeats)
PMLIII
exons 1-6
7a
7ab*
7b
641aa
PMLIV
exons 1-6
7a
8a
8b
633aa
PMLV
exons 1-6
7a
7ab*
611aa
PMLVI
exons 1-6
7a
560aa
intron seq.
GTAGGGAG
PMLVIIb
exons 1-4
7b
435aa

Chapter 2: Purification of PML NBs

Many of the cytoplasmic organelles have been biochemically fractionated and characterized. The isolation protocols were well established and have advanced over the past few decades (Spector *et al*., 1998). This has led to a good understanding of the composition and structure of several organelles which has suggested their potential functions. However, among the large number of subnuclear "organelles," only the nucleolus, Cajal bodies, the IGCs have been successfully purified (Mintz *et al.*, 1999; Lam *et al.*, 2002; Leung *et al.*, 2006). The technical difficulty is due to the fact that nuclear organelles are not encircled by phospholipid membranes. In addition, most of them are enmeshed with chromatin, and are possibly bound to the nuclear matrix. Therefore, it is far more difficult to isolate subnuclear domains than cytoplasmic organelles. As a result, more than 50 different proteins even though have been identified to associate with PML NBs, the complete proteome of PML NBs remains unknown.

I. PML NB Purification from Baby Hamster Kidney (BHK) Cells

Early biochemical studies showed that PML NBs were tightly associated with the nuclear matrix, and that their morphology was highly resistant to salt extraction and DNase or RNase treatments (Stuurman *et al.*, 1992). Since IGCs were successfully purified from the nuclear matrix fraction of mouse liver cells (Mintz *et al.*, 1999), a similar approach was adapted to isolate PML NBs.

i. Starting materials

A baby hamster kidney (BHK) cell line was chosen as the starting material for two reasons. First, PML NBs are usually more abundant in cell lines than in primary tissues. PML NBs in BHK cells are also physically bigger than their HeLa counterparts. The other reason is that in living cell studies, 12% of PML NBs in BHK cells were found to exhibit metabolic energy-dependent dynamic movement (Muratani *et al.*, 2002); however, the fast moving PML NBs were not found in

HeLa cells (Wiesmeijer *et al.*, 2002). It will be interesting to biochemically isolate this class of PML NBs and identify its components, which may contain nuclear motor proteins. In addition, this cell line has also been adapted to suspension culture, which is less cumbersome than an attached cell line or primary cells, in large scale biochemical purifications of PML NBs.

In order to monitor the integrity of PML NBs during initial biochemical preparation as well as to have an additional means for PML NB sorting, BHK suspension (BHK-S) cells was stably transfected with EYFP-Sp100, a fluorescently-tagged PML NB component protein. The resulting stable cell line, BHK-S 1-6, has fluorescently labeled PML NBs in over 90% of its population. This was confirmed by immunofluorescent labeling of PML NBs using mAb 5E10, which showed colocalization of EYFP-Sp100 and endogenous PML protein. Immunoblotting analysis using a monoclonal antibody against GFP also showed that the apparent size of the fusion protein is approximately 120 kDa (Fig. 7B). Although the predicted size of the fusion protein, including hSp100 (480 a.a.) and YFP (238 a.a.), is approximately 80 kDa, the observed aberrant migration is due to the acidic region of Sp100 protein (Sternsdorf *et al.*, 1997). In BHK-S 1-6 stable cell line, the EYFP-Sp100 expression level is low and steady. Also, as a suspension BHK line, it can grow in large quantities using suspension flasks and is suitable for biochemical purification.

ii. Preparation of a PML NB enriched fraction

The previously published purification protocol of IGCs (Mintz *et al.*, 1999) was adapted to isolate the nuclear matrix containing fraction from BHK suspension cells. A flow chart of the PML NB isolation protocol is shown in Fig. 4. It can be subdivided into several steps and each step has been optimized for BHK-S cells. One difficulty of nuclear domain purification is that, unlike cytoplasmic organelles or protein complexes, nuclear organelles usually do not have a signature enzymatic reaction which can be used to identify the fraction containing the target structure; therefore, it is difficult to follow the appropriate fraction during protocol development. In addition, during a traditional biochemical fractionation, the effectiveness can be easily verified by checking the persistence of enzymatic activity. If the enzyme is active, the purified complex is presumably still “intact.” However, the integrity of a nuclear domain can only be verified at best by comparing its ultrastructure and protein compositions before and after the

purification. Here, two methods were used to track the enrichment and integrity of PML NBs in each fraction. Because BHK-S 1-6 cell line stably expresses EYFP-Sp100, PML NBs in each fraction can easily be followed by detecting the EYFP fluorescent signal with a ZEISS Axioplan 2i fluorescence microscope (Fig. 5). Immunoblotting (IB) analysis was also performed to detect PML protein enrichment as well as contamination in each fraction, as shown in Fig. 6. Note that all of the fractions in the IB analysis were normalized by weight in order to show the enrichment of certain proteins in 10 μg protein of the fractions. The normalization for the subsequent IB analysis in this study was done by the same method as above.

Isolation of nuclei - Even though one of the PML splice variants, PMLVII, is cytoplasmic and appears in cytoplasmic bodies, we are primarily interested in nuclear PML NBs. Therefore, isolation of cell nuclei is the first step for PML NB purification, and, as such, cytoplasmic contamination needs to be minimized. BHK-S cells collected from suspension flasks were treated with hypotonic RSB buffer, which was described in the standard isolation protocol for HeLa nuclei (Spector *et al*., 1998) In order to obtain clean nuclei with minimal cytoskeletal contamination, 2 mM $CaCl_2$ was added during the hypotonic treatment to provide better separation of cytoplasm and nucleus, and to prevent nuclear clumping (Nathanson *et al.*, 2003). As shown by the differential interference contrast (DIC) image in Fig. 5A, isolated nuclei had very little cytoplasmic contamination. IB indicated that PML protein accounted for only a small portion of the isolated nuclear proteins (Fig. 6A, lane 1-Nu), while cytoplasmic vimentin was still present in the nuclear fraction (Fig. 6C, lane 1-Nu). This may be due to the tight association of the cytoskeleton with the nuclear periphery in suspension cells that allows for cells to withstand mechanical forces in spinner culture. Further fractionation is needed to remove vimentin.

Permeablization and DNase I digestion - The conditions used for permeablization and DNase I digestion from the previous protocol (Mintz *et al.*, 1999) have been further optimized for BHK-S cells. Triton X-100 treatment was used to permeablize and remove the nuclear membrane to allow DNase I to access the chromatin. Little PML protein was present in the Triton X-100 extracted supernatant while majority of it remained in the pellet (Fig. 6A, lane2-TxS and lane3-TxP). Since EYFP-Sp100 fluorescent signal remained colocalized with

immunofluorescent-labeled PML protein, indicating that the PML NBs were intact after Triton X-100 treatment (Fig. 5B).

The incubation time of DNase I digestion was extended to 1.5 hours to ensure the completion of DNA digestion. Complete digestion is critical to successfully remove chromatin in the subsequent salt extraction step. Failure to remove all the chromatin will cause the nuclear matrix to exhibit higher resistance to mechanical forces after the extraction, and will therefore be harder to break in the disruption step. Most PML NBs would then be retained in the unbroken nuclear matrix, rather than being released into solution. In addition, chromatin associated proteins may co-fractionate with PML NBs if the majority of chromatin is not removed. Therefore, the completion of DNase I digestion is critical for the disruption of the nuclear matrix and the release of PML NBs in the downstream steps of fractionation.

Salt extraction - Salt extraction is used to obtain the nuclear matrix fraction which is highly enriched with PML NBs. High salt treatment extracts the soluble pool of various proteins, the digested DNA, and most of the histones from the nuclei. Meanwhile, many proteins will also precipitate onto the nuclear matrix as described by Lam *et al.*, (2002) such that the high Mg^{2+} concentration will cause Cajal bodies to associate with the matrix preventing their later separation. Therefore, Mg^{2+} concentration of the salt extraction buffer is crucial for how tightly the nuclear substructure associates with nuclear matrix. Different concentrations of Mg^{2+} in salt extraction buffer were titrated for efficient release of PML NBs from the matrix with the most effective concentration being 0.5 mM. After extraction, the nuclei were DAPI negative, but EYFP-Sp100 signal was still retained, indicating absence of chromatin contamination, but retention of intact PML NBs. The TEM image also showed that even though the nucleus was mostly depleted, the PML NBs were still intact (Fig. 5C). Only a small amount of soluble PML was extracted into the solution as shown in Fig. 6A by IB (lane4-DS1, lane5-DS2, and lane6-DS3) while the majority of PML protein was enriched in the nuclear matrix fraction (lane7-DSP). These results agree with previous studies that PML NBs are retained in the nuclear matrix fraction (Stuurman *et al.*, 1992).

Mechanical disruption - In order to release PML NBs from the nuclear matrix without disrupting their structure, gentle mechanical force was applied to break the nuclear matrix. Previously, Mintz *et al.* (1999) first treated the salt

extracted pellets with 1 mM DTT to partially disassemble the nuclear lamina and then used needle shearing followed by homogenization to effectively break the nuclear matrix. In the case of PML NBs, as long as the initial nuclear isolation was clean and DNase I digestion was efficient, extracting nuclei with low Mg^{2+} concentration made nuclei very fragile. Most of the PML NBs can be released from the matrix by simple homogenization. Therefore, the shearing step was omitted, and 10% glycerol was also added to the buffer to protect PML NBs from over-disruption which may lead to contamination by nuclear lamins, nucleoli, and other residual nuclear components in later isolation steps. IB shows at least five-fold enrichment of PML protein in this fraction (Fig. 6A, compare lane1 and lane8-MDP).

Low speed centrifugation - The crude separation of PML NBs from matrix remnants was done by brief centrifugation at low speed. The low speed supernatant (LSS) was enriched with smaller nuclear organelles, e.g. PML NBs, IGCs, and Cajal bodies while nuclear lamina, nucleoli, and unbroken nuclei were present in the low speed pellet (LSP). To further optimize the separation of the nucleoplasm from nuclear matrix remnants, various centrifugation speeds were tested. As shown in Fig. 7 (lane4 to lane9), the enrichment of PML protein in the supernatant shows little to no difference between the different centrifugation speeds, as varied from 7,000 rpm (7K) to 13,000 rpm (13K). In addition, contaminants, such as vimentin, were also present in LSS, although in smaller amounts than the LSP. Interestingly, as shown by DIC image in Fig. 5E, it is very clear that the LSS fraction only contains small particles, some of which colocalize with the fluorescently labeled PML NBs. This indicated that the PML NBs present in the LSS fraction were freed from nuclear matrix entanglement and that the contaminants were present either as soluble proteins or as the small particles broken down from the larger nuclear matrix components.

iii. Isolation of PML NBs by fluorescent-activated cell sorting (FACS)

PML NBs exist in various densities and sizes, due to their heterogeneous nature. It is very unlikely that they can be resolved into a single band in a gradient system. In order to isolate all of the PML NBs at once, two different approaches have been pursued.

Fluorescent sorting by fluorescent activated cell sorting (FACS) can actively

sort particles according to their fluorescent intensity. Each particle is first separated into single buffer droplet. A sample stream of continuous droplets is then passed through a laser beam which can excite each particle to generate profiles based on its fluorescent properties. Beside fluorescent intensity, two additional properties of each particle are also determined by the detectors. Forward scattered (FSC) light readings indicate relative size of the particles while Side scattered (SSC) light readings indicate the relative complexity of their components.

Since the PML NBs in BHK-S 1-6 cell line are labeled with EYFP-Sp100 fusion protein, we first attempted to isolate PML NBs using FACS. The PML NB enriched fraction, LSS, was prepared from both wt BHK-S and BHK-S 1-6 cells. YFP signal intensity was used to gate the particle sorting. As shown in Fig. 8A and 8B, each particle analyzed is represented as a data point and plotted by size versus fluorescent intensity. The population of particles with high fluorescent intensity in the BHK-S 1-6 LSS fraction is dramatically larger than the corresponding population in the wild type fraction. A gate was applied to separate the fluorescent particles from the non-fluorescent ones, as indicated in Fig. 8C and 8D. Both fractions were collected and analyzed by IB to check the protein composition. As shown in Fig. 7, the last 2 lanes of each blot were the “waste” (non-fluorescent) and the “sort” (fluorescent) fractions. The presence of several component PML NBs proteins (PML, Daxx, and Sp100), proteins of other nuclear organelles (B23, SF2, SC35 and coilin) and of cytoplasmic contaminants (vimentin) was assayed by IB. The results indicated that all of the proteins showed equal distribution between the 2 fractions. This indicated that FACS did not further partition PML NBs from the rest of nucleoplasmic proteins. Therefore, other isolation methods were needed to isolate PML NBs from the LSS fraction.

iv. Isolation of PML NBs by magnetic microbead sorting

PML protein is the major structural component of PML NBs and is localized at the outermost layers of PML NBs. Therefore, immunoprecipitation (IP) using specific antibodies against PML protein should potentially pull down PML NBs regardless of their size and composition. Traditional methods of IP use protein A- or protein G-conjugated Sepharose beads to precipitate protein complexes that were specifically bound by the primary antibodies. The protocol requires centrifugation to collect beads in several steps.

The LSS fraction is enriched for PML NBs, along with other nuclear organelles. All of these structures, up to 1 μm in diameter, are relatively very large protein complexes. As such, consecutive centrifugations may precipitate all of the complexes, without specificity. In order to specifically pull down PML NBs labeled by the primary antibodies, a protein G-coated magnetic bead sorting system (μMACS protein G microbeads from Miltenyi Biotech) was chosen as a more suitable method for this IP application. The system is able to effectively isolate small cytoplasmic organelles, e.g. Golgi vesicles and endosomes (Perrin-Cocon *et al.*, 1999; Mura *et al.*, 2002).The small size of the microbeads, about 50 nm in diameter, allows them to coat the exterior of the organelles without damaging their structural integrity.

μcolumns containing ion matrices, with 30 μm clearance, were primed and placed in the strong magnetic field of the μMACS separator. The mixture of LSS, microbeads, and mAb 5E10 were rotated at 4˚C for one hour before being applied to the separator. As the mixture passed through the column in the magnetic field, the microbead coated PML NBs were specifically retained in the ion matrix, while the flow-through was collected. The PML NBs were subsequently released and eluted by removing the column from the magnetic field. As shown by IB in Fig 9, PML protein and EYFP-Sp100 were enriched in the eluate while lamin A/C and vimentin were mainly present in the flow-through.

There were several problems with the microbead approach. The first was that a fair amount of vimentin contaminated the eluate. Different IP protocols were attempted to minimize vimentin contamination, including pre-IP with vimentin specific antibody. However, none of these approaches was successful. In addition, the efficiency of microbead recovery from the μcolumn was very poor, more likely due to the large size of the immunocomplexes bound to the beads than due to poor function of the microbeads themselves, as microbead recovery in the absence of a PML-specific antibody is robust and efficient. Indeed, the bound immunocomplexes were likely larger than the clearance of the μcolumn (30 um) and therefore were too large to be eluted from the column even after the removal of the magnetic field. The ultrastructure of the eluate, as revealed by immunoEM, also showed fibrous structures labeled by microbeads (Fig. 10). Many of these formed hollow, ring-like structures as well, but nothing that resembled endogenous PML NBs. Therefore, another approach was still needed to isolate PML NBs while maintaining their apparent structure.

II. PML NB Purification from Mouse Tissue

Although BHK-S 1-6 cells have several advantages for PML NB purification, such as large number of PML NBs per nucleus and easy tracking of EYFP-Sp100 labeled PML NBs, it also has several disadvantages. One is the absence of a cell line that lacks PML NBs to be used as a negative control. Additionally, many antibodies that recognize specific human or mouse proteins fail to recognize their hamster homologs in the BHK-S cell lines. Since there is no equivalent BHK cell line that contains no PML NBs, one possible method to establish a negative control is to induce sub-lethal cellular stress to disrupt PML NB structures at the beginning of the isolation process. Cadmium treatment was a feasible approach to achieve this goal (Nefkens *et al.*, 2003). However, lower dosages of cadmium were insufficient to completely disrupt PML NBs in the cells. Only about 50% of the cells lost PML NB after the treatment. Meanwhile, higher dosages of cadmium proved to be cytotoxic and killed half of the cells by the beginning of the isolation protocol. Therefore, a different starting material was required to provide a feasible negative control to facilitate the development of the isolation protocol.

i. Starting materials

In order to have a proper negative control to assess the efficacy of PML NB isolation, we switched our starting material from a hamster cell line to mouse tissue. PML knockout mice was the best negative control for PML NB isolation, as the mice have no apparent phenotype under normal physiological conditions (Wang *et al.*, 1998b). In addition, the isolation protocol of mouse nuclear matrix from liver tissue was well established (Mintz *et al.*, 1999). The protocol was also previously optimized in the BHK-S cell line to preserve the intact structure of PML NBs in the nuclear matrix, which was later used to prepare the PML NB enriched fraction. Therefore, beside the first step of nuclei isolation, the protocol only needed a few minor changes to accommodate the alternate starting materials.

Both mouse liver and spleen nuclei were isolated by different isolation protocols as described in the last chapter of material and methods. Both of the protocols were also optimized to obtain clean nuclei from the tissues with minimum cytoplasmic contamination. The total number of isolated nuclei from 10 livers was roughly equivalent to the number isolated from10 spleens, which was around 2×10^9 nuclei/ 10 organs. Even though the volume of a liver was much

larger than that of a spleen, most of the difference in mass was due to cytoplasmic organelles and extracellular matrices which were removed after collecting the nuclei through a sucrose gradient. Spleen cells, on the other hand, have little cytoplasm. However, as shown in Fig. 11, the nuclear fraction from spleen cells contained a higher level of vimentin protein as compared to a corresponding fraction from liver cells. This may be due to the vimentin cage surrounding the splenocyte nuclei, which sustains their rigidity (Brown *et al.*, 2001; Tolstonog *et al.*, 2002). The other observation is that the number of PML NBs in the liver nuclei was also about the same as that in the spleen nuclei. Since liver nuclei were much bigger than spleen nuclei and filled with higher number of other nuclear organelles, spleen nuclei exhibited higher PML protein enrichment than liver nuclei as shown in Fig. 11.

ii. Preparation of a PML NB enriched fraction

After nuclear isolation, further fractionation of mouse nuclei was similar to the protocol used on BHK-S cells. Nuclei were first permeablized by the Triton X-100 treatment followed by DNase I digestion. Salt extraction removed most of the chromatin to reveal the nuclear matrix, which was later disrupted by homogenization. After a brief low-speed centrifugation, PML NBs were enriched in the LSS supernatant fraction. The efficiency of fractionation using either wt mice or *pml*$^{-/-}$ mice showed no apparent difference other than an absence of PML protein in the *pml*$^{-/-}$ fraction (Fig. 12) One small modification was the addition of N-ethylmaleimide (NEM) in all buffers to prevent deSUMOylation by SUMO-1 hydrolase during fractionation (Suzuki *et al.*, 1999). As shown in Fig. 13, the higher molecular weight species of PML protein are now visible after NEM treatment.

PML NBs from mouse liver or spleen nuclei were less highly enriched in the LSS fraction than those from the BHK-S cells. In comparing the LSS and the LSP fractions in Fig. 11, much of the PML protein was still present in the LSP fraction indicating that the release of PML NBs from the nuclear matrix was not efficient. Many different conditions were attempted to increase the enrichment of PML NBs in the LSS. For example, 300 mM ammonium sulfate (AS) substituted for 500 mM sodium chloride during salt extraction in order to prevent precipitation of nuclear organelles onto the nuclear matrix. pH9 buffer and 1 mM DTT were used at the mechanical disruption step to partially disassemble the nuclear lamina to facilitate

matrix disruption. However, although the combination of AS extraction and pH9 buffer treatment yielded satisfactory PML protein enrichment in the LSS fraction, it also over-disrupted the nuclear matrix and increased contamination, which could not be eliminated, even after PML-specific IP (Fig. 13, lane 5). Moreover, the intact PML NB structure was no longer detected in the LSS fraction by immunoEM. Therefore, although a portion of PML NBs are lost in the LSP fraction by the original protocol, further isolation steps could yield a cleaner fraction of PML NBs, provided there is a sufficient, intact abundance of them in the LSS.

iii. Isolation of PML NBs by Dynabeads

Further isolation of PML NBs was carried out by using a different type of magnetic bead-based separation system developed by Dynal Biotech. The major difference of the Dynabeads from Miltenyi's microbeads is that the Dynabeads are larger and are about 250 μm in diameter. Therefore, instead of collecting microbeads by passing the bead/ lysate mixture through a μcolumn on the magnet, Dynabeads can be quickly separated from the mixture by applying the magnet on the side of the tube without centrifugation. They are also conveniently conjugated with either protein A, which binds to the Fc region of primary antibodies, or with sheep anti-mouse IgG antibodies, which recognize both heavy and light chains of mouse IgG.

Specific antibodies against PML protein (mAb PML 37) were covalently crosslinked to Dynabeads and used to immunoprecipitate PML NBs from the LSS fraction. As shown in Fig. 14, the PML37 conjugated protein A Dynabeads pulled down PML protein from both liver and spleen tissues with minimum levels of proteins from nuclear lamina, IGCs, and nucleoli. Vimentin was still present in the eluates, and was noticeably present in spleen isolates. However, without comparing against samples from *pml*$^{-/-}$ mice, it is difficult to elucidate whether these proteins were part of the PML NBs or rather contaminants present due to non-specific binding of the beads.

Subsequently, the LSS fractions prepared from both wt mice and *pml*$^{-/-}$ mice were used for IP. The immunoblots in Fig. 15A showed that using either PML37 conjugated protein A Dynabeads or Sheep-anti Mouse IgG Dynabeads effectively pulled down PML protein from the wt mouse LSS, while there was no PML protein present in the *pml*$^{-/-}$ samples. Moreover, lamin B, vimentin, and hnRNP M were present in both wt and PML-null eluate fractions, indicating that they are true

contaminants due to the non-specific binding of the beads, with notably higher levels in protein A Dynabead isolations (Fig. 15C, D, and E). In addition, nucleolar protein (B23) and SR proteins recognized by mouse monoclonal antibody 3C5 were absent in the eluates indicating that nucleoli and IGCs were efficiently separated from PML NB fractions (Fig. 15F and G). Interestingly, lamin A/C, while absent from *pml*$^{-/-}$ eluates, was specifically pulled down by anti-PML antibody (Fig. 15 B). This was further verified by IF labeling of the endogenous PML and lamin A/C proteins in mouse embryonic fibroblast (MEF) cells. As shown in Fig. 16, internal lamin A/C bodies were colocalized with PML NBs in the mouse primary cell line (MEFs). This may explain the tight association of PML NBs with mouse nuclear matrix and its inefficient release of PML NBs from the matrix fraction after mechanical disruption.

The integrity of PML NBs in the eluate of Sheep-anti Mouse IgG Dynabeads was verified by immunoEM. Fig. 17 presents several types of PML NBs found in the IP eluate. Many of them formed ring- or donut-shaped complexes with a PML-labeled shell, as indicated by immunogold particles, and a hollow center. Some of them have multilayer PML protein shells and a few of them have a PML shell with a solid center. These data indicated that the IP with dynabeads effectively purified structurally intact PML NBs from mouse tissue.

iv. Analysis of PML NB proteome by mass spectrometry

The purified PML NBs were analyzed further by mass spectrometry to identify their protein composition. Mass spectrometry is a powerful approach to quickly identify protein components of large macromolecular complexes such as the spliceosome (Zhou et al., 2002), the nucleolus (Andersen et al., 2002), and IGCs (Mintz et al., 1999). Due to the complexity of PML NB protein composition, the component proteins of the isolated PML NBs were first denatured and separated on a SDS-PAGE gel. The gel was pre-stained with GelCode Blue Stain Reagent (Estey *et al.*, 1997) and sliced into ten sections to separate different size of proteins. Each slice was subjected to in-gel trypsin digestion and the digested peptides were then analyzed by liquid chromatography-tandem mass spectrometry (LC-MS/MS). This approach greatly reduced the complexity of protein samples and therefore increased the sensibility of detect less abundant peptides.

The protein profiles of IP eluates from both wt mice and *pml*$^{-/-}$ mice are

summarized partially in Table 1. In the wt eluate, there were 195 proteins that were identified by at least two peptide hits in LC-MS/MS while there were only 80 proteins in the PML-null eluates. Table 1 lists the 48 proteins in the wt sample that have at least 8 peptide hits. The proteins that were present in both the wt and PML-null fractions were considered to be contaminants. PML protein has the third highest amount of hits on the list, indicating that the IP successfully enriched PML protein in the eluate fraction as in agreement with the IB results that we showed earlier. However, beside PML, none of the other known PML NB component proteins appeared on the list. Instead, many of the well known nuclear matrix proteins, e.g. matrin 3 and hnRNP family proteins, have the highest peptide hits. Interestingly, vimentin was identified by 24 peptides in the wt sample, while none of them were present in the PML-null sample. These results indicate that PML protein has a tight association with nuclear matrix proteins; however, we do not know if this association exists *in vivo* or was induced by the isolation protocol. Further study is needed to distinguish between these two possibilities.

Figure 4: Flow chart of PML NB isolation protocol.

The PML NB isolation protocol is depicted in the step-by-step flow chart. The fraction obtained after each step is indicated in the frame and the abbreviation for each fraction is indicated in red. The treatment for each step is stated on the right of the arrow. After salt extraction, the nuclear matrix is retained in the DSP fraction. Low speed centrifugation after mechanical disruption further separates nucleoplasm containing PML NBs, CBs, and IGCs from nuclear matrix remnants including nuclear lamina and nucleoli.

Flow Chart of PML NB Isolation

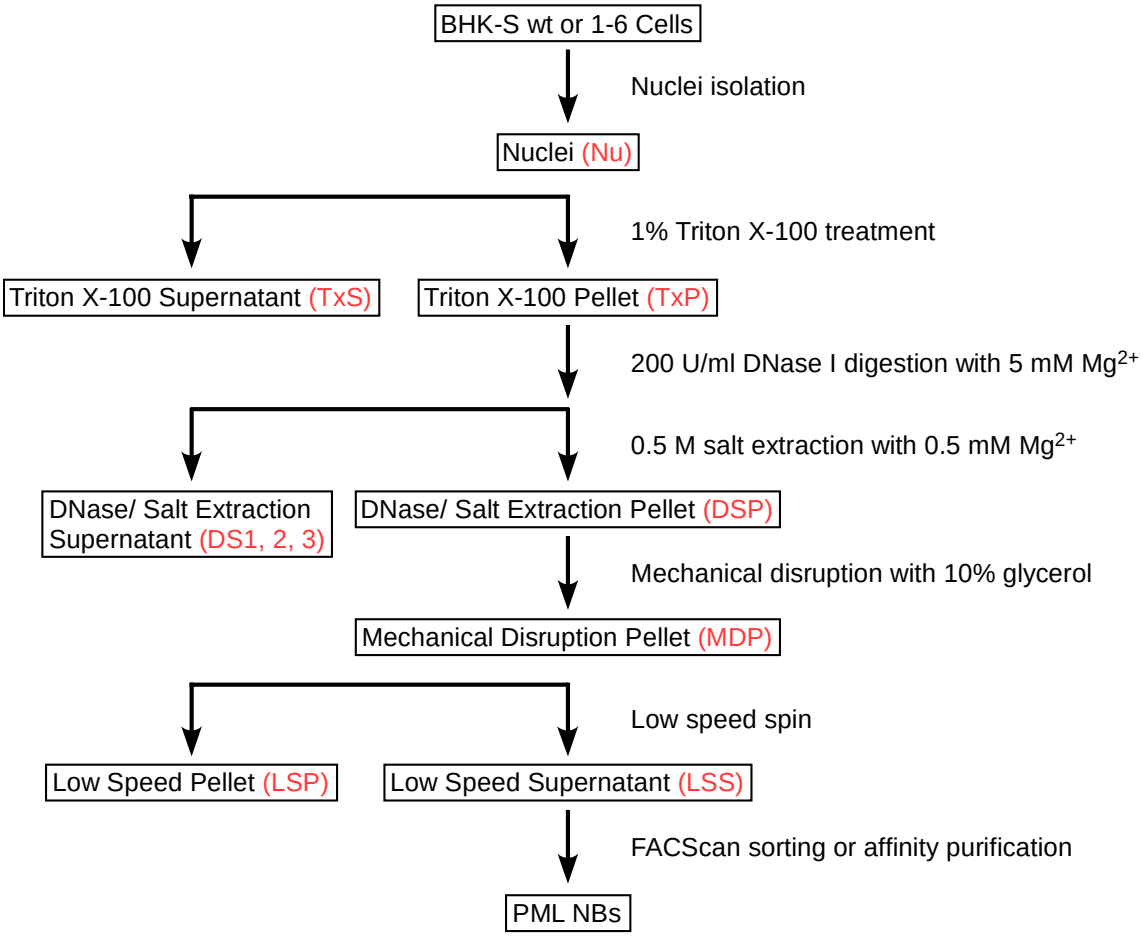

Figure 5: Selected fractions from the PML NB isolation protocol

To check the efficiency of each isolation step and verify the structure of PML NBs, a sample from each fraction was visualized by IF, DIC, or immunoEM. A few selected fractions are shown as follows.
(A) Nu: DIC image shows that purified nuclei had very little cytoskeleton contamination. (B) TxP: PML NBs were still intact after permeablization. DNA was stained by DAPI shown in blue. (C) DSP: After the salt extraction step, nuclei appeared extracted with little to no chromatin present as shown by TEM. The PML NBs labeled by mAb PML37 (10nm gold particles) were still well preserved (arrowhead). (D) MDP: IF staining of PML NBs (red) shows that PML NBs were released from the nuclear matrix after mechanical disruption. The colocalization of EYFP-Sp100 (green) with PML NBs indicates the preservation of the NB structure. (E) LSS: IF and DIC images show the enrichment of PML NBs with less nuclear matrix contamination. Colocalization of PML NBs with particles in DIC shows that PML NBs were released from the nuclear matrix. In (D) and (E), PML NBs were labeled with mAb 5E10. DNA (blue) was stained by DAPI. The colocalization is shown in yellow. Bars for all except C, 10 μm; for C, 500 nm.

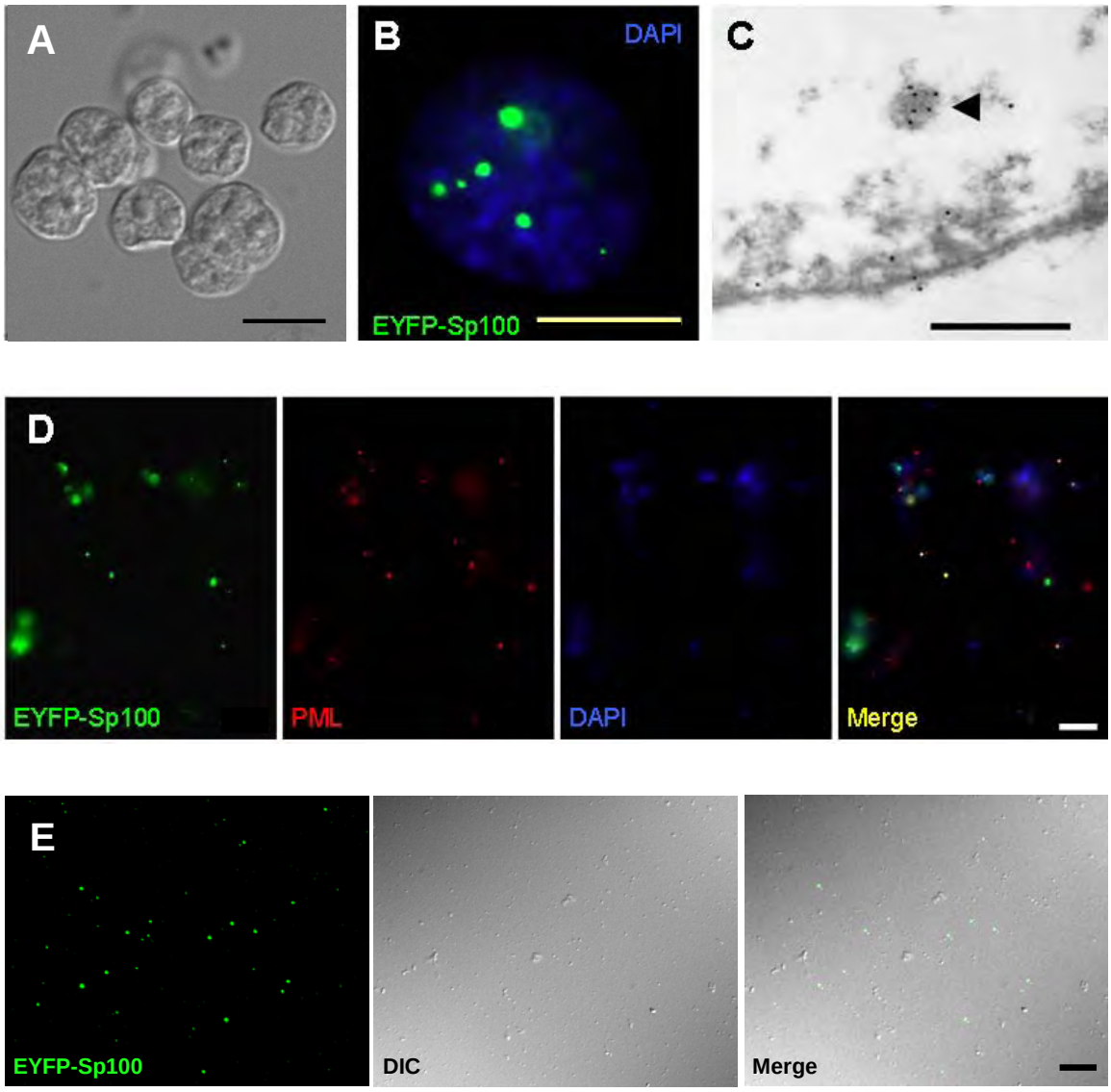
A
B
DAPI
EYFP-Sp100
C
D
EYFP-Sp100
PML
DAPI
Merge
E
EYFP-Sp100
DIC
Merge

Figure 6: Immunoblotting of fractions from PML NB isolation.

10 μg of total proteins from each fraction were separated on a 10% SDS-PAGE gel. Immunoblots using antibodies against (A) PML, (B) Daxx, and (C) vimentin are shown here. IB shows that after permeablization and salt extraction, the majority of PML, Daxx, and vimentin are retained in the pellet fractions while little to none is extracted in the supernatants (compare lane 2 to lane 3 and also lane 4-6 to lane 7). As shown in lane 9 and lane 10, PML and Daxx are enriched in the LSS fraction while the amount of vimentin is reduced in LSS.

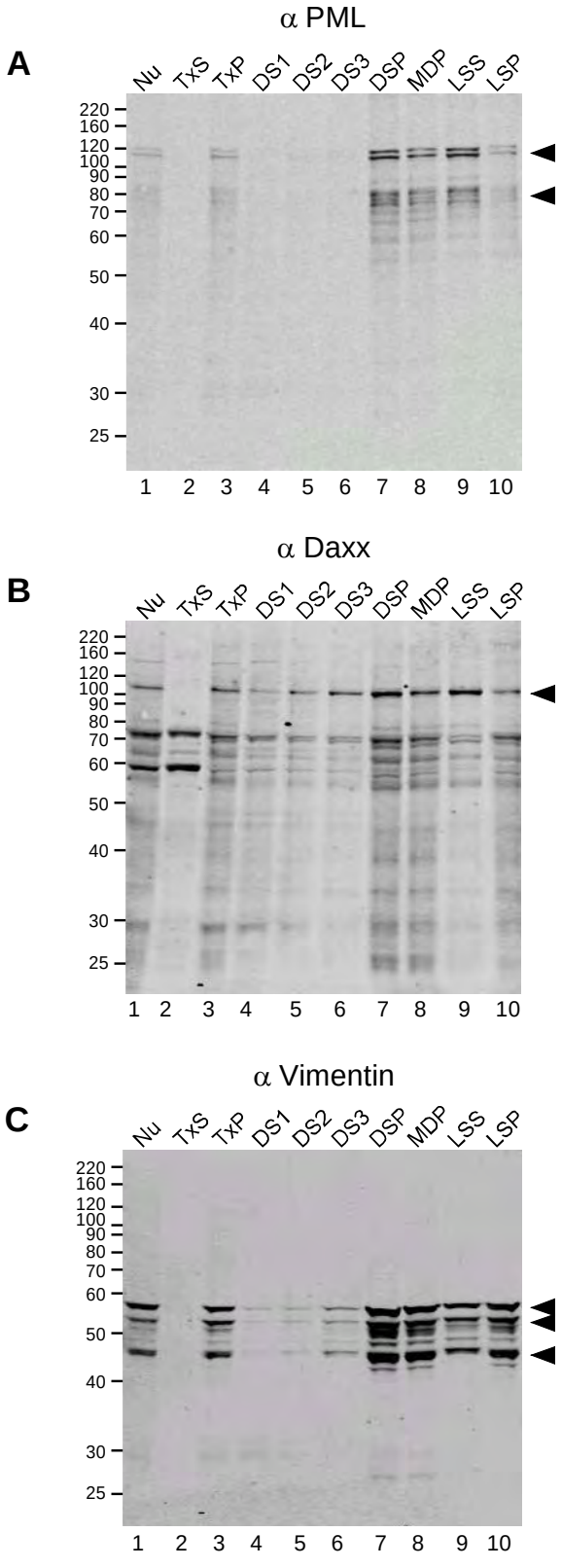
α PML
A
Nu
TxS
TxP
DS1
DS2
DS3
DSP
MDP
LSS
LSP
220
160
120
100
90
80
70
60
50
40
30
25
1 2 3 4 5 6 7 8 9 10
α Daxx
B
Nu
TxS
TxP
DS1
DS2
DS3
DSP
MDP
LSS
LSP
220
160
120
100
90
80
70
60
50
40
30
25
1 2 3 4 5 6 7 8 9 10
α Vimentin
C
Nu
TxS
TxP
DS1
DS2
DS3
DSP
MDP
LSS
LSP
220
160
120
100
90
80
70
60
50
40
30
25
1 2 3 4 5 6 7 8 9 10

Figure 7: Immunoblotting of fractions from fluorescent activated cell sorting (FACS).

The waste and the sort fractions from FACS were first precipitated by TCA and then dissolved in 50 mM Tris buffer, pH 8.8 before quantification. 10 μg of total proteins from each fraction were separated on a 10% SDS-PAGE gel. Immunoblots using antibodies against (A) PML, (B) GFP, (C) Daxx, (D) vimentin, (E) B23, (F) coilin, (G) SF2, and (H) SC35 are shown. The arrow heads indicate the specific bands for each protein and the bracket in (A) shows different PML isoforms. Various centrifugation speeds did not change the enrichment of PML or the reduction of vimentin in the LSS fraction (compare lane 4 to 9 in (A) and (D)). In addition, since all the proteins tested show equal distribution between the waste and the sort fractions (lane 10 and 11 in each blot), FACS sorting did not further partition PML NBs from the rest of the nucleoplasmic domains in the LSS fraction.

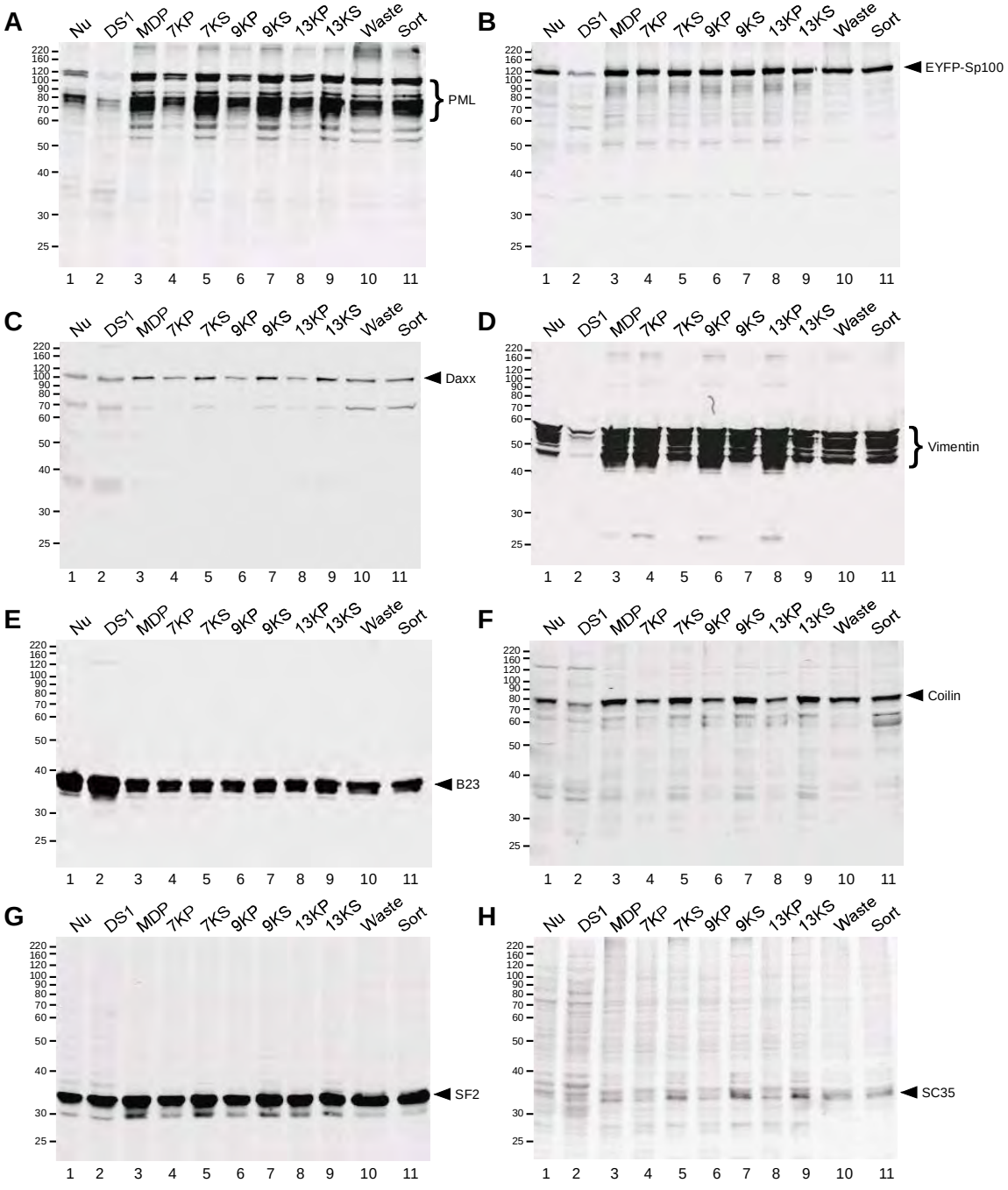
A
Nu DS1 MDP 7KP 7KS 9KP 9KS 13KP 13KS Waste Sort
220 160 120 100 90 80 70 60 50 40 30 25
PML
1 2 3 4 5 6 7 8 9 10 11
B
Nu DS1 MDP 7KP 7KS 9KP 9KS 13KP 13KS Waste Sort
220 160 120 100 90 80 70 60 50 40 30 25
EYFP-Sp100
1 2 3 4 5 6 7 8 9 10 11
C
Nu DS1 MDP 7KP 7KS 9KP 9KS 13KP 13KS Waste Sort
220 160 120 100 90 80 70 60 50 40 30 25
Daxx
1 2 3 4 5 6 7 8 9 10 11
D
Nu DS1 MDP 7KP 7KS 9KP 9KS 13KP 13KS Waste Sort
220 160 120 100 90 80 70 60 50 40 30 25
Vimentin
1 2 3 4 5 6 7 8 9 10 11
E
Nu DS1 MDP 7KP 7KS 9KP 9KS 13KP 13KS Waste Sort
220 160 120 100 90 80 70 60 50 40 30 25
B23
1 2 3 4 5 6 7 8 9 10 11
F
Nu DS1 MDP 7KP 7KS 9KP 9KS 13KP 13KS Waste Sort
220 160 120 100 90 80 70 60 50 40 30 25
Coilin
1 2 3 4 5 6 7 8 9 10 11
G
Nu DS1 MDP 7KP 7KS 9KP 9KS 13KP 13KS Waste Sort
220 160 120 100 90 80 70 60 50 40 30 25
SF2
1 2 3 4 5 6 7 8 9 10 11
H
Nu DS1 MDP 7KP 7KS 9KP 9KS 13KP 13KS Waste Sort
220 160 120 100 90 80 70 60 50 40 30 25
SC35
1 2 3 4 5 6 7 8 9 10 11

Figure 8: The sample profiles from FACS

The PML NB enriched LSS fraction from both wt BHK-S cells and BHK-S 1-6 cells were subjected to FACS sorting. The sample profiles were plotted either by the forward scattered light intensity (FSC) against the fluorescent intensity (GFP-A), (A) wt and (B) 1-6, or by GFP-A and particle counts, (C) wt and (D) 1-6. The gate for sorting was set by fluorescent intensity. The positive particles, which exhibit fluorescent intensity above the gate value, were collected into the sort fraction, shown in green, while the negative ones were collected into the waste fraction, shown in red.

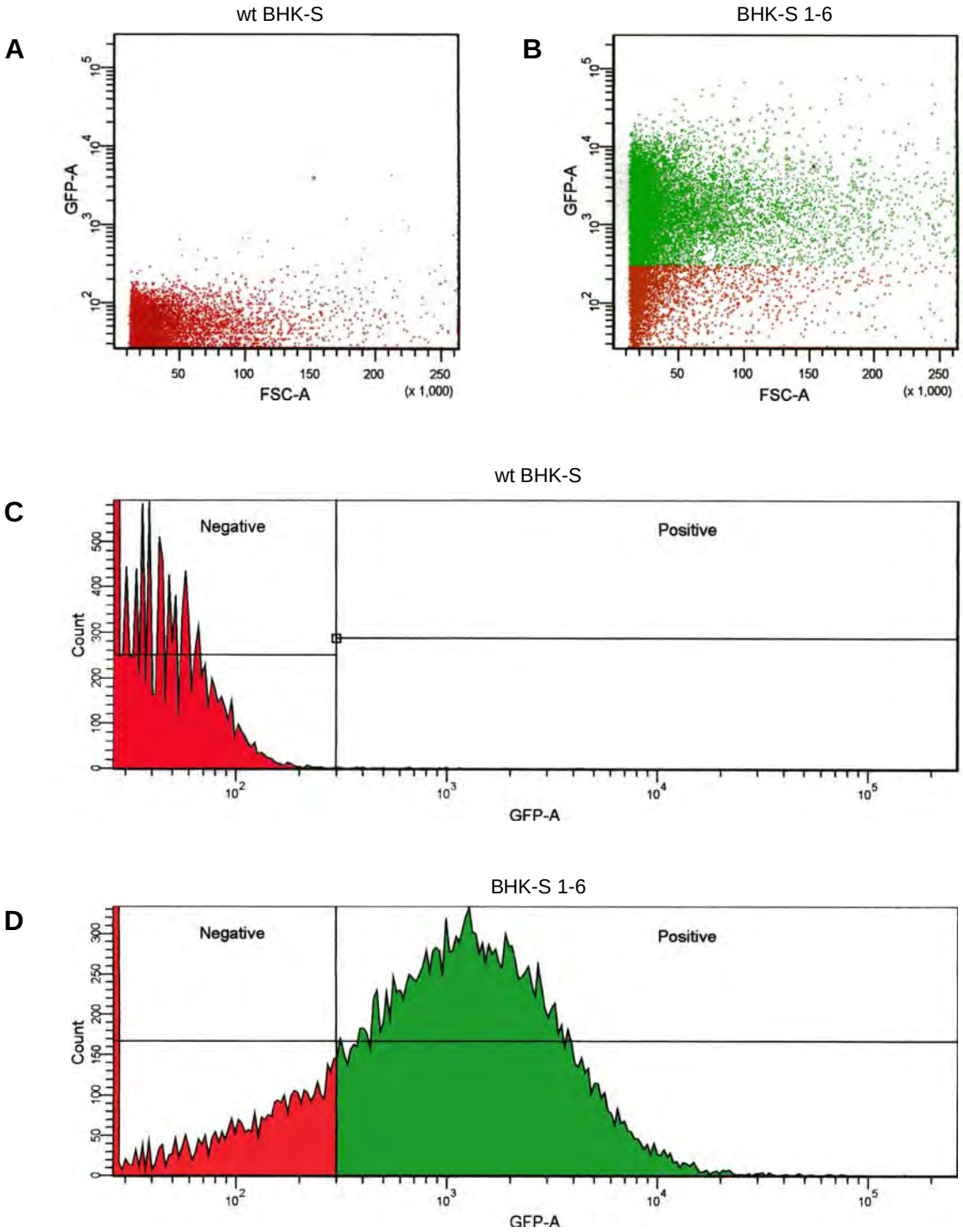
A
wt BHK-S
GFP-A
FSC-A
(x 1,000)
B
BHK-S 1-6
GFP-A
FSC-A
(x 1,000)
C
wt BHK-S
Negative
Positive
Count
GFP-A
D
BHK-S 1-6
Negative
Positive
Count
GFP-A

Figure 9: Immunoblotting of magnetic microbeads sorted fractions

Immunoprecipitation (IP) assay by the microbeads system was used to further isolate PML NBs in the LSS fraction. Immunoblots using antibodies against (A) PML, (B) GFP, (C) vimentin, and (D) lamin A/C are shown here. The arrow heads indicate the specific bands for each protein and the brackets in (A) and (C) show different PML or vimentin isoforms. The antibody heavy chain and light chain recognized by the secondary antibodies are indicated by asterisk. Comparing lane 4 and lane 6, both PML and EYFP-Sp100 protein are highly enriched in the eluates while lamin A/C is minimized in the same fraction. Little to no protein eluted in the negative control. However, vimentin is still present in the eluate fraction. NC, negative control without adding mAb in the mixture. IP, immunoprecipitation using PML specific mAb. FT, the flow-through fraction. E, the eluate fraction.

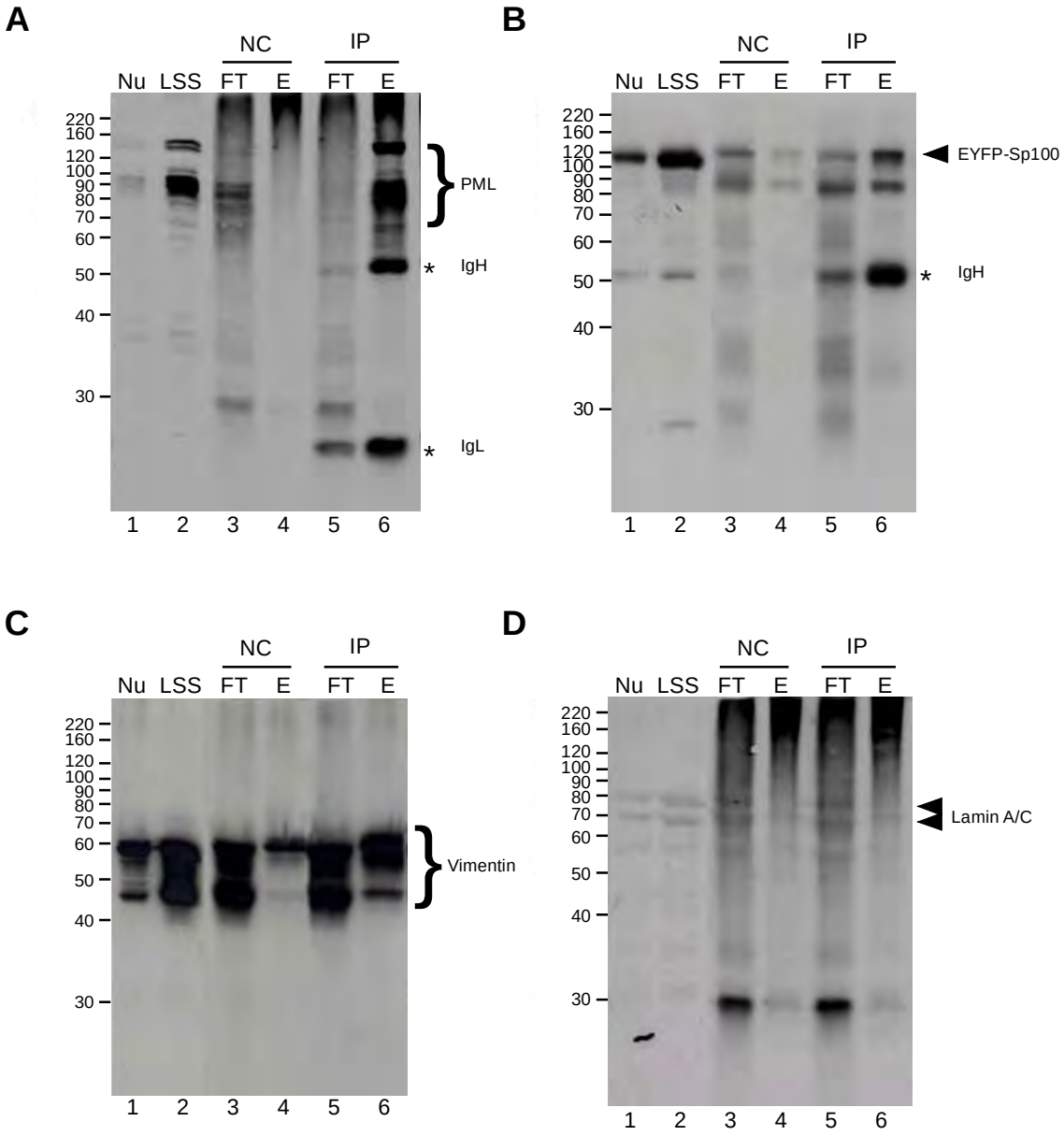
A
NC
IP
Nu LSS FT E FT E
220
160
120
100
90
80
70
60
50
40
30
PML
IgH
IgL
1 2 3 4 5 6
B
NC
IP
Nu LSS FT E FT E
EYFP-Sp100
IgH
1 2 3 4 5 6
C
NC
IP
Nu LSS FT E FT E
Vimentin
1 2 3 4 5 6
D
NC
IP
Nu LSS FT E FT E
Lamin A/C
1 2 3 4 5 6

Figure 10: Morphological characterization of the eluate fraction from the magnetic microbead sorting

TEM images of thin sections from the microbead IP eluates shows fibrous structures that were labeled with microbeads in the fraction. The arrowheads indicate some ring-like structures. The bar is 1 μm.

A

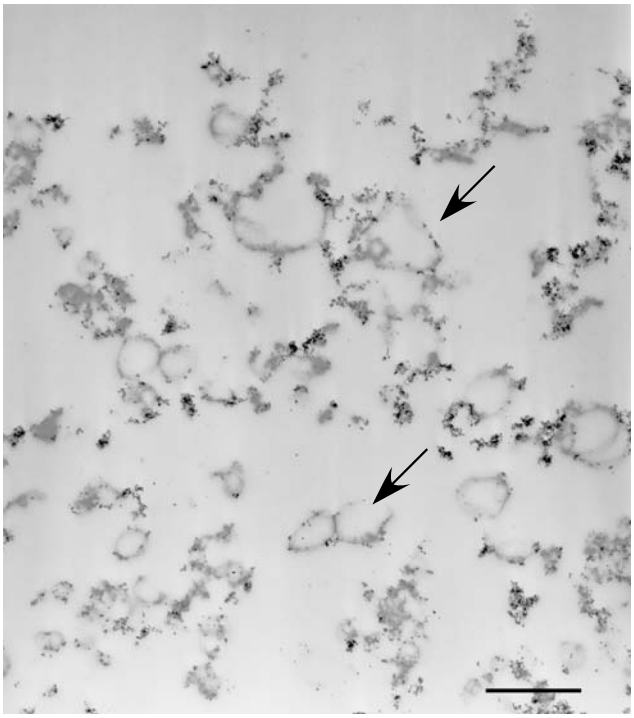

B

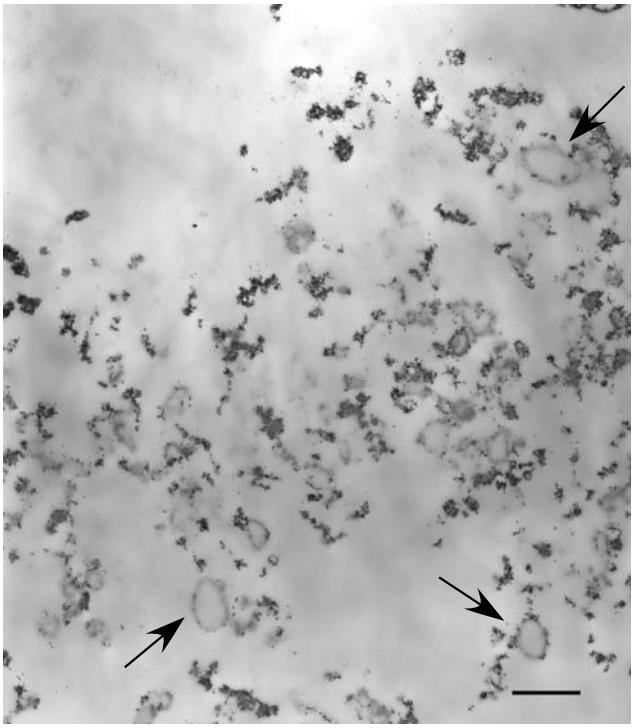

Figure 11: Fractionation from mouse spleen and liver tissues

10 μg of total proteins from each fraction were separated on a 10% SDS-PAGE gel. Immunoblots using antibodies against (A) PML and SF2, (B) Daxx and vimentin, (C) hnRNP M and U2 snRNP B", and (D) lamin A/C are shown here. Comparing lane 9 and 12, the spleen LSS shows higher enrichment of PML and Daxx proteins than the liver LSS. The amount of lamin A/C and vimentin are reduced in both liver and spleen LSS (compare lane 8 and 9, also lane 11 and 12).

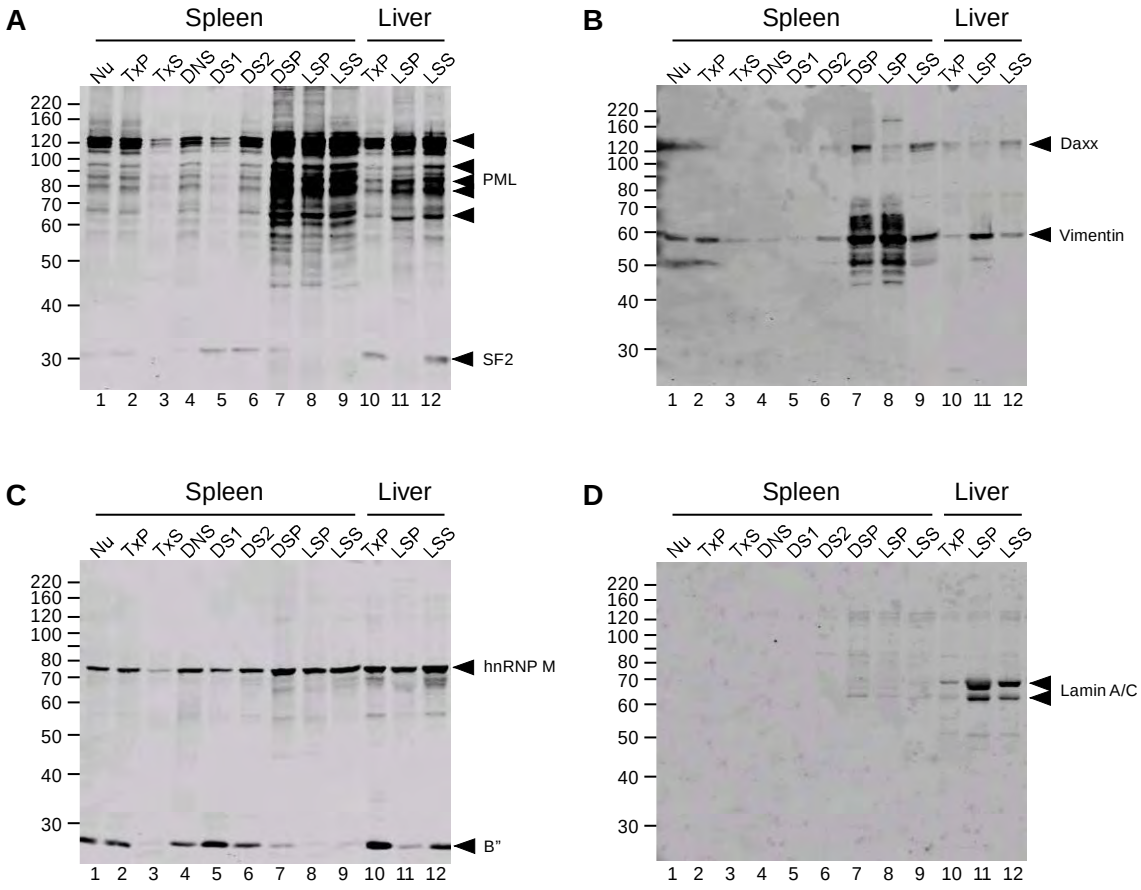
A
Spleen
Liver
Nu
TxP
TxS
DNS
DS1
DS2
DSP
LSP
LSS
TxP
LSP
LSS
220
160
120
100
80
70
60
50
40
30
PML
SF2
1 2 3 4 5 6 7 8 9 10 11 12
B
Spleen
Liver
Daxx
Vimentin
C
Spleen
Liver
hnRNP M
B"
D
Spleen
Liver
Lamin A/C

Figure 12: Immunoblotting of fractionation from wt and *pml*$^{-/-}$ mouse livers

Immunoblots using antibodies against (A) PML, (B) SR proteins, (C) vimentin, and (D) lamin A/C are shown here. The arrow heads indicate the specific bands for each protein. The fractions from wt and *pml*$^{-/-}$ mice show similar protein profiles besides there is no PML protein present in *pml*$^{-/-}$ fractions.

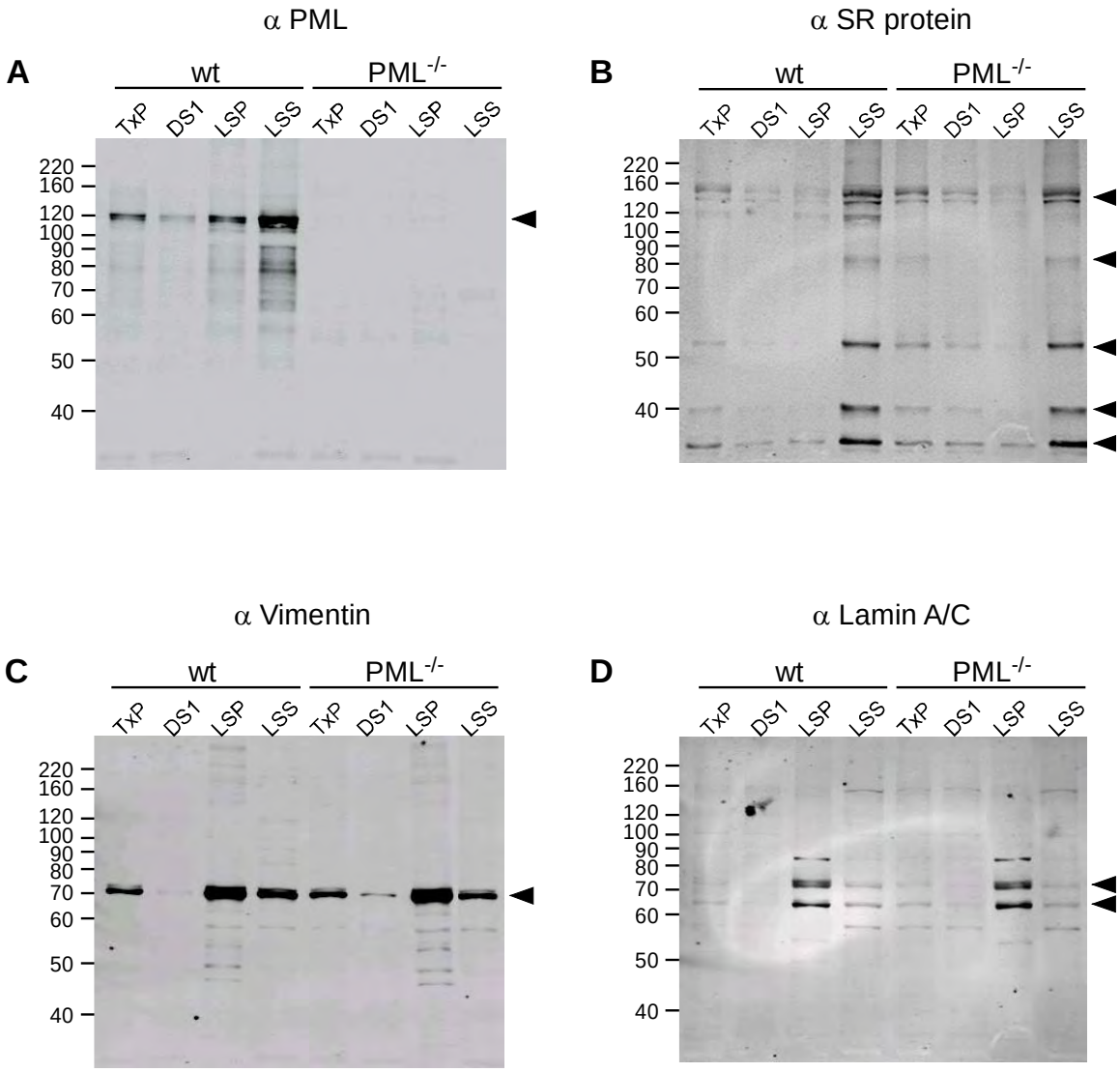
α PML
A
wt
PML-/-
TxP
DS1
LSP
LSS
220
160
120
100
90
80
70
60
50
40
α SR protein
B
α Vimentin
C
α Lamin A/C
D

Figure 13: Immunoblotting of fractionation from ammonium sulfate extraction and pH9 buffer treatment

Immunoblots using antibodies against (A) PML and SF2, (B) vimentin, (C) hnRNP M and U2 snRNP B", and (D) lamin B are shown here. The arrow heads indicate the specific bands for each protein. The bracket in (A) shows different PML isoforms. The asterisk in (A) shows the SUMOylated PML proteins and the asterisk in (C) shows the antibody light chain recognized by the secondary antibodies. After ammonium sulfate extraction, the nuclear matrix fraction, DSP, was treated with pH9 buffer to facilitate the disruption of the nuclear matrix. The enrichment of PML protein in the LSS was more prominent. PML protein was further enriched in the eluate fractions while B" and SF2 were depleted. However, vimentin, lamin B1, and hnRNP M were also present in the LSS fraction (lane 3) and can not be depleted even after PML-specific IP (lane 5).

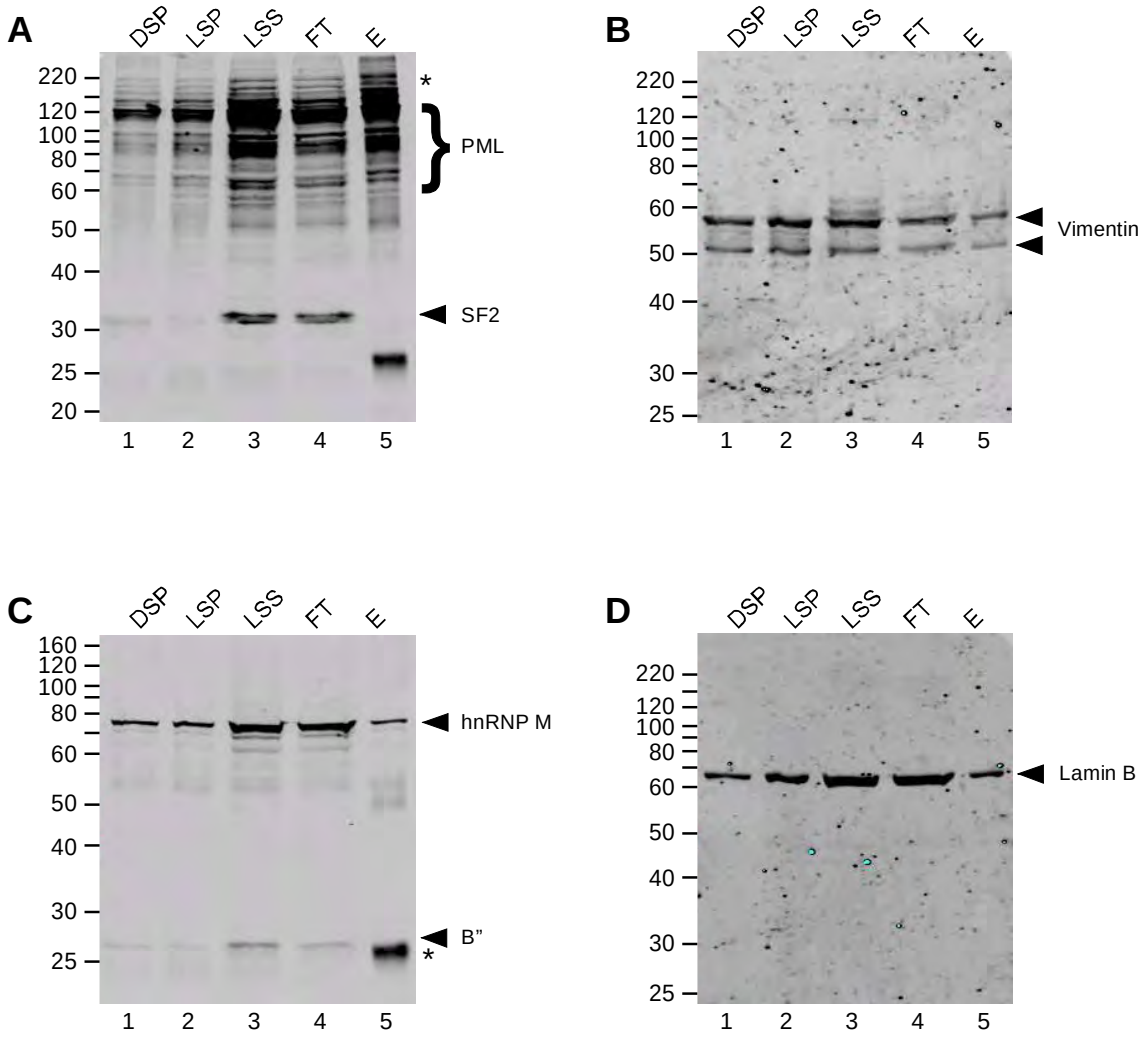
A
DSP
LSP
LSS
FT
E
220
120
100
80
60
50
40
30
25
20
*
PML
SF2
1
2
3
4
5
B
DSP
LSP
LSS
FT
E
220
120
100
80
60
50
40
30
25
Vimentin
1
2
3
4
5
C
DSP
LSP
LSS
FT
E
160
120
100
80
60
50
40
30
25
hnRNP M
B”
*
1
2
3
4
5
D
DSP
LSP
LSS
FT
E
220
120
100
80
60
50
40
30
25
Lamin B
1
2
3
4
5

Figure 14: Immunoblotting of Dynabeads immunoprecipitation fractions from mouse spleen and liver tissues

Immunoblots using antibodies against (A) PML and SF2, (B) Daxx and vimentin, (C) hnRNP M and U2 snRNP B", and (D) lamin A/C are shown here. The arrow heads indicate the specific bands for each protein. The bracket in (A) shows different PML isoforms. The asterisk in (A) shows the SUMOylated PML proteins and the asterisk in (C) shows the antibody light chain. Comparing lane 2 and lane 4, the eluates from spleen and liver tissues show similar protein profiles. However, vimentin is still present in the spleen eluate (lane 2 in (B)).

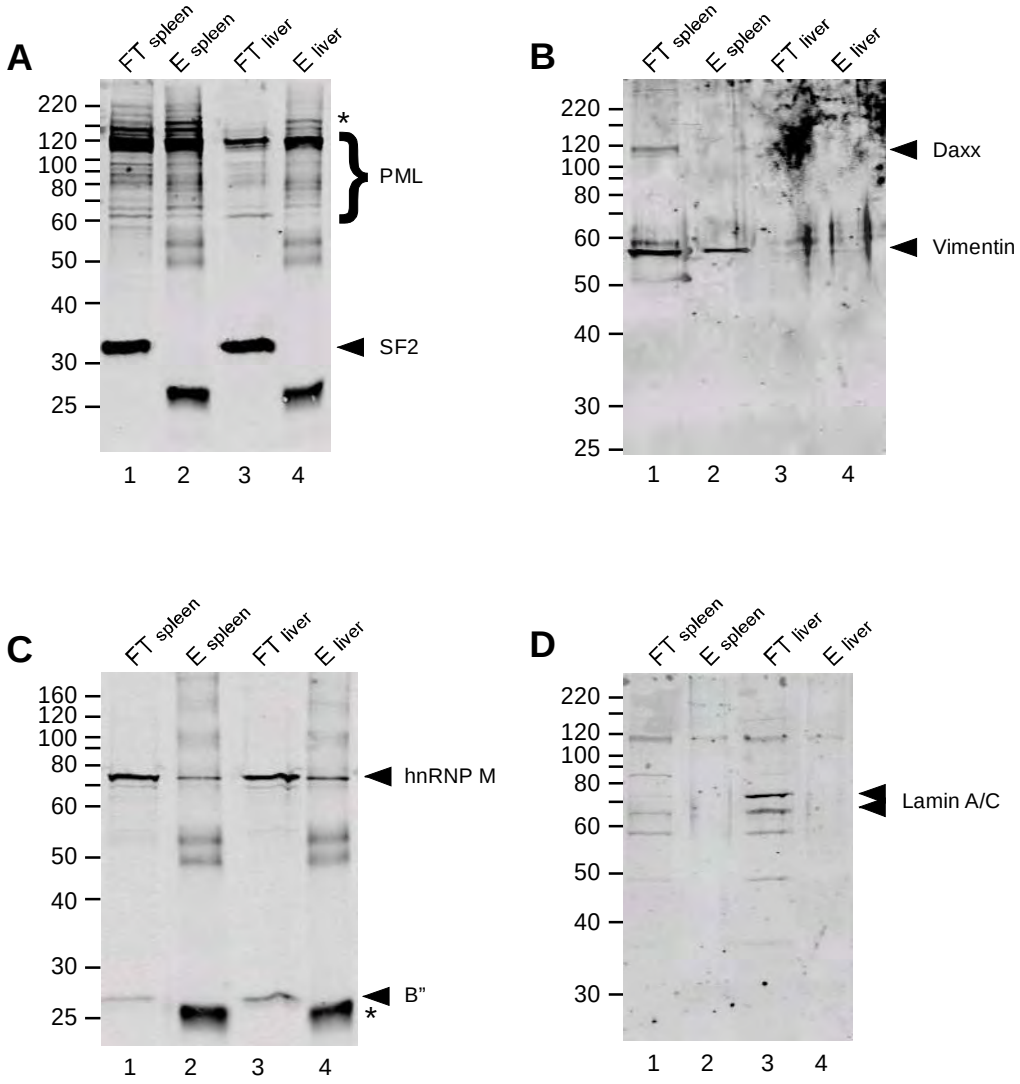
A
FT spleen
E spleen
FT liver
E liver
220
120
100
80
60
50
40
30
25
*
PML
SF2
1
2
3
4
B
FT spleen
E spleen
FT liver
E liver
220
120
100
80
60
50
40
30
25
Daxx
Vimentin
1
2
3
4
C
FT spleen
E spleen
FT liver
E liver
160
120
100
80
60
50
40
30
25
hnRNP M
B”
*
1
2
3
4
D
FT spleen
E spleen
FT liver
E liver
220
120
100
80
60
50
40
30
Lamin A/C
1
2
3
4

Figure 15: Immunoblotting of Dynabeads immunoprecipitation fractions from wt and *pml*$^{-/-}$ mice

Both mAb PML 37 conjugated protein A Dynabeads or Sheep-anti Mouse IgG Dynabeads were used for PML-specific IP in wt and *pml*$^{-/-}$ samples. Immunoblots using antibodies against (A) PML and SF2, (B) Daxx and vimentin, (C) vimentin, (D) lamin B, (E) hnRNP M, (F) SR proteins, and (G) B23 are shown here. The arrow heads indicate the specific bands for each protein. The bracket in (A) shows different PML isoforms. The asterisk show the non-specific bands recognized by secondary antibodies after re-probing. Comparing lanes 3, 5, 7, and 9 in each blot, the eluates from both protein A Dynabeads or Sheep-anti Mouse IgG Dynabeads are enriched with PML protein in wt sample but not in *pml*$^{-/-}$ control. The contamination by vimentin and hnRNP M are minimized in SαM eluates while lamin A/C is specifically precipitated by Sheep-anti Mouse IgG Dynabeads. A, protein A Dynabeads. SαM, Sheep-anti Mouse IgG Dynabeads. FT, the flow-through fraction. E, the eluate fraction.

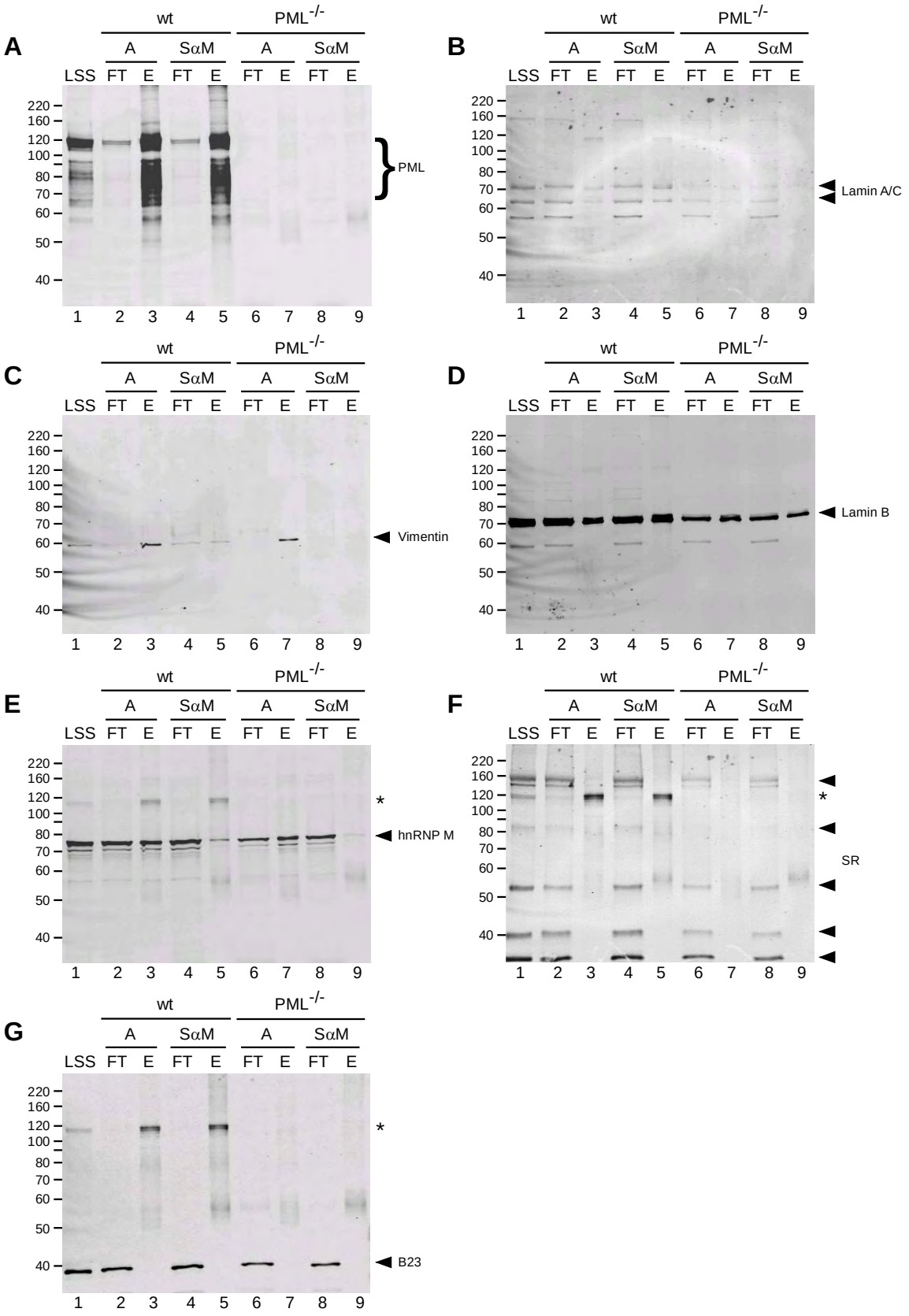
A
B
C
D
E
F
G
wt
PML-/-
A
SαM
LSS FT E FT E FT E FT E
1 2 3 4 5 6 7 8 9
220
160
120
100
80
70
60
50
40
PML
Lamin A/C
Vimentin
Lamin B
hnRNP M
SR
B23
*

Figure 16: Colocalization of endogenous PML and lamin A/C in MEF cells

Primary MEF cells were fixed and permeablized according to previously published procedures (Spector *et al*., 1998). Cells were then labeled with anti-PML antibody and anti-lamin A/C antibody. The images show the projection of a Z-stack of images collected by DeltaVision RT system. PML NBs colocalized with internal lamin A/C bodies (white arrowheads). The bar is 10 μm.

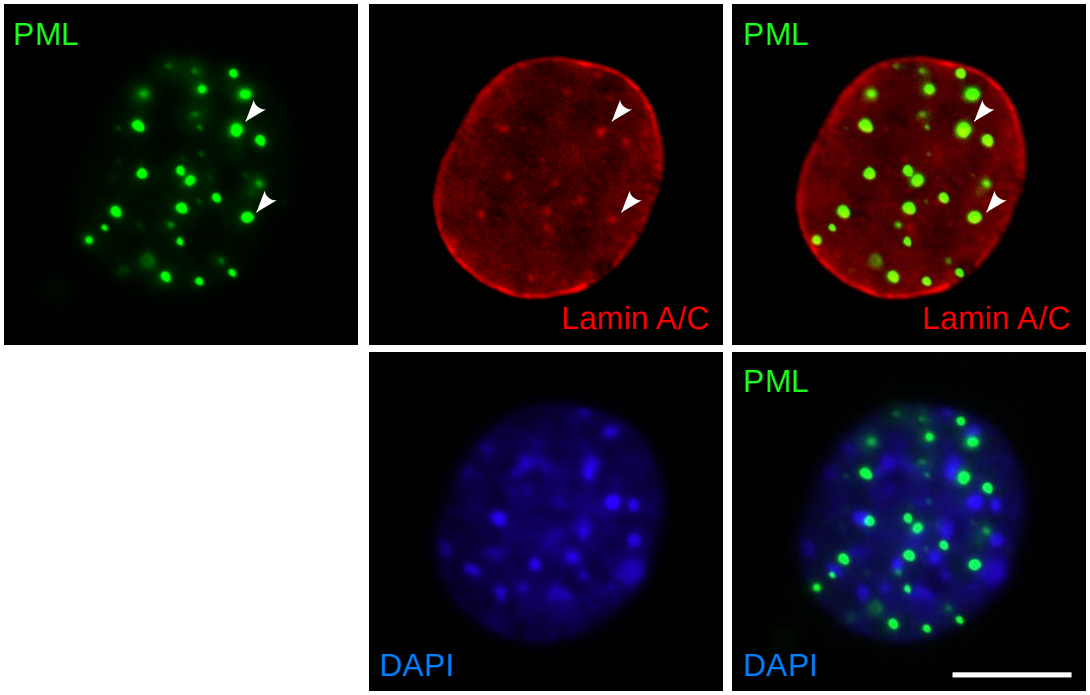
PML
Lamin A/C
PML
Lamin A/C
DAPI
PML
DAPI

Figure 17: Ultrastructure of purified PML NBs

Thin sections of PML NB enriched eluates showed different types of PML NBs. PML protein is labeled by 5 nm immunogold particles. The ring-like PML NBs and the multilayer PML NBs are shown in (A), (B) and (C), (D), respectively. The PML NBs in (E), (F), and (G) have electron dense contents. The arrows indicate the purified PML NBs. The asterisks are the Dynabeads. The bars are 500 nm.

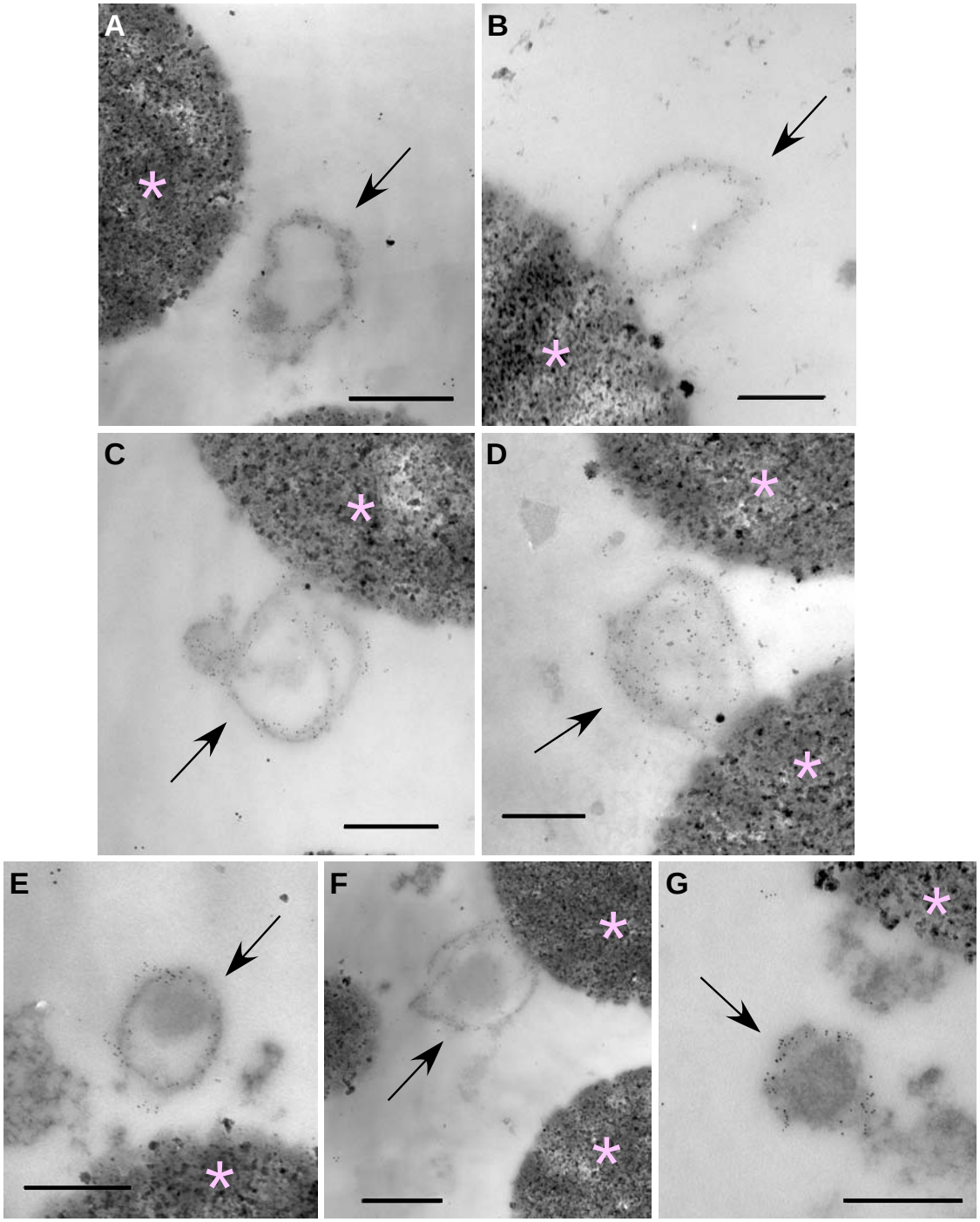
A
B
C
D
E
F
G

Table 1. Proteins identified by Mass Spectrometry and Protein Database Searching

	# of Peptides Identified in		
	wt mice	PML$^{-/-}$ mice	Gene ID
Potential PML NB components			
PML	44	0	18854
Thymopoietin	35	9	21917
Matrin3	25	1	17184
Torsin A interacting protein 1 (lamina-associated polypeptide 1B)	25	2	208263
Vimantin	24	0	22352
DEAD box polypeptide 5 (DEAD-box RNA helicase subunits)	23	2	13207
Similar to histone H2a, member O (H2aa3)	21	0	8337
Histone H2a, type3	20	0	
Histone H2B, type1h (H2bh)	18	0	319182
Nuclear mitotic apparatus protein 1 (Numa1)	18	1	101706
Similar to heat shock protein 8	15	7	621284
Pre-mRNA processing factor 40 homolog A (formin binding protein)	15	1	56194
DEAD box polypeptide 17 (DEAD-box RNA helicase subunits)	14	0	67040
Heterogeneous nuclear ribonucleoprotein D (hnRNP D)	14	0	11991
Nucleoporin 210	14	0	54563
Homeobox prospero-like protein 1	14	0	19130
Eukaryotic translation initiation factor 4A, isoform 3 (DEAD box polypeptide 48)	12	1	192170
Heterogeneous nuclear ribonucleoprotein H1 (hnRNP H1)	12	0	59013
Heterogeneous nuclear ribonucleoprotein K (hnRNP K)	12	1	15387
Nuclear receptor co-repressor 1 (N-CoR1)	12	0	20185
Poly(rC) binding protein 1 (hnRNP E1)	11	0	23983
Son cell proliferation protein	11	2	20658
Heterogeneous nuclear ribonucleoprotein F (hnRNP F)	10	1	98758
RuvB-like protein 1 (pontin 52)	10	0	56505
SWI/SNF-related matrix-associated actin-dependent regulator of chromatin c2	10	1	68094
Scaffold attachment factor B2	10	0	224902
RNA binding motif protein 25	9	0	67039
RAN GTPase activating protein 1 (RanGAP1)	9	0	19387
Similar to tubulin, alpha 2, isoform 2	8	2	668754
Splicing factor 3b, subunit 2	8	0	319322
Tubulin, alpha 1A	8	0	22142
Tubulin, alpha 4A	8	0	22145
YLP motif containing 1 (nuclear protein ZAP)	8	1	56531
Potential Contaminants			
Lamin A	59	51	16905
Nuclear pore complex-associated protein, Tpr	59	48	108989
Lamin B2	35	21	16907
Lamin B1	24	13	16906
Serine/arginine repetitive matrix 2	22	43	75956
Apoptotic chromatin condensation inducer 1	21	21	56215
Nucleoporin 153	20	44	218210
Pinin	15	25	18949
Keratin 10	11	12	16661
Thyroid hormone receptor associated protein 3	11	21	230753
Pre-mRNA 3'-end-processing factor (FIP1 like 1)	10	7	66899
Keratin 1	10	14	16678
BCL2-associated transcription factor 1	8	21	72567
Keratin 5	8	17	110308

Chapter 3: Dynamics of PML NBs during mitosis

I. The Establishment of Stable Cell Lines

In order to examine the dynamics of PML NBs during mitosis, I labeled PML NBs with fluorescently-tagged component proteins in live cells. The obvious marker protein candidate was the PML protein, the major structural component of PML NBs. PML has 7 major isoforms derived from alternative usage of 3' exons (for review see Jensen *et al.*, 2001). Each isoform contains a conserved amino-terminal region containing the RBCC motif, but with unique carboxyl-terminal tails (for review see Jensen *et al.*, 2001). Six of the seven isoforms are localized in the nucleus and present in all PML NBs, while isoform VII is cytoplasmic and has no nuclear localization signal (NLS). The specific functions of each isoform are still unclear. Previous studies have used PML isoform IV fused with GFP for live cell experiments by either transient or stable expression (Eskiw *et al.*, 2003; Dellaire *et al.*, 2006). However, overexpression of full length PML isoform IV has been shown to induce premature senescence in a p53 dependent manner (Fogal et al., 2000), thus the dynamic behavior of PML NBs may be affected by the isoform specific function of PML IV. In order to minimize the effect of ectopic expression of fluorescent-tagged PML protein, I fused isoform VI, which has a minimal C-terminus tail, with enhanced cyan fluorescent protein (ECFP) to generate a fusion protein.

In order to obtain stable double-transfected cell lines, I first generated a cell line, Cp89, which stably expresses a PML–ECFP fusion protein. The Cp89 cell line is derived from wild type (wt) U2OS cells and shows ECFP labeled PML NBs of comparable size and number to the PML NBs in the parental U2OS cell line. By using the Cp89 line, I further generated a double stable cell line, CpYs68, which expresses both PML-ECFP and EYFP-Sp100, in order to monitor the dynamic recruitment between PML NB component proteins. Whole cell extracts from both wt U2OS cells and CpYs68 cells were examined by immunoblotting (Fig. 18 A). As shown in Fig. 18A, several PML isoforms were expressed in both wt U2OS cells and CpYs68 cells (lane1 and lane 2). Sp100 has also been shown to have several splice variants as shown in lane 3 and lane 4 (Guldner et al., 1999). The arrowheads (lane2 and lane4) indicated that the ectopically expressed

PML-ECFP and EYFP-Sp100 are of the correct size and correspond to the fluorescent fusion protein (lane 5 and lane 6).

It has been reported that transient overexpression of Sp100 generates small Sp100 foci in the nucleoplasm, which contain no PML protein (Wiesmeijer *et al.*, 2002). Therefore, I examined the localization of the fusion proteins by immunofluorescence experiments. CpYs68 cells were fixed and labeled with mouse anti-PML and rabbit anti-Sp100 antibodies. As shown in Fig. 18B, both fusion proteins colocalized with the endogenous proteins. In addition, all of the Sp100 foci present in the nucleus, either visualized by EYFP signal or by antibody labeling, colocalized with PML protein. Therefore, the CpYs68 cell line contains PML NBs that are properly labeled by fluorescently-tagged PML and Sp100 proteins and are suitable for live cell studies.

II. Live Cell Imaging with 4D Tracking of PML NBs in Prophase

When cells enter mitosis, several dramatic structural rearrangements occur in the nucleus. Chromatin condensation and nuclear envelope breakdown (NEBD) are the two major events that occur during early prophase (for review see Margalit *et al.*, 2005; Belmont, 2006). At the same time, various nuclear compartments are reorganized into cytoplasmic structures or are disassembled into a diffuse pool of proteins (for review see Hernandez-Verdun et al., 2002). PML NBs also undergo compositional and structural changes at the initiation of mitosis (Everett *et al.*, 1999b; Dellaire *et al.*, 2006). However, without live cell imaging of high temporal and spatial resolution, the data from the previous studies failed to show the dynamic progression of events in detail during this period of time. Here, I first demonstrate three dimensional time lapse imaging of PML NBs from G2/ prophase transition to prometaphase.

i. Z-sweep acquisition of PML NB movements in prophase

I first checked the dynamics of PML NBs in prophase by using the Z-sweep acquisition (OAI^{TM}) function on the DeltaVision RT system. Images were taken every 5 seconds and a 4 μm Z-section projection with multicolor channels was collected at each time point. I stained the CpYs68 cells with a DNA dye, Hoechst 33342, to visualize early chromosome condensation as a mark for prophase entry. By precise identification of the cells that were at the appropriate phase, I can avoid excessive photodamage during image acquisition. In addition, cells can generally complete mitosis after intensive imaging in prophase. As shown in supplementary video 1, PML NBs exhibited highly dynamic movements when they progressed from prophase to prometaphase. The fast moving PML NBs moved within the interchromatin space and fused together to form aggregated MAPPs, in agreement with a previous study (Dellaire *et al.*, 2006). In addition, Sp100 still colocalized with PML protein in MAPPs when cells went into prometaphase and did not leave MAPPs until cells were in metaphase. Even though the OAI^{TM} function can allow fast acquisition of image stacks, a 4 μm Z-stack projection is insufficient to capture all of the PML NBs during prophase, given their highly dynamic movement and the dramatic morphological changes of the cells. Therefore, a larger Z-stack image collection is required to monitor the dynamics of all of the PML NBs in prophase.

ii. Comparison of PML NB tracking by PML-ECFP and EYFP-Sp100

In order to capture all of the PML NBs during prophase, a series of Z sections with 0.5μm steps expanding 8μm in Z axis was collected on the DeltaVision RT system. As shown in Fig. 19A, the high spatial resolution of Z-stack projection at selected time points included all of the PML NBs in the cells. The live cell movies were taken in CFP and YFP channels to visualize PML NBs that were labeled by both PML-ECFP and EYFP-Sp100 proteins. A single Z section reference image at the middle of the cell was also taken in the Hoechst channel to follow the progression of prophase by DNA staining. I clearly observed multiple fusion events that resulted in the formation of MAPPs and the reduction of PML NB number from 16 ± 5 bodies/ cell to 7 ± 5 bodies/cell, which is comparable to the previous study (Dellaire *et al.*, 2006).

The movement of nuclear bodies can be categorized into three types according to the coefficient of anomalous diffusion, α, as shown previously in the study of Cajal body dynamics (Platani et al., 2002). In order to determine the types of PML NB movements during prophase, the global movements of the cells were first corrected by using Hoechst reference channel to register the images by using the ImageJ TurboReg plugin. Then I tracked all of the PML NBs by using a 4-D image processing platform (TIKAL) (Gorisch *et al.*, 2004).

During prophase, PML NBs exhibited all three different types of movements: simple diffusion, constrained diffusion, and directed movement. As shown in Fig. 19A, PML NBs were manually assigned a number and checked by eye to correct the automatic tracking. Mean square displacement for each track was then calculated and fitted to the power law $MSD = 6D\Delta t^{\alpha}$ to obtain the value of α. Fitting graph examples of each movement type are shown in Fig. 19B. An overview of the trajectory of each PML NB in this 4D image data set is shown as ball-and-stick representations in Fig. 19C. The initial position of each PML NB is indicated by a green volume. The percentage of PML NBs that showed directed movement in a cell increased to 40% in prophase as compared to 10% in interphase. A high percentage of the PML NB population moved within the interchromatin space and notably, a subpopulation of fast moving PML NBs fused with each other to form MAPPs. As I tracked 16 ± 4 PML NBs per cell, the average percentage of PML NBs per cell to form MAPPs is 40% ± 30%. These data suggest that even though the frequency of MAPP formation through fusion may vary from cell to cell, the increase of PML NB dynamics is related to the formation

of MAPPs in prophase.

Using either CFP or YFP channels, the tracking of PML NBs by PML-ECFP or EYFP-Sp100 signals showed no difference (Fig. 20). Therefore, the following live cell movie data shown here were only taken in EYFP-Sp100 channel to avoid using the shorter wavelength fluorophore, ECFP.

iii. Different types of PML NB movement in prophase

During the tracking of PML NBs, I noticed that the MSD plot of many tracks exhibited a bi-phasic pattern. As shown in Fig. 19D, the PML NBs showed constrained movement during the first one-third of the plot but changed to directed movement by the end of the time points measured (green line). To further investigate this bi-phasic pattern and to determine whether it was indeed genuine and significant, I needed to visualize DNA in a higher spatial resolution in order to obtain better 3D registration. Since the Hoechst excitation wavelength is 405nm, close to ultraviolet light, intensive imaging using the Hoechst channel induces severe photodamage to the cells, which leads to incomplete mitosis. Therefore, I changed strategy by using transient transfection of a mCherry-H2A fusion protein into CpYs68 cells to visualize DNA. Since mCherry has longer maximum excitation wavelength at 587nm, I can collect, at each time point, a full Z stack as a DNA reference, instead of a single Z section image. 4D live cell movies taken in both YFP and mCherry channels started at early prophase and ended at late prometaphase with 8 second time intervals and 0.5 μm Z steps.

When tracking the PML NBs in this new series, two observations were made. First, when the PML NB displacement was plotted against time, several PML NB tracks showed a sudden increase in displacement near the same time point (Fig. 19E). This change in PML NB displacement seems to correlate with the phase transition between phases of the bi-phasic MSD plots observed earlier. Second, I noticed that when the full condensation of chromatin and the distortion of the nucleus occurred at later prophase, the diffused EYFP-Sp100 background signal also dissipated from the nucleus into the cytoplasm. The time point of diffuse EYFP-Sp100 release from the nucleus may indicate the time point of NEBD, which traditionally marks the transition from prophase to prometaphase. These observations may reflect the dramatic structural rearrangements in the cell upon mitotic entry. Therefore, in order to track PML NBs more accurately during the early stages of mitosis and also to correlate the dynamic changes of PML NBs to

major mitotic events, I decided to use the time point of Sp100 dissipation from the nucleus to divide our live cell movies in this series into two phases. Phase 1 begins from the time zero to the time I observed Sp100 dissipation. Phase 2 starts from the time of Sp100 dissipation to the end of the movies.

The intensity of mCherry-H2A was used to obtain the position of chromosomes and also the progress of prophase during the course of image. PML NBs labeled with EYFP-Sp100 were analyzed by TIKAL and their movements were then categorized by the equation of anomalous diffusion. The dynamic movements of PML NBs in 10 interphase cells and 20 prophase cells were tracked, and categorized into three different movement types: directed, diffusive, and constrained. The percentages, which are summarized in Fig. 21, represents the PML NB population in each movement type in each cell. In the interphase cells, about 10% of the PML NBs exhibited directed movement, which is in agreement with a previous study (Muratani *et al.*, 2002). In phase 1 and phase 2 of prophase, the percentage increased to 18% and 30% respectively. The population of PML NBs exhibiting diffusive motion remained constant at approximately 60% during both interphase and prophase. Interestingly, during phase 2, the percentage of PML NBs showing directed movement increased from 18% to 30%, while the population of PML NBs showing constrained movement decreased from 20% to 10%. Moreover, when I compared every MSD plot from both phases, I found that some PML NBs did change their movement types between phase 1 and phase 2. However, not all of the PML NBs that ceased their constrained movement in phase 1 shifted to directed movement in phase 2. Some of the PML NBs shifted their movement types from constrained motion to diffusive motion as well. Therefore, the increase of directed PML NBs in phase 2 was contributed to by both the diffusive and constrained population of PML NBs in phase 1.

However, the global increase of directed PML NBs and the global decrease of constrained PML NBs during the phase transition may be caused by two possibilities. First, chromosome condensation is mostly complete in phase 2 creating additional interchromatin space. This may allow constrained PML NBs to simply increase their movement when their confinement by chromatin is reduced. The second possibility is that material exchange between the nucleoplasm and the cytoplasm during NEBD may generate a physical flow that may force PML NBs to move passively. Experiments in the next two sections were designed to distinguish between these two possibilities.

iv. Dynamics of PML NBs upon induction of premature chromosome condensation

First, I wanted to determine if the increase of interchromatin space can also increase dynamic movement of PML NBs. Premature chromosome condensation (PCC) was first accurately described by Johnson and Rao in 1970 and can be induced by several methods (Johnson and Rao, 1970). PCC was used for the preparation of chromosome spreads that are independent of cell cycle stage, and have minimal culturing artifacts. Traditionally, PCC is induced by fusing test cells with mitotic cells in the presence of either virus or chemical fusing agent (Johnson and Rao, 1970; Pantelias and Maillie, 1983). However, cell fusion is too laborious and technically difficult to be routine. Therefore, alternative methods have been developed by using chemical inhibitors of type 1 and type 2A protein phosphatases (PP1 and PP2A), such as calyculin A (CA) and okadaic acid (OA) (Asakawa and Gotoh, 1997). CA and OA treatments have been shown to efficiently induce PCC, usually within an hour of treatment, in over 20% of the cells tested (Durante *et al.*, 1998). Therefore, I decided to use CA to induce PCC in the CpYs68 double stable cell line in order to determine if PCC affects the dynamics of PML NBs.

CpYS68 cells were transiently transfected with mCherry-H2A for chromatin visualization. Cells were imaged 30 min after 40 nM CA treatment. 4D live cell image stacks with 0.5 μm steps were collected in mCherry and CFP channels every 10 sec for 8 min. As indicated by arrowheads shown in Fig. 22, PML NBs did not change their relative position, and PML NBs displayed limited movement when chromosome condensation was already visible. It is clear that the dynamic behavior of PML NBs in CA treated cells is dramatically different from that in normal prophase cells. After CA treatment, PML NBs exhibited close association with the chromatin, and their limited movement was concurrent with the movement of condensed chromatin. In addition, few PML NB fusion events were observed during the course of imaging. This indicates that upon the induction of PCC by CA, PML NBs do not move within the increased interchromatin space.

v. Dynamics of PML NBs upon nuclear envelope breakdown

Another possible explanation for the increase of directed PML NB movements during the second phase is the physical flow between the

nucleoplasm and the cytoplasm. It occurs upon nuclear envelope breakdown (NEBD) and may be the driving force of PML NB movements in phase 2. As previously mentioned, the time of Sp100 dissipation from the nuclei may correspond to the time of NEBD. This time point was therefore used to roughly divide the prophase movies into two phases in order to achieve a better fit of the mean square displacement plots. Here, I more precisely determined the timing of NEBD and its temporal relationship with the increase of PML NB dynamics.

I used a construct containing the importin-β binding domain (IBB) of importin α fused with 2 copies of HcRed. This IBB fusion protein is actively imported into the nucleus as long as a functional nuclear envelope is maintained. The IBB-HcRed signal is restricted within the nucleus during interphase, but appeared in the cytoplasm during the transition from prophase to prometaphase, marking the initiation of NEBD (Leung *et al.*, 2004). I therefore generated a triple stable cell line, CpYsRi89, stably expressing PML-ECFP, EYFP-Sp100, and IBB-HcRed for the 4D live cell analysis. The cells at G2/prophase transition were identified by the partially condensed chromatin, as visualized by Hoechst DNA staining. As shown in the still images in Fig. 23, the IBB-HcRed signal was restricted within nucleus even when chromosome condensation was near completion. The timing of IBB-HcRed release from the nucleus coincided with the timing of Sp100 dissipation. Surprisingly, even before IBB-HcRed signal appeared in the cytoplasm, the long distance displacements (green arrowheads) and the fusion of PML NBs (red arrowheads) have already occurred. The data suggest that the increase of PML NB dynamics was triggered in late prophase (phase 1) prior to NEBD.

vi. A window of increased PML NB dynamics during prophase

The global increase of PML NB dynamics during phase 1 of prophase may be triggered by other mitotic events prior to NEBD. It has been shown that the cyclin B1/ cyclin dependent kinase 1 (Cdk1) complex commits the cell to mitosis and promotes metaphase progression by phosphorylating a variety of substrates, including nuclear lamins and condensins (for review see Marcello *et al.*, 2003). Cyclin B1 forms an active complex with Cdk1 in the cytoplasm and is later translocated from the cytoplasm into the nucleus during late prophase (Jackman *et al.*, 2003). Therefore, I investigated whether the translocation of cyclinB1 correlated with the increase of PML NB dynamics. I generated a new double

stable cell line, CpYcb165, stably expressing PML-ECFP and EYFP-cyclin B1 based on the master line, Cp89. Transient transfection of mCherry-H2A allowed us to visualize DNA and to identify early prophase cells. 4D live cell images were collected in both CFP and YFP channels to visualize PML NBs and cyclin B1. A Z-stack of 0.5 μm steps expanding to 8 μm was collected every 8 seconds over 30 minutes. The reference image of one mCherry channel Z section in the middle of the cell allowed us to follow the progression of prophase at each time point.

As shown in Fig. 24, YFP panel, when cells were in G2/prophase transition, cyclin B1 was mainly diffuse throughout the cytoplasm and was excluded from the nucleus. It was also concentrated at the duplicated centrosomes as reported in a previous study (Jackman *et al.*, 2003). In addition, when the two EYFP-cyclin B1 labeled centrosomes separated to the opposite poles of the nucleus, marking the end of G2 phase, the cell usually enters mitosis within 30 minutes despite no apparent chromatin condensation at the time of observation. Chromatin condensation is initiated by other protein kinases at the initiation of mitosis, possibly by cyclin A/ Cdk1 (Hagting *et al.*, 1999). Indeed, I first observed partially condensed chromatin in the mCherry channel approximately 10 minutes prior to the rapid entry of EYFP-cyclin B1 into the nucleus. By the time of cyclin B1 nuclear entry in late prophase, chromosome condensation has mostly completed, and nuclear envelope breakdown was visualized, within 6 minutes, by release of cyclin B1 from the nucleus through out the mitotic cell. These observations indicated that the EYFP-cyclin B1 fusion protein in the stable cell line retained its function *in vivo* as described in the previous study (Hagting *et al.*, 1999).

The cells that are in G2/prophase transition can be precisely identified by the observation of partially condensed chromatin and separated centrosomes, provided that the centrosomes are labeled by EYFP-cyclin B1 and DNA is labeled by mCherry-H2A. During this time, as shown in Fig. 24, CFP panels, PML NBs did not significantly change their relative positions at the beginning of the prophase (Fig. 24, the arrowheads, T = 0 min to T = 10 min). Only when cyclin B1 was translocated into the nucleus were long range displacements of PML NBs and PML NB fusion resulting in MAPPs formation observed (Fig. 24, the white and red arrowhead, respectively, T = 15 min to T = 30 min). The NEBD, as indicated by dissipation of cyclin B1 from the nucleus to the cytoplasm, occurred near the 30 min time point. Taken with the previous results, these data indicate that the increase of PML NB dynamics and the formation of MAPPs occur during a window between cyclin B1 nuclear entry and NEBD.

III. Newly Assembled PML NBs in Early G1 Cells

From prometaphase to metaphase, PML NB components, such as Sp100 and Daxx, leave newly formed MAPPs and diffuse into the mitotic cytoplasm. The reformation of interphase PML NBs occurs in early G1. Previous studies suggested that MAPPs may contribute to PML NB reformation in G1 phase since no new PML protein is synthesized during mitosis (Dellaire *et al.*, 2006). The PML protein accumulation in MAPPs may be recycled back to the nucleus to form PML NBs in daughter nuclei. Fixed cell studies also suggested that the recruitment of Sp100 and Daxx began in early G1, and that the percentage of PML NBs associated with Sp100 at this stage was higher than that with Daxx, suggesting that Daxx accumulation in the newly formed PML NBs occurred later than Sp100 recruitment (Dellaire *et al.*, 2006). However, higher temporal resolution studies using live cells are still needed to determine how reassembly occurs in daughter nuclei.

The double stable cell line, CpYs68, expressing both PML-ECFP and EYFP-Sp100 was used to examine the reassembly of PML NBs upon exit from mitosis. 4D live cell images were collected from anaphase through early G1 phase with 1 μm steps of 20 μm Z-stack every 1 minute for 3 hours. The cells were also transiently transfected with the HcRed-IBB construct to monitor the functional nuclear envelope reformation in daughter nuclei. As shown in Fig. 25A, the functional daughter nuclear envelope was reformed around 7 min after the beginning of imaging. Few MAPPs were trapped within the newly formed nuclei, while Sp100 protein was still diffused throughout the daughter cells. The first indication of Sp100 protein recruitment into the nucleus was observed at the18.5 min time point. However, the recruitment of Sp100 into the PML NBs (blue arrowheads in Fig. 26) occurred much later than the recruitment of Sp100 protein into the nucleus.

Next, I transiently transfected EYFP-Daxx and IBB-HcRed in the Cp89 cell line, which stably expresses ECFP-PML, in order to monitor the recruitment of Daxx during early G1 phase. 4D live cell imaging began at telophase and proceeded through early G1 phase with 1 μm steps of 20 μm Z-stack every 1.5 minute for 5 hours. At the beginning of the movie, as shown in Fig. 25B, the IBB-HcRed signal was already detectable in daughter nuclei indicating the reformation of a functional nuclear envelope. However, the recruitment of Daxx into the daughter nuclei did not occur until much later. The first time point at which

Daxx protein could be detected in newly formed PML NBs was 57 min after the start of imaging. However, it was not until the cells were well into G1 phase that the normal interphase localization of Daxx was re-established.

The time point of Daxx nuclear recruitment, relative to the reformation of a functional nuclear envelope, is much later than that of Sp100. However, even after Sp100 and Daxx proteins were both present in the daughter nuclei, additional time was required to complete the recruitment into newly formed PML NBs, as shown by the still images with higher temporal resolution in Fig. 27. The delay between nuclear entry and recruitment of PML NB component proteins to the PML NBs suggests that additional modifications may be needed before the recruitment of PML NB component proteins can occur. Even though I did not compare the recruitment of Sp100 and Daxx proteins in the same cell, the delayed nuclear entry of Daxx protein after the reformation of a functional nuclear envelope suggests a sequential recruitment of PML NB component proteins into early G1 PML NBs, in agreement with the previous fixed cell studies (Dellaire *et al.*, 2006).

Figure 18: Characterization of double stable cell line

(A) U2OS cells were stably transfected with PML-ECFP and EYFP-Sp100. Whole cell extracts from both parental U2OS cells (wt) and double stable cells (CpYs68) were analyzed by immunoblot. Rabbit polyclonal antibody against PML (A gift from Dr. Paul Freemont) shows several PML isoforms in both wt cells and double stable cells. Rabbit anti-Sp100 antibody (A gift from Dr. Gerd G. Maul) also shows several Sp100 isoforms. The arrowheads indicate the bands representing PML-ECFP and EYFP-Sp100 fusion proteins.
(B)Fixed double stable cells were labeled with mouse anti-PML antibody (PG-M3, Santa Cruz Biotech.) and rabbit anti-Sp100 antibody (rSpGH, a gift from Dr. Hans Will). The projected 3D Z-stacks, collected using a DeltaVision RT microscope, show the colocalization of PML-ECFP and EYFP-Sp100 fusion proteins with endogenous PML and Sp100 proteins, respectively. The bar is 10 μm.

A

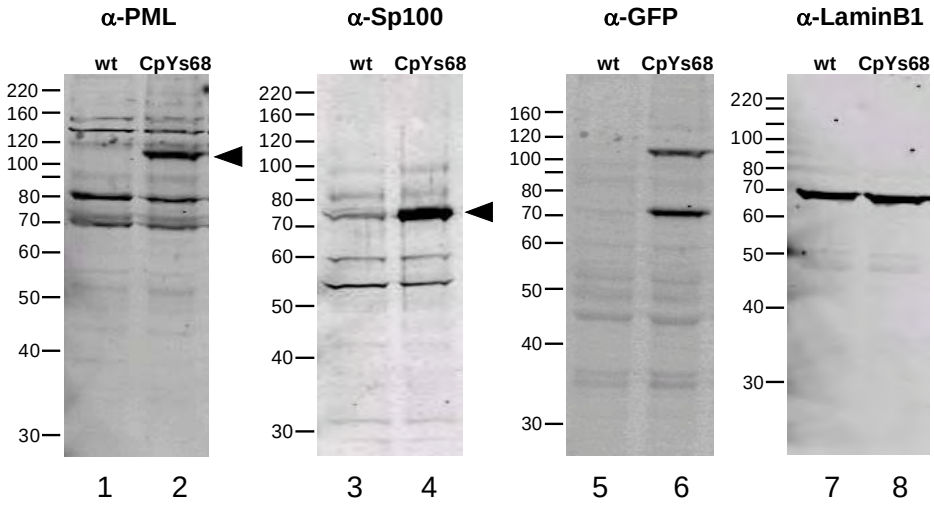
α-PML
α-Sp100
α-GFP
α-LaminB1
wt
CpYs68
220
160
120
100
80
70
60
50
40
30
1
2
3
4
5
6
7
8

B

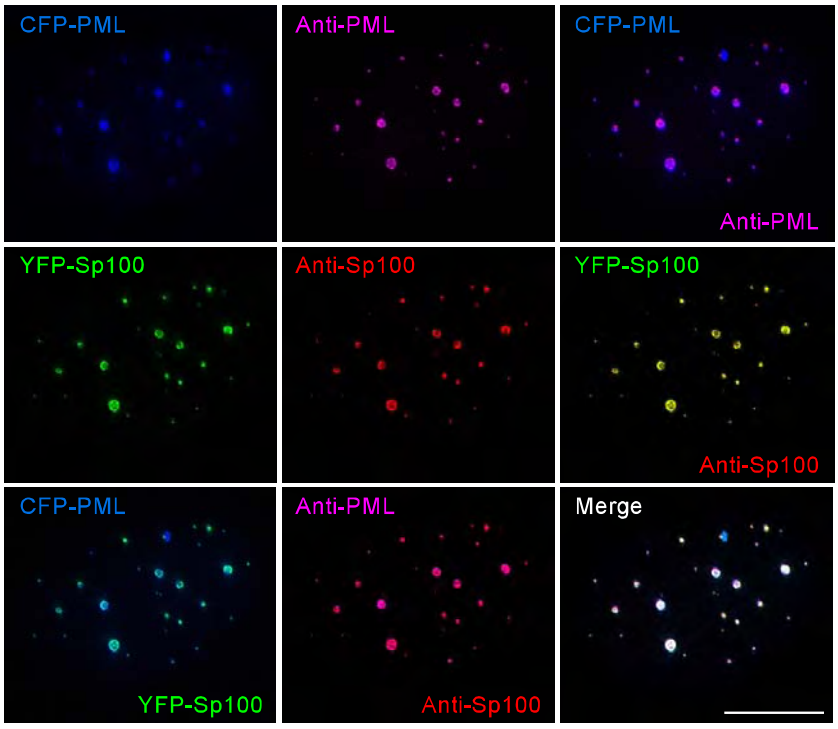
CFP-PML
Anti-PML
CFP-PML
Anti-PML
YFP-Sp100
Anti-Sp100
YFP-Sp100
Anti-Sp100
CFP-PML
YFP-Sp100
Anti-PML
Anti-Sp100
Merge

Figure 19: 4D tracking of PML NBs from prophase to prometaphase in living cells

(A) Double stable cells, CpYs68, stably expressing PML-ECFP and EYFP-Sp100. Chromatin was visualized by Hoechst 33342 staining. A 7μm Z-stack of 0.5 μm steps were collected in the CFP and YFP channels every 8 sec for 26 min. One Z section at the middle of the cell was collected in the Hoechst channel, at each time point, as the reference image for DNA. The 3D projected still images of selected time points are shown here. Each PML NB was manually assigned a number and tracked by TIKAL 4D viewer in order to determine their displacement. The examples of PML NBs with different motions are indicated by colored arrowheads. The red arrowhead, directed motion. White arrowhead, diffusive motion. Blue arrowhead, constrained motion. Red, pseudocolored PML-ECFP. Green, EYFP-Sp100. Blue, DNA stained by Hoechst 33342. The bar is 10 μm. See also supplementary video 2.
(B) The trajectories of bodies were exported into MATLAB in order to calculate the mean square displacement (MSD), which is plotted in the Y-axis against Δt in the X-axis. The MSD is fitted to the power law $MSD = 6D\Delta t^{\alpha}$ with α as the coefficient of anomalous diffusion. A non-linear relationship between the MSD and Δt indicates non-standard diffusion. Classification into movement types is performed according to $\alpha \sim 1.5$ for directed movement, $\alpha \sim 1$ for simple diffusion, and $\alpha \sim 0.5$ for constrained diffusion. The representative MSD plot of each movement type is displayed here with the actual data (blue circles) and the fitted curve (red line).
(C) Overview of the trajectory of each PML NB in this 4D image data set is summarized by ball-and-stick representations to show the displacement of each body. The initial position of each PML NB is indicated by a green volume.
(D) An example of a MSD plot, showing a bi-phasic curve. The green line shows the real data and the blue line shows the fitted curve.
(E) An example of displacement plot includes all the tracks in a cell. Each track is plotted using different color lines, and the black circles indicate the average displacement of all tracks at each time point.

A

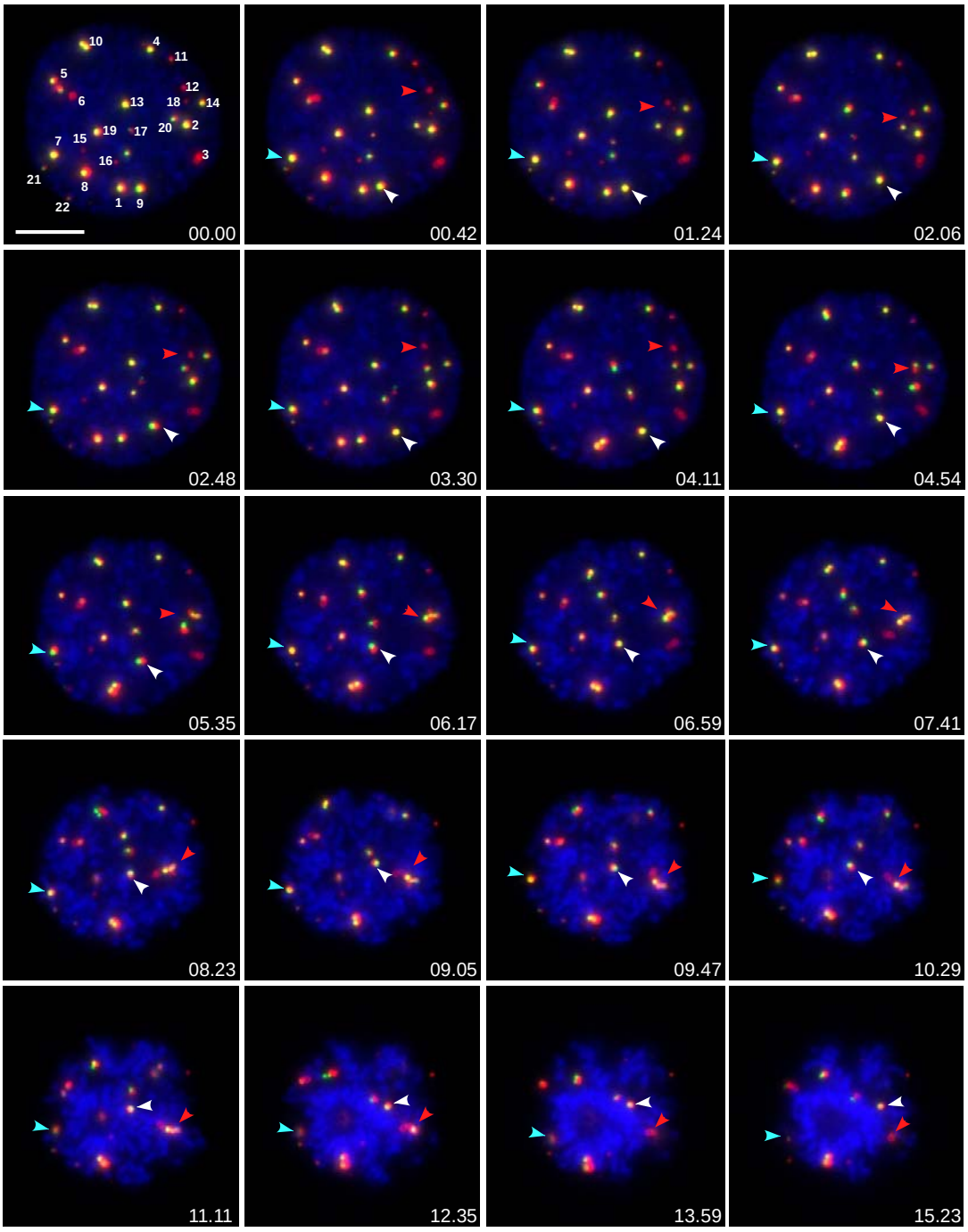
10
4
11
5
12
6
13
18
14
19
17
20
2
7
15
16
3
21
8
1
9
22
00.00
00.42
01.24
02.06
02.48
03.30
04.11
04.54
05.35
06.17
06.59
07.41
08.23
09.05
09.47
10.29
11.11
12.35
13.59
15.23

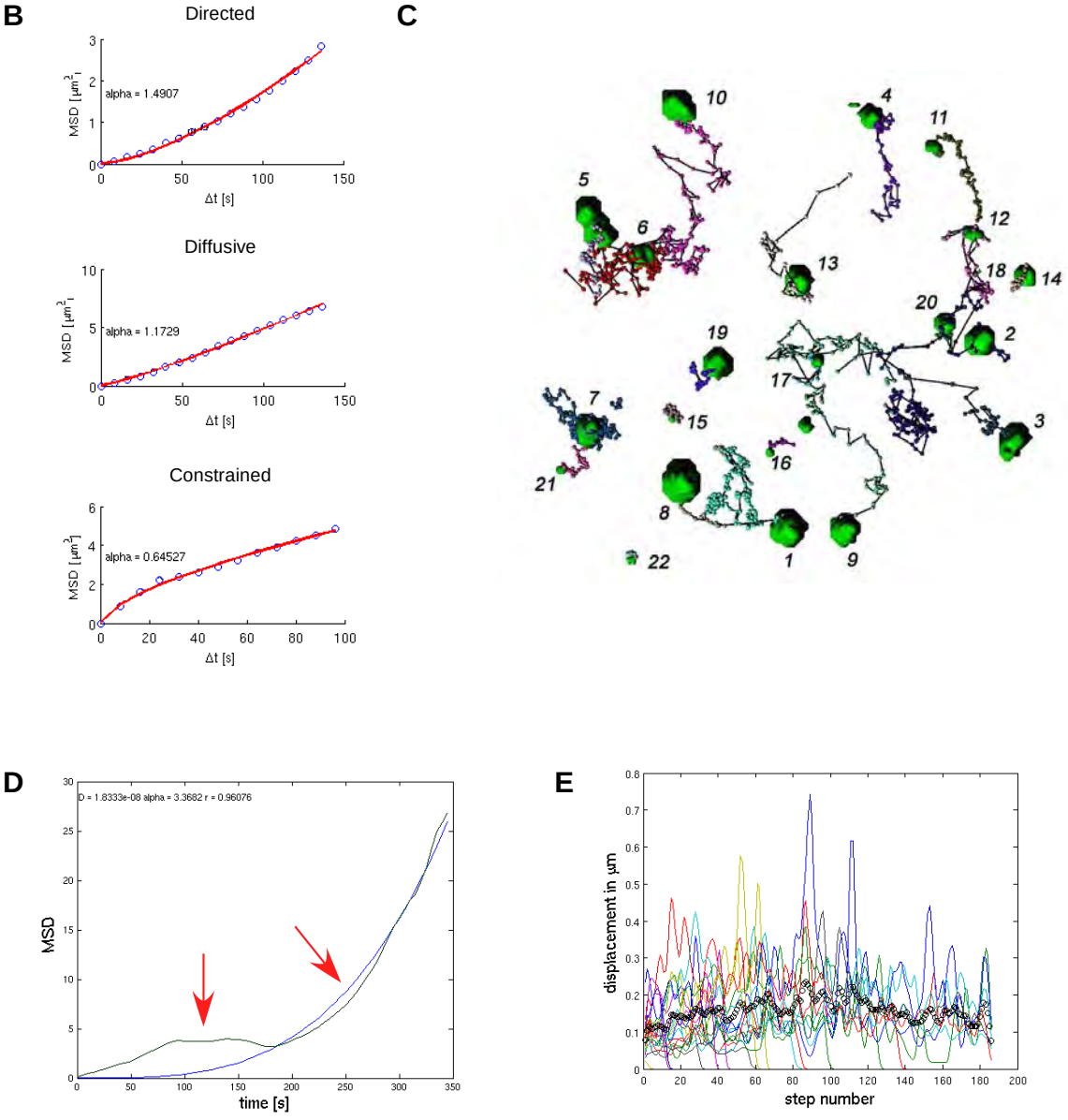
B
Directed
alpha = 1.4907
MSD [μm²]
Δt [s]
Diffusive
alpha = 1.1729
MSD [μm²]
Δt [s]
Constrained
alpha = 0.64527
MSD [μm²]
Δt [s]
C
10
4
11
5
6
12
13
18
14
20
2
19
17
7
15
3
16
21
8
22
1
9
D
D = 1.8333e-08 alpha = 3.3682 r = 0.96076
MSD
time [s]
E
displacement in μm
step number

Figure 20: Summary of PML NB movement types from PML-ECFP tracks and EYFP-Sp100 tracks

The box plot summarizes the distribution of the PML NB population in a cell that exhibiting particular movement types during prophase. The y-axis indicates the percentage of PML NB population and x-axis indicates the data from two different sets of cells (PML set: N =12 and Sp100 set: N = 20). The PML NBs in set 1 were tracked by ECFP signal, while set 2 is by EYFP. The red line indicates the median of the data set. The box indicates 50% of the data points. The notch of the box indicates the significance of the difference of the mean values in the two data sets. If the notch area overlaps between the two sets, the mean values of the two sets are not significantly different. If there is no overlap, the difference is significant with 95% of confidence. (A) Directed movement. (B) Diffusive movement. (C) Constrained movement. Although there is a low level of cell to cell variation between datasets, the global distribution of each movement type is similar.

A

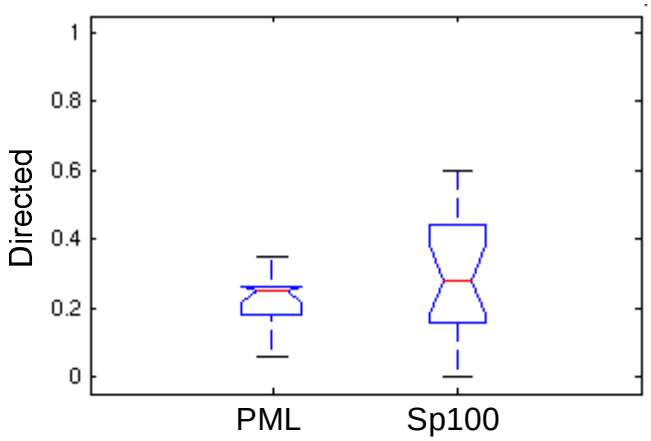
Directed
1
0.8
0.6
0.4
0.2
0
PML
Sp100

B

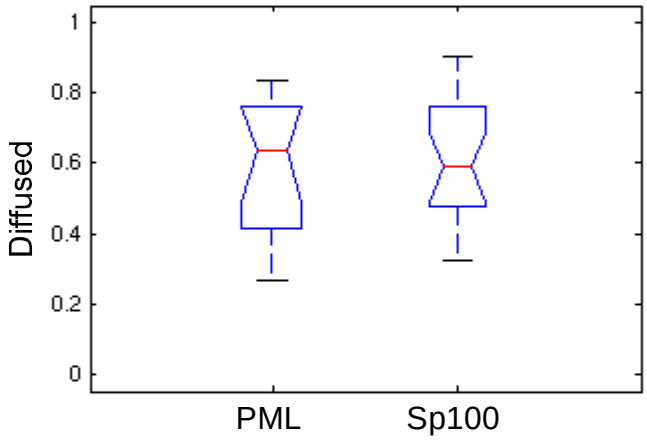
Diffused
1
0.8
0.6
0.4
0.2
0
PML
Sp100

C

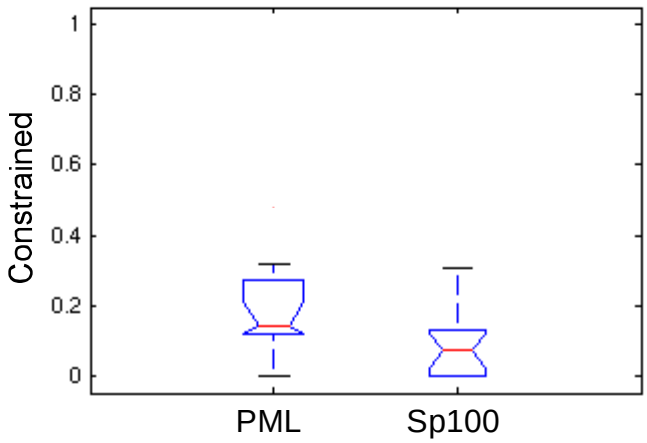
Constrained
1
0.8
0.6
0.4
0.2
0
PML
Sp100

Figure 21: Summary of PML NB movement types in interphase and prophase

The box plots summarize the movement types of PML NBs from both interphase cells (N = 10) and prophase cells (N = 20). The y-axis indicates the percentage of PML NB population that exhibits certain movement types and x-axis indicates the data from different phases, notably the two phases in the prophase data sets. The red line indicates the median of the data set. The box indicates 50% of the data points. The notch of the box indicates the significance of the difference of the mean values in the two data sets. If the notch area overlaps between the two sets, the mean values of the two sets are not significantly different. If there is no overlap, the difference is significant with 95% of confidence. (A) Directed movement. The median of directed movement increased from 10% in interphase to 18% in phase 1 of prophase and again to 30% in phase 2 of prophase. (B) Diffusive movement. The percentage of the PML NB population exhibiting diffusive movement is maintained at about 60% throughout the three phases. (C) Constrained movement. In contrast to directed movement, the median of constrained movement decreased from 30% in interphase to 20% in phase 1 of prophase and to 10% in phase 2 of prophase.

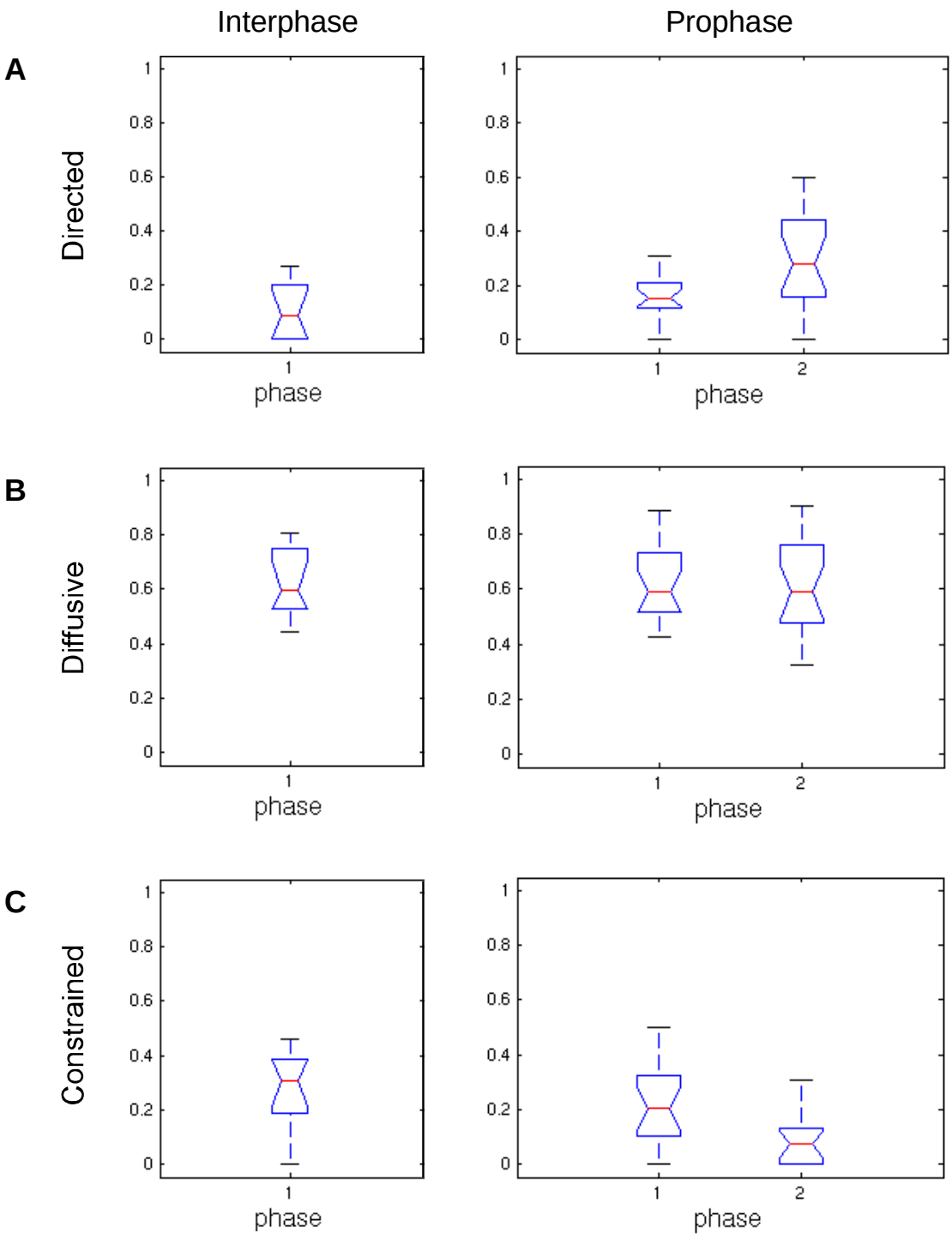
Interphase
Prophase
A
Directed
B
Diffusive
C
Constrained
0
0.2
0.4
0.6
0.8
1
1
2
phase

Figure 22: PML NB dynamics upon calyculin A induced premature chromosome condensation

A double stable cell line, CpYs68, was transiently transfected with mCherry-H2A construct. Cells (N = 10) were then treated with 40 μM Calyculin A for 30 min to induce premature chromatin condensation before 4D live cell imaging by the DeltaVision RT microscope. A 24 um Z-stack of 1.5 um steps was taken in the CFP and mCherry channels every 10 sec for 33 min. The 3D projected still images from selected time points are shown here. Condensed chromosomes can be visualized by the mCherry-H2A fluorescent signal (pseudocolored in green). PML NBs (pseudocolored in red, the white arrowheads) do not exhibit dynamic movement within the increased interchromatin space. The bar is 10 μm. See also supplementary video 3.

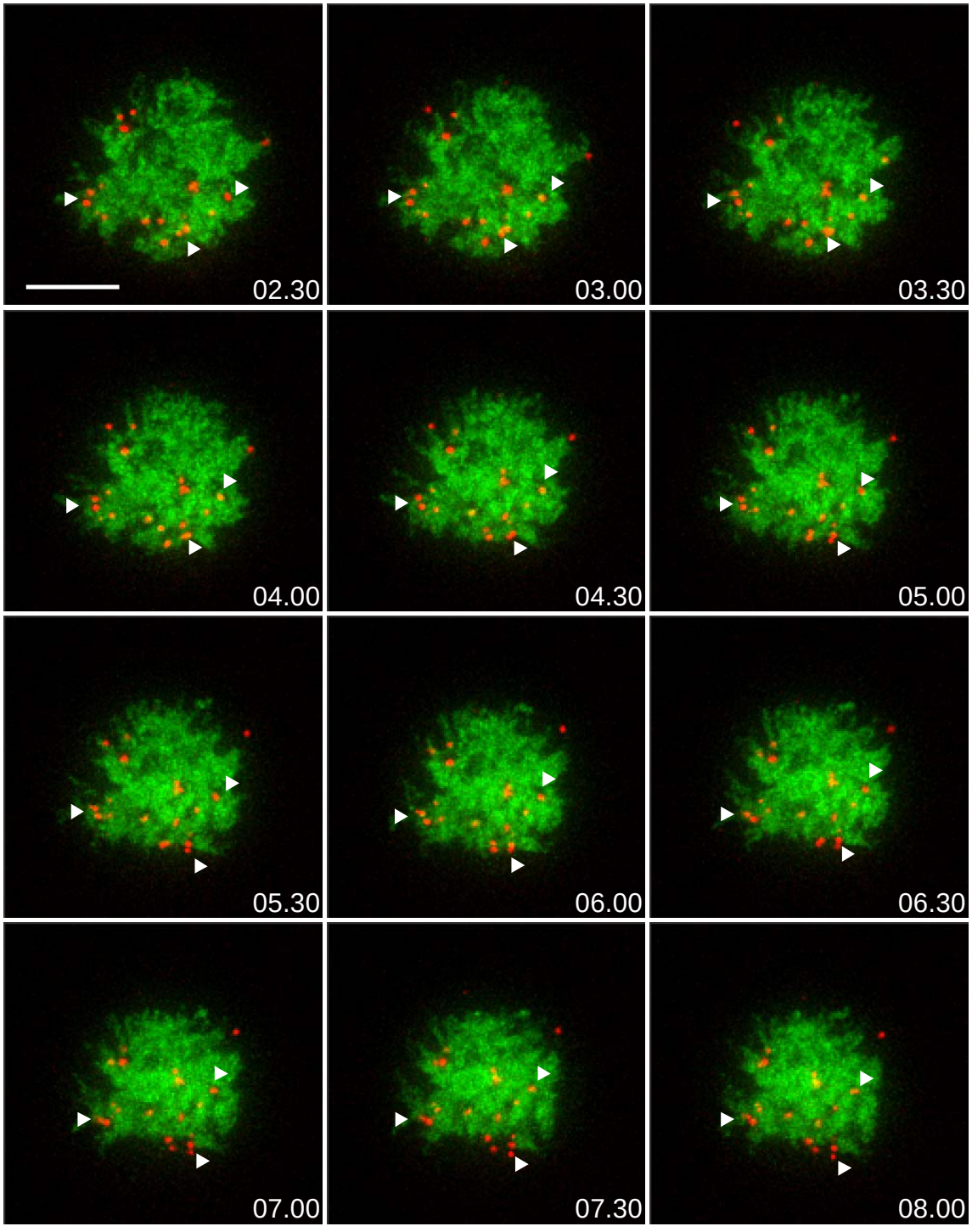
02.30
03.00
03.30
04.00
04.30
05.00
05.30
06.00
06.30
07.00
07.30
08.00

Figure 23: PML NBs dynamics upon nuclear membrane breakdown

Double stable cell line, CpYs68, was transiently transfected with the importin-β binding domain (IBB) of importin α fused to HcRed (IBB-HcRed). An 8 μm Z-stack of 0.6 μm steps is collected every 8 sec for 20 min in the YFP and the mCherry channels. A single Z section at the middle of the cell was taken every time point in the Hoechst channel as the reference image for DNA. Nuclear membrane breakdown was visualized by the release of the HcRed signal from the nucleus into the cytoplasm. The 3D projected images show that PML NBs are highly dynamic even before nuclear membrane breakdown. White arrowheads, PML NBs with long distance displacement. Red arrowheads, the fusion of PML NBs. The bar is 10 μm. See also supplementary video 4.

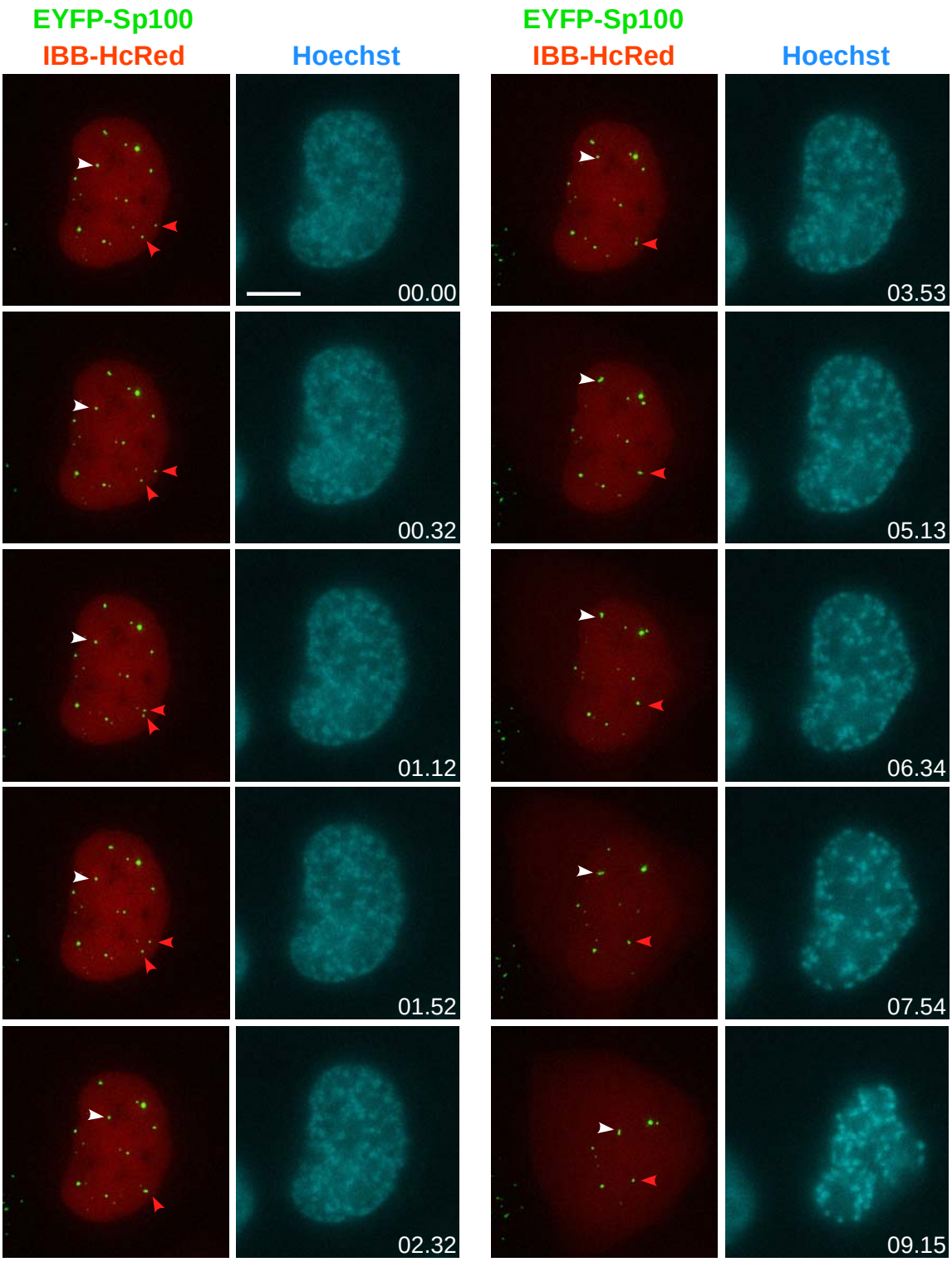
EYFP-Sp100
IBB-HcRed
Hoechst
EYFP-Sp100
IBB-HcRed
Hoechst
00.00
00.32
01.12
01.52
02.32
03.53
05.13
06.34
07.54
09.15

Figure 24: PML NBs dynamics upon nuclear entry of cyclin B1

Double stable cell line, CpYcb165, stably expresses PML-ECFP and EYFP-cyclin B1. Cells were transiently transfected with mCherry-H2A construct. An 11 μm Z-stack of 1 μm steps was collected every 15 sec for 35 min in CFP and YFP channels. The 3D projected images show that PML NBs exhibited limited movement before cyclin B1 entered the nucleus. After the nuclear entry of cyclin B1, PML NBs became dynamic, and long distance displacement and fusion of PML NBs were observed. White arrowheads, PML NBs with long distance displacement. Red arrowheads, the fusion of PML NBs. The bar is 10 μm. See also supplementary video 5.

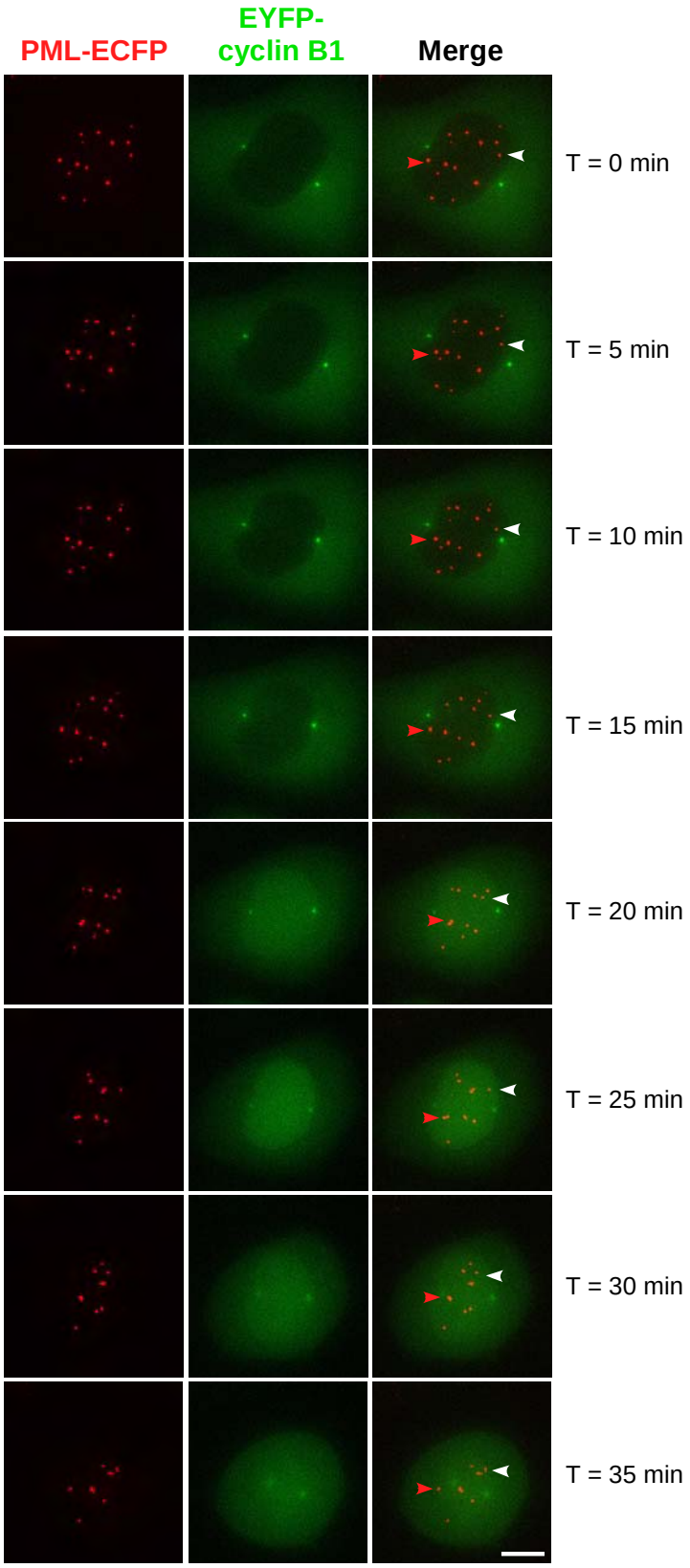
PML-ECFP
EYFP-cyclin B1
Merge
T = 0 min
T = 5 min
T = 10 min
T = 15 min
T = 20 min
T = 25 min
T = 30 min
T = 35 min

Figure 25: The formation of PML NBs in G1 cells upon the establishment of a functional nuclear envelope

(A) Double stable cell line, CpYs68, expressing PML-ECFP (blue) and EYFP-Sp100 (green) was transiently transfected with IBB-HcRed (red). A 21 μm Z-stack of 1.5 μm steps was taken every 30 sec for 75 min in 3 channels. The establishment of a functional nuclear membrane can be visualized by the import of the HcRed signal from the cytoplasm into the nucleus. The 3D projected images show that the entry of Sp100 protein into the daughter nuclei occurs after the establishment of a functional nuclear envelope. The recruitment of Sp100 into the PML NBs occurs much later than the recruitment of Sp100 protein in the nucleus (white arrowheads). See also supplementary video 6.
(B) Single stable cell line, Cp89, expressing PML-ECFP (blue) was transiently transfected with EYFP-Daxx (green) and IBB-HcRed (red). A 21.5 μm Z-stack of 1.5 μm steps was taken every 3min for 100 min in 3 channels. The establishment of a functional nuclear membrane can be visualized by the import of the HcRed signal from the cytoplasm into the nucleus. The 3D projected images show a long delay of Daxx nuclear entry after the establishment of a functional nuclear envelope. The normal interphase localization of Daxx was re-established much later, well into G1 phase (white arrowhead). See also supplementary video 7.

A

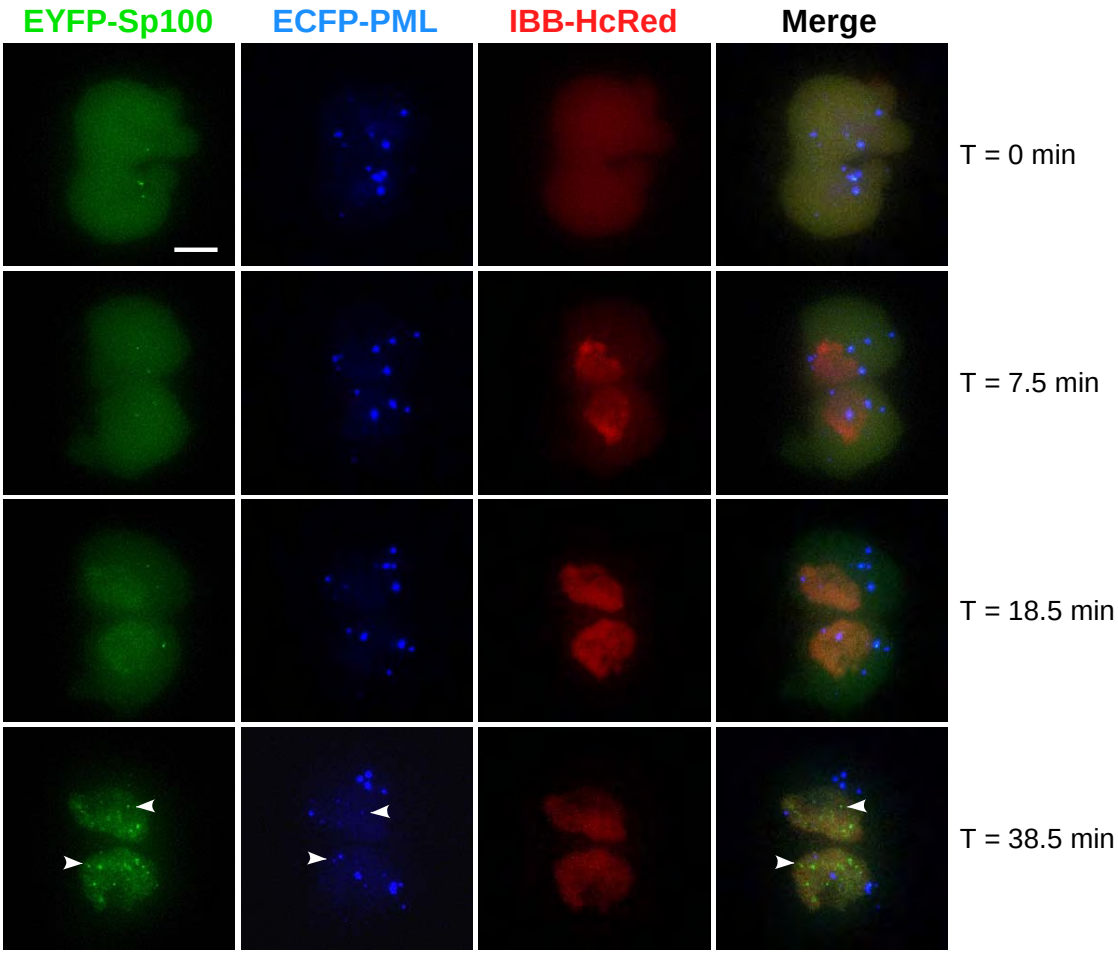
EYFP-Sp100
ECFP-PML
IBB-HcRed
Merge
T = 0 min
T = 7.5 min
T = 18.5 min
T = 38.5 min

B

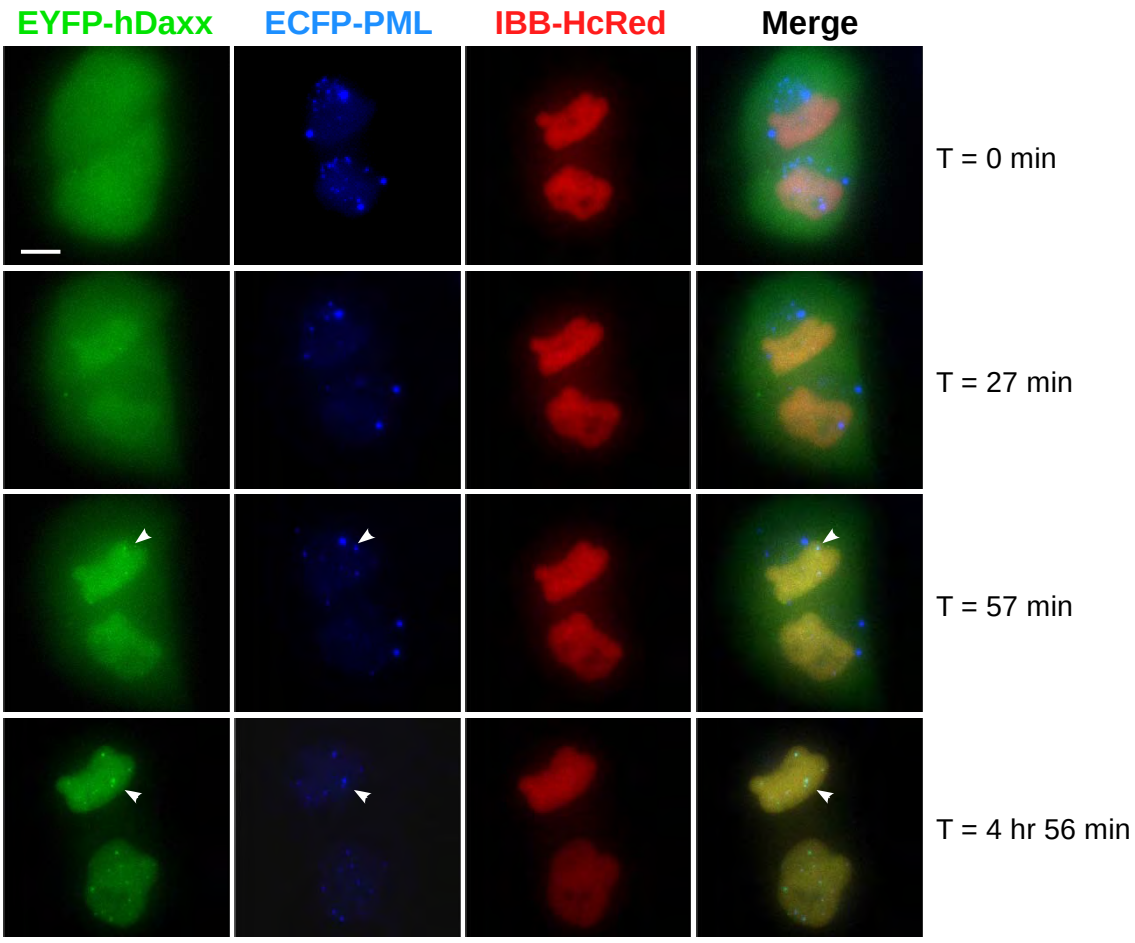
EYFP-hDaxx
ECFP-PML
IBB-HcRed
Merge
T = 0 min
T = 27 min
T = 57 min
T = 4 hr 56 min

Figure 26: Visualization of PML NB formation in G1 cells with high temporal resolution

(A) Double stable cell line, CpYs68, stably expresses PML-ECFP (red) and EYFP-Sp100 (green). A 23 μm Z-stack of 1.5 μm steps was taken every 1 min for 200 min in 2 channels. Selected 3D-projected images show that Sp100 protein (green) enters daughter nuclei prior to PML protein (red). However, the recruitment of Sp100 to PML NBs (yellow) occurs only after PML NBs reform (white arrowhead). See also supplementary video 8.
(B) Single stable cell line, Cp89, expressing PML-ECFP (red) was transiently transfected with EYFP-Daxx (green). A 21.5 μm Z-stack images of 1.5 μm steps was taken every 3 min for 100 min in 2 channels. Selected 3D-projected images show that Daxx protein enters daughter nuclei first before its recruitment into newly formed PML NBs (white arrowhead). See also supplementary video 9.

A

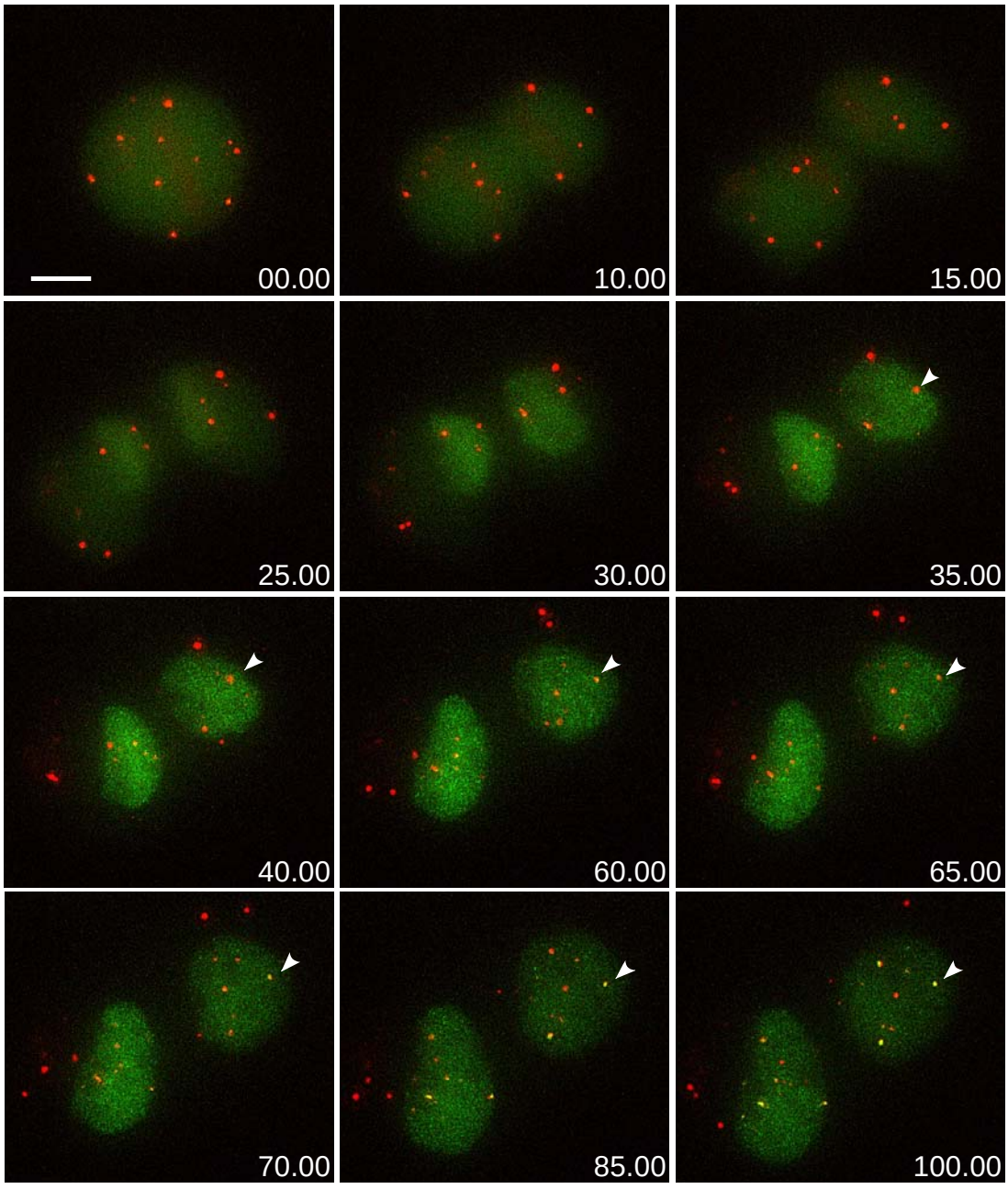

B

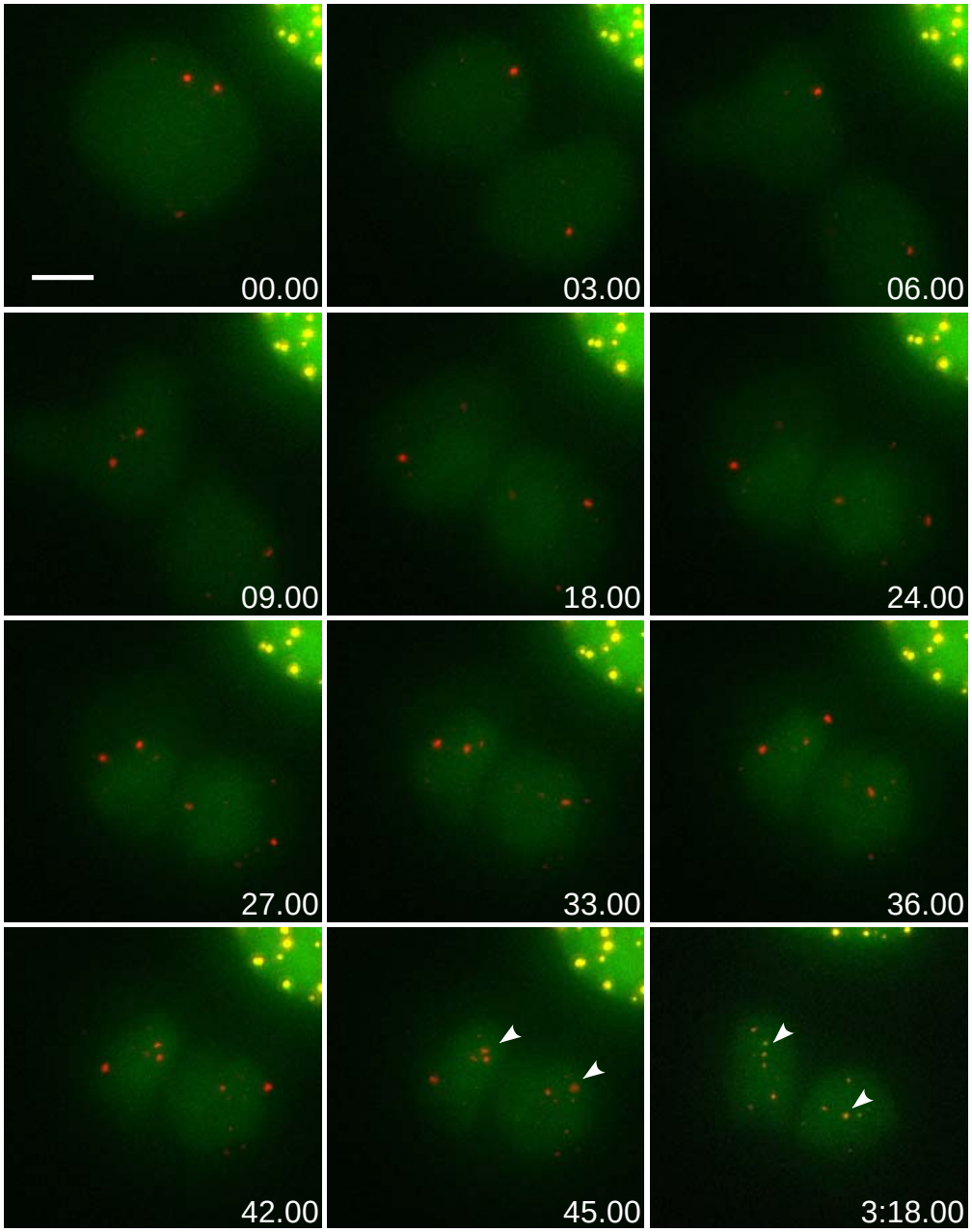

Chapter 4: Conclusions and Discussion

I. Function(s) of PML NBs

Since their first description made by de Thé in 1960 (de *et al.*, 1960), PML NBs have been studied extensively. Amazingly, in only 15 years, our understanding of these nuclear domains has expanded from a mere morphological description to a detailed molecular and mechanistic elaboration. One of the major reasons why PML NBs have drawn so much attention over the past two decades is due to their apparent association with the onset and progression of human diseases, particularly acute promyelocytic leukemia and viral infections (for review see Everett, 2001; Pandolfi, 2001). Additionally, more than 50 proteins have thus far been identified as associated with PML NBs, a number which is still growing. Many of these proteins are involved in different cellular pathways, such as growth control, tumor suppression, apoptosis, premature (Ras induced) senescence, transcription activation/repression, viral defense, protein degradation, DNA repair, DNA replication, and RNA transport (for review see Borden, 2002). It is clear that PML NBs play an important role in the physiological functions of the cell and are actively involved in different regulatory pathways. However, the mechanisms by which they integrate all of these distinctive pathways are still unknown.

The interpretation of PML NB function by protein association may have two major drawbacks stemming from the nature of these nuclear domains. First, PML protein may play different roles than PML NBs proper in certain pathways (Bischof *et al.*, 2002). Proteins that are purported to interact with PML protein may not be directly linked to the functions of PML NBs. Second, PML NBs may function as a depository site of excess proteins in the nucleus as overexpressed foreign proteins have been reported to localize in PML NBs (Maul, 1998; Tsukamoto *et al.*, 2000). Therefore, protein localizations identified by overexpression systems may be misleading in the case of PML NBs.

Indeed, the heterogeneity of PML NB composition makes it difficult to interpret their precise function, but paradoxically, that heterogeneity may very well be a result of those functions. More evidence in recent years indicates that PML NBs may serve as catalytic scaffold domains for the post-translational

modification of cellular effector proteins. A strong illustration of this phenomenon is the connection between p53 and PML NBs.

Many studies have shown that p53 activity is regulated by several post-translational modifications that affect its functions (for review see Hofmann and Will, 2003). For example, upon the expression of the active Ras oncogene, p53 is acetylated by CBP and then activates transcription of target genes that induce apoptosis or senescence (Pearson *et al.*, 2000). This process can be inhibited by the p53 deacetylase hSIR2 (Langley *et al.*, 2002). Also, in response to other stimuli, the p53 degradation pathways are activated by a phosphorylated E3-ubiquitin ligase, HDM2, and are inhibited by an ubiquitin-protease, Ubc7/HAUSP (Li *et al.*, 2002). Moreover, p53 SUMOylation by PIASy, a SUMO ligase, can induce the transactivating property of p53 (Bischof *et al.*, 2006). And lastly, in conditions of oncogenic stress, the p14ARF tumor suppressor can induce p53 activation via its competitive binding to p53 ubiquitin ligase, MDM2, and the SUMOylation of HDM2, the human homolog of MDM2 (Xirodimas *et al.*, 2002). Interestingly, all of these key modulators have been found to accumulate in PML NBs, in specific scenarios. These studies suggest that PML NBs may play a scaffold role, concentrating protein modulators under certain physiological conditions for more efficient post-translational modification of substrates. Therefore, it is important to understand what types of proteins reside in PML NBs in a normal, non-stressed cellular environment. Those proteins could potentially contribute to PML NB function as a catalytic scaffold. Additionally, it is equally important to examine the dynamic behavior of PML NBs upon mitotic entry and exit when most of the cell-growth modulator proteins are potentiated to take actions. Dramatic structural and composition changes of PML NBs during the mitotic disassembly and re-assembly process may reflect the intrinsic property of PML NBs to function as a scaffold domain. Therefore, I used both biochemical and cell biological approaches to gain further insight into this aspect of PML NB function as discussed in the following sections.

II. Biochemical Purification of PML NBs

Isolation of PML NBs has been attempted by many researchers in the field of PML NB studies. However, this study represents the first success in this endeavor. Several immunoprecipitation experiments with endogenous or tagged PML proteins have been reported, but these have only served to identify direct interactions between the proteins of interest and PML NBs. A large scale purification of PML NBs towards elucidating the complete proteome of PML NBs has yet to be done.

There are three layers of difficulty in PML NB purification which need to be resolved to achieve success, all of which are due to the structural nature of PML NBs. First, PML NBs are spherical with their key structural protein, PML, forming the outer most layer of the NB surface (Fig. 2B). One can presume that it is difficult to maintain the structure of a hollow, spherical, proteinaceous structure lacking a bi-layer membrane for shielding, during the rigorous process of biochemical purification. Second, because PML NBs are heterogeneous in size and composition, the traditional biochemical approach for protein complex purification, e.g. density gradient centrifugation, is not suitable for PML NBs. Lastly, the full length PML protein tends to form aggregates *in vitro* when the concentration of the PML protein is high. It has also been suggested that the RING domain of PML may facilitate self-assembly (Kentsis and Borden, 2004). Several studies have suggested that PML protein can form premature PML NBs *in vivo* in the absence of SUMOylation, and that these premature PML NBs (or PML aggregates) contain none of the well established PML NB resident proteins, e.g. Sp100 and Daxx (Muller *et al.*, 1998; Zhong *et al.*, 2000; Lallemand-Breitenbach *et al.*, 2001). Therefore, even though PML protein (and PML NBs?) can be successfully enriched through fractionation, it is difficult to interpret whether or not the proteins in the PML fraction are, in fact, genuine PML components without individually verifying each putative component's direct interaction with PML NBs by stringent criteria.

Here, I have developed a PML NB isolation protocol which has tackled the first two limitations successfully. However, our data suggest that the last limitation may not be resolved with the current state of technology, due to the intrinsic properties of PML NBs as discussed below.

i. Verification of PML NB integrity by structure and composition

During the development of the PML NB purification protocol, I assessed the efficiency of fractionation by examining the structure of PML NBs and by verifying their composition. Using BHK-S 1-6 cells stably expressing EYFP-Sp100 allowed me to follow the fractionation by visualizing EYFP-Sp100 labeled PML NBs. As shown in previous studies, the dispersal of Sp100 in the nucleoplasm was correlated with the loss of PML NB integrity under various cellular stresses, such as induction of PML-RARα protein in APL, viral infection, or heat shock treatment (for review see Dellaire and Bazett-Jones, 2004). Therefore, the colocalization of Sp100 with PML protein is a strong indicator that PML NBs maintained their apparent structure during the purification.

BHK-S 1-6 cells were therefore used to develop the first version of my PML NB isolation protocol. First, nuclei isolation was performed, based on well established protocols for suspension cells (Spector *et al*., 1998), which were further modified and refined for BHK-S cells, as described in chapter 5. After isolation of the nuclei, the colocalization of Sp100 and PML was observed. Subsequently, the procedure to generate a nuclear matrix fraction also successfully maintained the structure of PML NBs, as verified by both IF and immunoEM. Moreover, in the LSS fraction, PML protein is highly enriched, as shown by immunoblot, and PML NBs still maintain their colocalization with Sp100 protein. Based on these results, the first version of the isolation protocol, which was developed using BHK-S 1-6 cells, was able to allow me to isolate a fraction that is enriched for structurally intact PML NBs.

Following the promising initial results with BHK-S cells, I switched the starting material from cell line to mouse tissue in order to use *pml*$^{-/-}$ mice as a negative control. The second version of the protocol was designed for mouse tissue. The nuclear isolation step was performed, based on well established nuclear isolation procedures for isolating mouse liver and spleen nuclei (Spector et al., 1998; Mintz *et al.*, 1999). After the nuclear isolation step, the second version of the protocol only contained slight modifications to the nuclear matrix isolation section. The structure of PML NBs in the LSS fraction was also verified by IF and/or immunoEM. However, the nuclear matrix preparation step resulted in tight association between PML NBs and the nuclear matrix. Different salt extraction conditions and harsher matrix disruption treatments led to improved PML NB enrichment in the LSS fraction from mouse tissues when compared to the level

yielded from BHK-S cells. However, the increased yield also let to increased contamination. As such, I shifted my focus to the enhancement of purity over the efficiency of the isolation protocol.

ii. Purification of heterogeneous PML NB by immunoprecipitation

Traditional biochemical isolation methods are not suitable for PML NB purification, due to the heterogeneity of both PML NB structure and composition. In order to specifically extract PML NBs from the LSS fraction, I chose an approach that utilized immunoprecipitation. Using an antibody with specificity against PML protein, in combination with the magnetic bead sorting, PML NBs can be successfully immunoprecipitated regardless of their size and density. As shown by immunoEM, the structurally intact PML NBs, of a variety of shapes and content, are bound to the magnetic Dynabeads after IP. When using Dynabeads conjugated with a sheep anti-mouse secondary antibody, the protein profile of the eluate fraction showed strong enrichment of PML protein, with relative low amounts of contamination, particularly vimentin and hnRNP M. Intriguingly, lamin A/C, previously categorized as a contaminant, is actually enriched in the wt eluate but not in the *pml*$^{-/-}$ eluate, suggesting it was specifically pulled down with PML NBs. Indeed, while checking the fractionation efficiency via IF, lamin A/C colocalized with PML protein in every fraction from both liver and spleen tissues. This association was further confirmed in MEF cells and may account for the inefficient release of PML NBs from the mouse nuclear matrix.

Lamins are known to be the building blocks for the nuclear lamina underlying the inner nuclear membrane. It has been suggested that the function of the lamina may be to maintain the integrity of the nuclear envelope and to provide anchoring sites for chromatin (Goldman *et al.*, 2002). In the past decade, many studies have demonstrated the existence of intranuclear lamins and their association with DNA replication centers during S-phase (Moir *et al.*, 1994), and with IGCs during interphase (Jagatheesan *et al.*, 1999). It has also been reported that during myoblast differentiation, intranuclear lamin A foci undergo rearrangement while the peripheral organization of lamin A/C remains unchanged (Muralikrishna *et al.*, 2001). This indicates that intranuclear lamins may play important roles in nuclear organization. Here, I report the association of PML NBs with intranuclear lamin A/C for the first time.

iii. Nuclear matrix and the crowding effect

I have developed a PML NB isolation protocol that largely relies on the isolation of the nuclear matrix. Although first described and patented in 1948 (Zbarskii, 1948), and well defined and isolated in 1974 (Berezney and Coffey, 1974), the definition of “nuclear matrix” is still under debate. There is evidence from both sides that the observed nuclear matrix may exist as a true internal framework for nuclear compartment organization or as an artifact due to the isolation protocol (for review see Pederson, 2000). One of the major challenges of the nuclear matrix model is that the preparation step requires extraction with high salt concentration for the removal of chromatin. This type of procedure has been shown to create new macromolecular interactions which results in otherwise extractable proteins deposited in the matrix (Hancock, 2000).

This raises the concern that the salt extraction step in my PML NB isolation protocol may precipitate PML NBs onto the nuclear matrix, and therefore the nuclear matrix proteins may irreversibly contaminate the PML NB fraction. Interestingly, when I examined the DSP fraction from BHK-S 1-6 cells using the fluorescent microscope, some of the PML NBs moved freely within the nuclear matrix. In addition, after 0.5 M NaCl extraction, the ultrastructure of the DSP, shown by immunoEM, did not reveal filamentous structures as described in the previous studies after 2 M NaCl extraction (Berezney and Coffey, 1974). In addition, after mechanical disruption and short low-speed centrifugation, PML NBs in the LSS fraction appeared as free particles, and were not attached to large aggregates. This suggests that in BHK-S cells, PML NBs are not tightly attached with nuclear matrix after salt extraction.

Mass spectrometry analysis showed that most of the proteins that were present in the wt eluate, but not in the *pml*$^{-/-}$ eluate, were nuclear matrix proteins, particularly matrin 3 and various heterogeneous nuclear ribonuclear proteins (hnRNPs). It has been shown that hnRNP proteins can form filaments once they are released from their RNA binding sites, and that fibrous structures they form are similar to the 10 nm fiber observed in the nuclear matrix preparation (Tan *et al.*, 2000). This may suggest that although I did not observe filamentous or network-like nuclear matrix remnants associated with PML NBs in the LSS fraction following matrix disruption, the aggregation of nuclear matrix proteins with PML NBs can occur during the incubation period of the IP. Indeed, after overnight IP incubation of the LSS fraction with PML antibody conjugated Dynabeads, large

aggregates over 5 μm were sometimes observed in the eluate fraction. High concentrations of nuclear matrix proteins in a high salt buffer can potentially induce “crowding effects” (Hancock, 2004).

The nucleus is well known to be a highly compartmentalized organelle; however, little is known how this compartmentalization is achieved. The “nuclear matrix” model postulates that a protein scaffold may help position the subnuclear domains, as well as establish and maintain their structure. However, a simple experiment done by R. Hancock proved otherwise (Hancock, 2004). Previous studies have suggested the formation of nuclear compartments is generated by macromolecular crowding forces, since the global concentration of macromolecules within the nucleus is estimated to be ~100 mg/ml (Busch and Daskal, 1977; Minton, 1993; Zimmerman, 1993). R. Hancock showed that by simply reducing the monovalent cation concentration in the cell culture medium, PML NBs and nucleoli are dissembled in the expanded nuclei, a process that is reversible through the addition of inert, penetrating macromolecules, such as polyethylene glycol (PEG) and 10.5 kDa dextran, in the same medium even with low monovalent cation concentration (Hancock, 2004). This indicates that the formation of PML NBs (or PML protein aggregation) may largely depend upon the surrounding macromolecular milieu.

It is not surprising that vimentin is present in the fractions since it has been reported that vimentin is associated with the nuclear matrix and may be involved in nuclear matrix attachment regions’ (MARs) organization of genomic DNA (Tolstonog *et al.*, 2002). I found that after the overnight incubation step of PML-specific IP, vimentin can also be enriched in the eluates. Intriguingly, this phenomenon is PML protein specific, i.e. the eluates from neither *pml*$^{-/-}$ mice nor minus-antibody controls did not show enrichment of vimentin after the overnight incubation. This suggests that the crowding effect, mediated by PML protein, may account for the subsequent aggregations. This may also explain why I consistently found vimentin as a contaminant in the eluate fractions.

It is worth mentioning that even though mass spectrometry analysis did not show the presence of the most common PML NB components, such as Sp100, Daxx, and SUMO, one of the known PML partner proteins, nuclear co-repressor (NcoR), was specifically detected in the wt sample. It is not a common nuclear matrix contaminant like matrin 3 or DDX5 (Cronshaw *et al.*, 2002) and its localization to PML NBs requires PML protein (Khan *et al.*, 2001). Although I have not yet detailed the molecular interactions between NcoR and PML NBs, it is

interesting that of all partner proteins, NcoR, specifically, was immunoprecipitated with PML. More work needs to be done to verify the association of NcoR with PML NBs.

In summary, I have successfully enriched structurally intact PML NBs from the immunoprecipitation eluate of mouse tissues. However, due to the molecular nature of PML NBs, enriched PML NBs *in vitro* may induce aggregation of nuclear matrix proteins by the macromolecular crowding effect. Avoiding this PML-mediated crowding effect during the IP incubation remains a hurdle for efficient PML NB purification. Crowding agents, such as glycerol, actually facilitate the preservation of PML NB structure during the mechanical disruption step since more intact PML NBs were observed in an LSS fraction containing 10% glycerol than one without glycerol. However, when the concentration of the buffer is reduced to a level that precludes the crowding effect, PML NBs nonetheless dissembled. Regardless, it remains possible that PML NBs intrinsically are able to associate with nuclear matrix proteins and therefore are part of nuclear matrix network. I have not yet verified the localization of other nuclear matrix proteins in PML NBs *in vivo* besides lamin A/C. It is certain that PML NBs are connected to the intranuclear lamin network as I first described the colocalization of PML and lamin A/C in primary mouse cells. My data suggest PML NBs are closely associated with nuclear matrix proteins and may play a scaffolding role in the organization of the nucleus. Therefore, I postulate that due to this intrinsic property of PML NBs, one may not be able to isolate PML NBs with their endogenous constituents *in vitro* by currently available technology.

II. The Dynamics of PML NBs during Mitosis

i. Introduction

The most dramatic nuclear reorganization occurs during mitosis, the final stage in the cell cycle Therefore, analyzing the disassembly and reassembly of nuclear domains upon entry into and exit from mitosis provides important insights into the formation of nuclear domains under endogenous regulation of mitotic progression (Bubulya *et al.*, 2004; Leung *et al.*, 2004). In this study, I examined the dynamics of PML NBs during mitosis, and based upon my studies, I suggested that their association with chromatin may indicate their role as a scaffold domain in the nucleus.

Traditionally, the classification of mitotic stages is based on the morphological changes of the cell during mitosis. The starting point of mitosis is when the condensing chromosomes first become visible within the nucleus during prophase. NEBD marks the end of prophase and the initiation of prometaphase, during which time the mitotic spindle is formed, and microtubules capture the kinetochore of each chromosome. When all chromosomes are aligned near the spindle equator, the cell is in metaphase. Anaphase initiates when the two sister chromatids are separated longitudinally and move towards the opposing spindle poles. Finally, during telophase, chromosomes decondense to form the two daughter nuclei, and a microtubule-based midbody is assembled near the original spindle equator to participate in the ensuing cytokinesis. However, gross staging by morphology sometimes may occasionally be problematic, as not all mitotic structures are conserved between organisms during evolution (Nicklas and Arana, 1992).

As a more detailed molecular map of mitotic progression was developed, Pines and Rieder proposed a new staging of mitosis based on the activity of defined cell-cycle regulators (Pines and Rieder, 2001). From the traditionally defined late G2 phase to early prophase, several protein kinases are activated to prepare the cell for mitosis in the absence of significant cyclin B/ Cdk1 activity. For example, cyclin A/ Cdk1 is responsible for the initiation of chromosome condensation, and inhibition of this kinase can prevent G2 cells from prophase entry and induce the reversal of early prophase cells back into G2 (Furuno *et al.*, 1999). Other kinases, such as polo-like kinases (Plks) and aurora B, are also activated during this period (Lane and Nigg, 1996; Hsu *et al.*, 2000). At this stage,

chromosomes begin their condensation, but the cells are not yet committed to mitosis, since chromosomal condensation remains reversible by a wide variety of cellular stresses (Rieder and Cole, 1998). Therefore, they define this stage as transition 1, in which cells are prepared for mitotic entry.

They particularly stressed a “point of no return,” when mitotic entry becomes irreversible during late prophase (Rieder and Cole, 1998). This coincides with the activation of cyclin B/ Cdk1 complexes, which are the main component of M-phase-promoting factor (MPF). The activation of cyclin B/ Cdk1 is governed by two levels of regulation (for review see Bassermann *et al.*, 2005). First, the two inhibitory phosphates at the N-terminus of Cdk1 must be removed by Cdc25 phosphatase for Cdk1 activation. Second, the accumulation of cyclin B in the nucleus is also required for its full activation. Upon the sudden accumulation of active cyclin B/ Cdk1 in the nucleus, cells pass this “point of no return” and commit to mitosis until conditions change for them to escape from mitosis (Hagting *et al.*, 1998). Therefore, they define transition 2 as the period from cyclin B/ Cdk1 activation to NEBD.

Transition 3 is equivalent to the traditionally defined stage of prometaphase. After NEBD, the anaphase-promoting complex (APC), a large ubiquitin-ligase complex, is activated by cyclin B/ Cdk1. However, a cofactor of APC, Cdc20, is still sequestered via kinetochore-attachment (Morgan, 1999). This regulatory checkpoint allows APC to degrade cyclin A but not cyclin B or securin (Hunt *et al.*, 1992), allowing the cyclin B/ Cdk1 complex to remain active during transition 3.

Transition 4 begins when the kinetochore-attachment checkpoint is removed and the APC is fully activated. Cyclin B and securin are rapidly degraded by the APC, which results in Cdk1 inactivation and the separation of sister chromatids (Nasmyth *et al.*, 2000). Transition 4 replaces the traditionally defined metaphase and anaphase. Since removal of the checkpoint depends on the attachment of kinetochore to the spindle, rather than chromosome position, sister chromatid separation can occur without chromosomal line-up at the spindle equator, as shown in a previous study (Nicklas and Arana, 1992).

The initiation of the last transition before mitotic exit is marked by the substitution of APC cofactors (Pines and Rieder, 2001). Cdc20 is degraded at this stage and is replaced by Cdh1 (Visintin *et al.*, 1997). The switching of APC cofactors expands the range of APC substrate recognition and sustains APC activation into G1 phase (Pfleger and Kirschner, 2000). During transition 5, two daughter nuclei are reformed, a midbody assembles in between the two nuclei,

and the cell is ready to initiate cytokinesis.

ii. Change in PML NB dynamics reflects the new staging paradigm for mitosis

A previous live cell imaging study has demonstrated, with single particle tracking, that PML NBs exhibit dynamic displacement during mitosis (Dellaire *et al.*, 2006). However, in that study, the authors were unable to track the dynamic movement of PML NBs with high temporal and spatial resolution, and were therefore unable to resolve how and when the mobility of PML NBs changes upon mitotic entry. By using 4D live cell imaging with high temporal and spatial resolution, I demonstrated, for the first time, that the change of PML NB dynamics may correlate to specific mitotic events.

I first observed that PML NBs exhibit long range displacement from early prophase through prometaphase. Some of the PML NBs moved across the nucleus with speeds higher than 10 μm/ min, and the number of PML NBs per cell that exhibited this type of movement during prophase are 30% higher than those in interphase. Interestingly, when I categorized the PML NB movement by fitting to the MSD plot, several tracks showed a bi-phasic pattern indicating that PML NBs changed their movement types during the course of imaging. In order to further investigate how PML NBs change their dynamics, I attempted to obtain a better fit on the MSD plot by dividing each image track into two phases according to the time point at which NEBD was observed. Statistical analysis showed a global increase in the PML NB population exhibiting directed movement in phase 1, as well as a larger shift, either from diffusive or constrained movement to directed motion, in PML NBs in phase 2.

One possibility is that chromosomal condensation increases the interchromatin space during prophase, which leads to increased mobility of PML NBs. The pre-assumption of this explanation is that PML NBs are not tethered to either chromatin or nuclear matrix, and therefore are able to move freely within the additional space when the space constraints are removed, and to fuse together to form MAPPs during mitosis. However, the observation made in CA treated cells clearly proved otherwise. First, PML NBs did not show the same type of fast movements in CA treated cell as compared to that in prophase cells. Second, PML NBs appeared to be tethered onto prematurely condensed chromatin and did not change their relative position or fuse during the course of imaging. These

observations suggest that the additional interchromatin space created after premature chromosome condensation does not facilitate the fast movement of PML NBs by virtue of the release of PML NBs from chromatin.

Note that the fast movements of PML NBs are not completely equivalent to the directed motion, since PML NBs exhibiting diffusive movement can also move at high velocity. The “directed” movement only refers to that PML NBs being driven by certain physical forces, i.e. a flow of nuclear or cytoplasmic materials or dragging by nuclear matrix or chromatin. Interestingly, when I further analyzed the PML NB movement types in CA treated cells, over 60% of the PML NBs exhibited directed movement, and the trajectories of PML NBs showed that most of the tracks moved toward the center of the nucleus, which is probably due to the shrinkage of the cell. This suggests that PML NBs may be potentially dragged by prematurely condensed chromatin. Indeed, when analyzing the localization of PML NBs in CA treated cells, most of them colocalized with chromatin and remained attached during the course of imaging. An interesting point to consider is that the dynamic increase of PML NBs, especially in phase 2, may be partly affected by other dynamic events in mitotic cells. Most likely, the movement of PML NBs after NEBD is affected by the condensed chromosomes, which are pushed and dragged towards the metaphase plate by the newly formed spindle. However, this model still does not explain the dynamic increase of PML NB movement before NEBD.

A biochemistry study has reported that PML protein is phosphorylated and deSUMOylated during mitosis, and that the phosphorylation can be maintained by calyculin A (Everett *et al.*, 1999b). Moreover, unSUMOylated PML protein cannot recruit PML NB components into PML NBs but can still form immature PML protein aggregations (Dellaire *et al.*, 2006; Shen *et al.*, 2006). These studies indicate that post-translational modification of PML protein may play an important role in changing PML NB dynamics and MAPP formation during mitosis. However, it is not clear which kinase(s) directly targets PML protein during mitosis. While only one report has shown that PML protein can be directly phosphorylated by Casein kinase 2 at Ser517, which leads to PML protein degradation through a ubiquitin-mediated pathway (Scaglioni *et al.*, 2006), our own observations of PML NB dynamics in prophase may help to direct studies examining the role of post-translational modification in PML NB dynamics.

By 4D live cell imaging, I observed that the increase in PML NB dynamics occurred after the rapid nuclear entry of cyclin B1 and prior to NEBD. Interestingly,

this window of the PML NB dynamic increase coincides with the definition of transition 2 of the new mitosis staging paradigm proposed by Pines and Rieder, 2001. Shortly after the nuclear translocation of cyclin B1, the active cyclin B1/ Cdk1 complex phosphorylates different substrates, e.g. lamins and Cdc25, to commit the cells into mitosis (for review see Takizawa and Morgan, 2000). It is possible that PML protein may be one of the substrates of active cyclin B1/ Cdk1 or their downstream kinase(s), which modifies PML protein post-translationally and leads to the change of PML NB dynamics, as well as MAPP formation, during prophase.

One caveat from this set of experiments is that cyclin B1/ Cdk1 is not responsible for chromosome condensation in early prophase, as reported previously (Hagting *et al.*, 1999). Since PML NBs did not increase their dynamics prior to the nuclear entry of cyclin B1/ Cdk1, this indicates that chromosome condensation, per se, is not sufficient to induce an increase in PML NB dynamics. This also further supports our previous conclusion from the calyculin A experiments. It will be interesting to investigate, in future studies, whether PML protein is a true cyclin B1/ Cdk1 substrate.

iii. The association of PML NBs with chromatin

An association between PML NBs and chromatin has been suggested in many studies (Shiels *et al.*, 2001; Wang *et al.*, 2004; Dellaire *et al.*, 2006). The ultrastructure, as shown by composite electron micrographs, suggests that PML NBs may have a direct connection with chromatin (Dellaire *et al.*, 2006). A subpopulation of PML NBs are also known to associate with specific chromosomal regions, such as MHC gene clusters (Shiels *et al.*, 2001), telomeres (Yeager *et al.*, 1999), and centromeres (Everett *et al.*, 1999a). One recent study showed that PML NBs, in conjunction with special AT-rich sequence binding protein 1 (SATB1), can alter the chromatin loop structure and regulate transcription of the MHC I locus. Since most of these studies are performed on fixed cells, it is important to show how these chromatin associations of PML NBs affect PML NB dynamics in live cells.

Since 4D live cell imaging of mCherry-H2A and EYFP-Sp100 presents a 3D view of chromatin organization at high temporal and spatial resolution, I was able to analyze the correlation between chromatin association and the moving velocity of PML NBs during prophase. Preliminary data suggested that the velocity of PML

NBs is greatly affected by their association with chromatin, and that PML NBs exhibiting directed movement in phase 2 can be clearly distinguished into two types. One type of PML NBs moves freely without chromatin association, and the other type is dragged by chromatin. More statistic analysis is needed before these data are more conclusive. Intriguingly, Platani *et al*. (2002) has demonstrated that ATP depletion can affect the dynamics of Cajal bodies (CBs), and the authors suggest that tethering of CBs onto chromatin may require ATP (Platani *et al.*, 2002). It will be interesting to further investigate whether PML NBs also tether to chromatin through the same mechanism as CBs.

Taken together with my previous observations, I suggest that PML NBs may increase their dynamics by disassociation from chromatin upon entry into mitosis.

iv. Reassembly of PML NBs in G1

The formation of PML NBs requires proper post-translational modifications of PML protein (Sternsdorf *et al.*, 1999), whose regulation can alter PML NB structure and composition during mitosis (Everett *et al.*, 1999b). It has also been proposed that the formation of mature PML NBs requires several steps (Shen *et al.*, 2006). However, it is important to verify these observations under endogenous regulation in live cells as well. Therefore, I examined PML NB reformation in daughter nuclei upon exit from mitosis.

My data has demonstrated that there is a delay between the nuclear entry and PML NB recruitment of its component proteins, e.g. Sp100 and Daxx, suggesting that certain rate-limiting steps may prevent the maturation of PML NBs in early G1 cells. In addition, Sp100 and Daxx are recruited into PML NBs at different stage, from telophase to G1 phase transition. This suggests that the rate-limiting steps for Sp100 and Daxx may each be different, and ultimately result in their sequential entry into PML NBs. The defined sequence of events, regarding Sp100 and Daxx recruitment into newly formed PML NBs, needs to be verified by comparing the two proteins directly in the same cell.

Even though Sp100 and Daxx recruitment follow the recruitment of PML protein, suggesting that PML protein may be the seed for PML NB formation, I do not exclude the possibility that other unknown components may initialize the formation of PML NBs. When I followed MAPPs during telophase/G1 transition, I did observe that some MAPPs were trapped in the newly formed nuclear envelope as described previously by Dellaire *et al*., 2006. However, many PML

NBs are formed *de novo* at different sites in daughter nuclei, and the *de novo* formation of PML NBs seems to be synchronized at a specific time. Exactly where and when the reformation of PML NBs occurs is still unknown. Further investigation by live cell imaging is needed to answer these questions.

III. Prospects and Future Directions

A recent emerging model of PML NB assembly, which involved SUMO-mediated noncovalent binding, provides exciting insight into the potential explanation of the heterogeneity of PML NBs' functions (Lin *et al.*, 2006; Shen *et al.*, 2006). Since PML protein is SUMOylated at multiple sites and also contains a SUMO binding motif (SIM), it can form a PML network to recruit an assortment of proteins through SUMO moieties or SIMs of the proteins. This assembly model provides a potential mechanism for PML NBs to serve as a scaffold domain, which may explain the involvement of PML NBs in a variety of pathways.

My biochemistry purification data suggest that PML NBs may form *de novo* complexes with nuclear matrix proteins *in vitro*, and my live cell imaging data suggest that PML NBs may be released from chromatin upon entry into mitosis, which results in their increased dynamics. Since nuclear matrix proteins are known to interact with specific chromatin regions, known as nuclear matrix attachment regions (MARs), and to regulate the transcriptional activities of the genes in MARs (for review see Chattopadhyay and Pavithra, 2007), I speculate that besides their attachment to centromeres or telomeres, PML NBs may physically attach to chromatin through their interaction with nuclear matrix protein. Here, I propose several experiments to test this hypothesis.

First, I want to examine whether PML NBs are tethered to chromatin by specific nuclear matrix protein(s). As shown by mass spectrometry in Chapter 2, matrin 3, nuclear mitotic apparatus protein 1 (NuMA1), and scaffold attachment factor B2 (SAF-B2) were specifically co-immunoprecipitated with PML NBs. All of them are known to bind to MARs (Luderus *et al.*, 1994; Nayler *et al.*, 1998; Hibino *et al.*, 2006). In addition, PML NBs have been shown to alter the chromatin loop structure of the MHC class I locus through direct interaction with a MAR-binding protein, SATB1 (Kumar *et al.*, 2007). This suggests that SATB1 can be one of the candidates to attach PML NBs to chromatin. In particular, my study showed that intranuclear lamin A/C colocalizes with PML NBs in MEF cells. Lamin A/C is also shown to be one of the MAR binding proteins (Luderus *et al.*, 1994). Therefore, it will be interesting to investigate whether knocking down one or more of these nuclear matrix proteins can abolish the chromatin attachment of PML NBs. This can be evaluated by knocking down nuclear matrix proteins in CpYs 68 double stable cells and then analyzing the dynamic change of PML NBs during interphase. I anticipate that by depleting one of the nuclear matrix proteins, PML

NBs will lose their tethers to chromatin and increase their dynamics in the interphase.

Second, I want to investigate whether PML NBs tether to specific genomic loci. Even though PML NBs are known to be localized at the MHC I locus (Shiels *et al.*, 2001), only one study has suggested a global positioning of PML NBs in relation to genomic regions (Wang *et al.*, 2004). The authors used combined immunofluorescence and fluorescence *in situ* hybridization (immuno-FISH) to visualize both PML NBs and gene loci. By calculating the distance between the two, they demonstrated that PML NBs were positioned close to transcriptionally active genomic regions. However, they only selected a limited number of loci from 10 chromosomes, and therefore were not able to determine the precise location of each PML NB in the nucleus. Therefore, I propose to use a modified chromatin immunoprecipitation (ChIP) assay combined with comparative genomic array to identify chromatin regions that may tether PML NBs. The comparative genomic array technique allows genome wide analysis of DNA copy number by hybridizing patient DNA and normal reference DNA to arrays of genomic clones (for review see Gunn *et al.*, 2007). It is wildly used to detect global genomic lesions, e.g. unbalanced gains or losses of genetic material, in human disease. In order to distinguish chromatin associated with PML protein from that with PML NBs, I can modify the ChIP assay by pre-extracting the diffuse pool of PML protein before pull down PML NB associated chromatin regions by PML specific antibodies. The pre-extracted PML protein can still be pulled down as a control. For additional control, I can perform ChIP in both wild type and *pml*$^{-/-}$ mouse cells. By comparing the two ChIP samples on genomic DNA array, I can identify chromatin regions, or gene loci that are specifically associated with PML NBs, and further investigate whether PML NBs may functionally interact with those loci to regulate their gene activities.

Third, if the anchoring of PML NBs to chromatin is due to their association with nuclear matrix proteins, it is possible that nuclear matrix proteins may play a role in determining where and when the *de novo* formation of PML NBs occurs in early G1 cells. To test that, I will first determine which nuclear matrix proteins are colocalized with PML NBs by using IF with specific antibodies. Several candidates can be chosen from the list of proteins that were identified in my mass spectrometry analysis (Table 1). In addition, eIF4E can also be one of the candidates for initiating *de novo* PML NB assembly in early G1 cells since it can form nuclear bodies in the absence of PML protein (Cohen *et al.*, 2001). It will be

interesting to visualize the interaction between PML NBs and these proteins by using 4D live cell imaging, especially in early G1 cells. In particular, lamin A/C, one of the top candidates, may form nuclear bodies before the reformation of PML NBs occur, and therefore provide the anchoring sites for *de novo* PML NB formation. These experiments may give us insight into how the association between PML NBs and nuclear matrix protein leads to the PML NB assembly in early G1 cells.

Overall, by using biochemical and cell biological approaches, my study suggests that PML NBs have close association with nuclear matrix proteins and chromatin. Further investigation will be needed to verify these associations, and, hopefully, to help reveal the function of PML NBs in the cell nucleus.

Chapter 5: Materials and Methods

I. cDNA Constructs

The EYFP-Sp100 construct has been previously published by Muratani *et al*., 2002. The PML-ECFP containing PML VI isoform is provided by Dr. T. Tsukamoto (Himeji institute of Technology, Hyogo, Japan). IBB-HcRed was provided by J, Ellenberg and E. Zanin (EMBL, Heidelberg, Germany). EYFP-cyclin B1 and mCherry-H2A was provided by Dr. T. Nakamura (Tokyo Medical and Dental University, Tokyo, Japan). Daxx coding sequence was first amplified from human adult brain cDNA library by PCR to generate Kpn I and Xho I sites flanking the sequence and was subsequently cloned into pCR2.1-TOPO TA cloning vector (Invitrogen, Calsbad, CA). After sequencing, a correct clone was further sub-cloned into a modified pEYFP-C1 vector containing a SV2 promoter instead of a CMV promoter.

II. Cell Culture, Transfection, and Stable Cell Lines

MEFs, BHK, wt U2OS, and all of the U2OS derived stable cell lines were grown in Dulbecco's MEM (Gibco BRL, Gaithersburg, MD) supplemented with 50U/ml penicillin, 50U/ml streptomycin, and 10% fetal bovine serum (Hyclone Laboratories, Logan, UT). BHK-S and BHK-S 1-6 cells were grown in Glasgow's MEM (Gibco BRL) supplemented with 50U/ml penicillin, 50U/ml streptomycin, and 10% fetal bovine serum. Cells were grown at 37°C in 5% CO_2.

Electroporation (160 V, 950 μF) was performed using a MicroPulser Cuvettes with 0.4 cm gap (BioRad) on trypsinized cells resuspended in 250 μl of growth medium and transferred to cuvettes containing 2 μg of fusion protein plasmid plus 20 μg of sheared salmon sperm DNA. The cells were washed one time by 2 ml of growth medium and seeded onto either acid-washed coverslips for IF or MatTek glass bottom microwells (MatTek, Ashland, MA) for live cell imaging.

To make BHK-S 1-6 stable cell line, BHK-S cells were grown on 100-mm Petri dishes to 50% confluency and transfected with EYFP-Sp100 plasmid by

Fugene 6 reagent. Cells stably expressing EYFP-Sp100 were selected with 1 mg/ml G418, and then cells were serially diluted to pick out single cell clones. The clones were than screen using a fluorescence microscope (model Axioplan 2i; Carl Zeiss MicroImaging, Inc) equipped with Chroma filters (Chroma Technology Corp) to select a clone with more than 90% of its population expressing the fusion protein.

All U2OS cell derived stable cell lines were generated by the same protocol. U2OS cells were grown on 100-mm Petri dishes to 70 % confluency and transfected with plasmids by electroporation. Cells stably expressing the fusion protein(s) were selected with 1 mg/ml G418, and then single cell cloning was performed to further select a clone with more than 90% of its population expressing the fusion proteins. To generate double stable cell line from Cp89 single stable cell line, Cp89 cells were transfected with EYFP tagged fusion plasmid. Two days after transfection, EYFP expressing fluorescent cells were sorted using a FACSVantage SE cell sorter with DiVa option (Becton Dickinson, San Jose, CA) using a Helium-Neon laser at 488 nm. Sorted cells were further selected by single cell cloning to select a clone with more than 90% of its population expressing the fusion proteins.

III. Immunofluorescence

Cells were rinsed in PBS once and fixed for 15 min in 2% formaldehyde in PBS, pH7.4. After being washed in PBS for 10 min x 3 times, cells were permeablized 5 min in PBS with 0.2% Triton X-100 and 1% normal goat serum. After being washed in PBS plus 1% goat serum for 10 min x 3 times, the following primary antibodies were added for 1 hr at RT: mAb 5E10 (1:10, hybridoma supernatant provided by R. van Driel, University of Amsterdam, Amsterdam, Netherlands), mAb PML37 (1:50, ascites provided by S. Lowe, CSHL, Cold Spring Harbor, NY), and rabbit anti-lamin A/C (1:500). Cells were rinsed in PBS with 1% normal goat serum for 10 min x 3 times, and secondary anti-species-specific antibodies (Jackson ImmunoResearch Laboratories, West Grove, PA) were added for 1 hr at RT. Cells were rinsed in PBS for 10 min x 3 times and mounted in mounting media (90% glycerol in 0.2 M Tris-Cl, pH 8.0, with 1 mg/ml *p*-phenylenediamine). Fixed cells were examined using the Axioplan fluorescence

microscope 2i, and OpenLab software (Improvision) was used to collect digital images. Alternatively, fixed cells were observed on a DeltaVision RT system (Applied Precision, Issaqua, WA) equipped with Photometrics CoolSNAP *hq* Monochrome camera, and images were collected using SoftWorx software.

IV. Immunobloting

For all of the fractions from PML NB isolation protocol, the pellets were sonicated for 10 sec x 3 times at a constant cycle using a microprobe sonicator with Branson Sonifier (model S-250A). The protein concentration in each fraction was quantified by Bio-Rad protein assay (Bio-Rad Laboratories). 10 mg of protein sample from each fraction was separated on 10% SDS-polyacrylamide gels. The gels were transferred to nitrocellulose membrane (Bio-Rad Laboratories). Membranes were blocked in Odyssey blocking buffer (LI-COR Biosciences, Lincoln, NE) for 2 hr at RT. The following primary antibodies were incubated with membranes for 1 hr at RT: mAb PML 37 (1:1,000), rabbit anti-Daxx (1:1,000, provided by G. Maul, the Wistar Institute, Philadelphia, PA), rabbit anti-vimentin (1:10,000, provided by R. Goldman, Northwestern University Medical School, Chicago, IL), mAb anti-GFP (1:1,000, Roche, Basel, Switzerland), mAB B23 (1:2,000), mAb AK96 anti-SF2/ASF (1:2,000, provided by A. Krainer, CSHL, Cold Spring Harbor, NY), rabbit anti-coilin R228 (1: 2,000, provided by E. Chan, The Scripps Research Institute, La Jolla, CA), mAb anti-SC35 (1:1,000, provided by T. Maniatis, Harvard University, Cambridge, MA), rabbit anti-lamin A/C (1:5,000), rabbit anti-lamin B (1:5,000), mAb anti-B” (1:2,000, provided by W. van Venrooij, University of Nijmegen, Nijmegen, Netherlands), mAb anti-hnRNP M (1:4,000), mAb 3C5 (1:1,000), and rSpAB anti-Sp100 (1:1,000, provided by H. Will, Hamburg University, Hamburg, Germany). Membranes were washed by TBS with 0.2 % tween-20 for 10 min x 3 time, and then incubated with secondary antibodies, IR700 anti-rabbit and IR800 anti-mouse (Rockland Immunochemicals), for 1 hr at RT. Membranes were then washed by TBS with 0.2 % tween-20 for 10 min x 3 time and then TBS for 10min x 1 time. To visualize immunoblots, membranes were scanned by the Odyssey infrared imager (LI-COR Biosciences), and the images were processed by Odyssey software.

V. Transmission Electron Microscopy

Samples were fixed in 2% glutaraldehyde and 0.2% formaldehyde in 0.1M PBS overnight and then dehydrated in a graded ethanol series. Samples were then infiltrated by continuous mixing on a shaker table with 50% LR White resin (Electron Microscopy Sciences –EMS) in ethanol for 1 hour, followed by 100% LR White for 2 hours and then polymerized in gelatin capsules overnight in an oven at 50°C.

Samples were thin sectioned on an ultramicrotome model Ultracut UCT (Leica Microsystems Vienna, Austria) with a Diatome diamond knife (EMS). Immunogold labeling was done on 100 nm LR White sections collected on nickel grids. Sections were first incubated for 5 minutes in a blocking solution of 1% acetylated BSA (Aurion, EMS) and then transferred to drops of primary antibody to mAb PML 37 (a gift from Dr. Scott Lowe) diluted 1:10 in PBS. Grids were incubated in primary antibody for 2 hours at room temperature and then briefly rinsed in a jet of PBS and placed in drops of goat anti-mouse antibody conjugated to 10nm colloidal gold (Amersham Biosciences/GE Healthcare) for 30 minutes. Grids were then rinsed in distilled water, air dried and then counterstained in aqueous uranyl acetate. Positive and negative immunocytochemical controls done consisted of labeling sections of mouse cells containing PML nuclear bodies and doing gold labeling on the test sample from which the primary antibody was omitted or an irrelevant antibody was used in its place.

Ultrathin immunogold labeled sections were examined and photographed in a Hitachi HT-7000 electron microscope at 3000-17,000x magnifications, operated at 75kv and film negatives made of representative sample areas were digitally scanned with a Microtek ArtixScan 1800f at 1000 dpi resolution. Scanned images were viewed with Adobe Photoshop.

VI. Crosslinking Antibodies to the Dynabeads

1 ml Dynabeads (Invitrogen) were added into 25ml of mAb PML37 hybridoma culture supernatant. The mixture was rotated at 4°C overnight. Dynabeads were then pulled down by magnet and washed two times in 0.1 M sodium phosphate buffer pH 8.1 + 0.05% Tween-20. After washing two more times with 0.2 M sodium

borate + 0.05% Tween-20, Dynabeads were resuspended in the same washing buffer. 20 mM dimethyl pimelimidate (DMP) were then added into the Dynabeads suspension, and the mixture was rotated at RT for 30 min. Subsequently, Dynabeads were pulled down by magnet and washed 1 time by 0.2 M ethanolamine + 0.05% Tween-20. The reaction was stopped by re-suspending the beads in 0.2M ethanolamine and rotating at RT for 2 hr. After wash one time by 0.1 M sodium phosphate buffer pH 8.1 + 0.05% Tween-20, the mAb PML37 conjugated Dynabeads were stored at 4˚C.

VII. Isolation of BHK-S Cell Nuclei

All the buffers used here contained protease inhibitors (1 mM PMSF, 5 μg/ml leupeptin, 5 μg/ml aprotinin). All the procedures were done on ice or 4˚C.

6 liters of BHK-S cells were harvested and washed 2 times by PBS. Cells were resuspended in RSB buffer (10 mM Tris-HCl pH 7.4, 5 mM NaCl, 1.5 mM $MgCl_2$, and 2 mM $CaCl_2$) for 20 min. After the swelling of the cells were observed, cells were homogenized by a 55 ml Dounce homogenizer (VWR International, Inc., West Chester, PA). The nuclei were collected by centrifugation at 1,000g, 5 min, and washed 3 times by RSB buffer. The BHK-S nuclei were washed once in TMZ5 buffer (10 mM Tris-HCl, pH 7.4, 5 mM $MgCl_2$, and 1 μM $ZnCl_2$) and were ready for PML NB isolation.

VIII. Isolation of Nuclei from Mouse Tissues

All the buffers used here contained protease inhibitors (1 mM PMSF, 5 μg/ml leupeptin, 5 μg/ml aprotinin, and 5 mM NEM). All the procedures were done on ice or 4˚C.

Livers from 7- to 10-weekold C57BL/6 female mice were washed once in ice-cold TMZ5 buffer and minced into small pieces using a razor blade on a 10ml glass Petri dish. The minced liver was homogenized by a 55 ml Dounce homogenizer (VWR International, Inc) in TMZ5 buffer + 0.25 M sucrose. The homogenate was filtered twice through 2 layers of cheese cloth. An equal volume

of TMZ5 buffer + 2.2 M sucrose was added to the homogenate and mixed vigorously. The homogenate was transferred to 30 ml conical polycarbonate Oak Ridge centrifuge tubes (Nalgene Labware, Rochester, NY) containing 8 ml TMZ5 buffer + 2.2 M sucrose and was centrifuged at 39,000g for 2 hr at 4˚C. The nuclear pellet was washed once with TMZ5 and was ready for PML NB isolation.

Spleens from C57BL/6 female mice were washed once in PBS. Spleens were minced using the base of the plunger from a 5 ml syringe on a 5 ml glass Petri dish in 2 ml PBS. The minced spleen was filtered through a cell strainer with 40 μm pores (BD Bioscience) and washed by PBS once. The splenocytes were treated with RSB buffer for 20 min and then homogenized by a 55 ml Dounce homogenizer (VWR International, Inc). The homogenate was filtered through a cell strainer and centrifuged at 1,000g for 5 min. The spleen nuclei were washed once in TMZ5 buffer and were ready for PML NB isolation.

IX. Fractionation of PML NBs

All the buffers used here contained protease inhibitors (1 mM PMSF, 5 μg/ml leupeptin, 5 μg/ml aprotinin, and 5 mM NEM). All the procedures were done on ice or 4˚C.

The isolated nuclei were resuspended in TMZ5 buffer at the concentration of 5 x 10^8 nuclei/ ml and treated with 1% Triton X-100 for 5 min at RT. Nuclei were centrifuged at 780g for 5 min and resuspended in TMZ5 buffer. Permeabilized nuclei (5 x 10^8 nuclei/ ml) were treated with 200U DNase I (Roche), and the mixture was rotated for 1.5 hr at 4˚C. DNase I digested nuclei were centrifuged at 730g for 2 min and resuspended in TMZ0.5 buffer (10 mM Tris-HCl, pH 7.4, 0.5 mM $MgCl_2$, and 1 μM $ZnCl_2$) with 0.5 M NaCl or with 300 mM $(NH_4)_2SO_4$. The nuclei were incubated on ice for 5 min and then centrifuged at 730g for 5 min again. The pellet was resuspended in TMZ0.5 buffer + salt and extracted by the above step two more times. After the last extraction, the pellet (nuclear matrix) was either resuspended in TSG buffer (TMZ 0.5, 0.5 M NaCl, and 10% glycerol) or TSG_9 buffer (TMZ0.5, pH 9.0, 330 mM $(NH_4)_2SO_4$, 10% glycerol) + 1 mM DTT and homogenized by 1 ml Dounce homogenizer (VWR). The homogenate were centrifuged at 4,547g (7,000 rpm), 7,516g (9,000 rpm), or 15,682g (13,000 rpm). The supernatant was transferred to a new microcentrifuge tube and ready for

immunoprecipitation.

For immunoprecipitation, 200 μl mAb PML37 conjugated Dynabeads were washed once with TSG or TSG_9 buffer. The protein concentration of the supernatant was quantified by Bio-Rad protein assay. Total of 300 μg supernatant protein was mixed with the beads, and the final volume of the mixture was adjusted by TSG or TSG_9 buffer to 600 μl. The mixture was rotated for 2 hr at RT or overnight at 4˚C. The Dynabeads were then washed by TSG or TSG_9 buffer plus 0.05% Tween-20 for 3 times. For immunoblotting, PML NBs were eluted by SDS sample buffer (Spector *et al.*, 1998). For immunoEM, the beads were fixed in 2% glutaraldehyde and 0.2% formaldehyde in 0.1M PBS. For mass spectrometry, Dynabeads were pulled down by magnet, and the liquid was removed as much as possible before the samples were frozen at -80°C overnight and shipped to Amgen Inc. (Thousand Oaks, CA) for mass spectrometry analysis in collaboration with S. Patterson, Mike Davis, and Paul Auger (Amgen, Inc.).

X. Mass Spectrometry

Samples were thawed at 4°C and then stripped in boiling 1% SDS (Invitrogen) at 99°C for 5 min. Samples were removed from heat and allowed to cool. The extracted beads were concentrated using a magnetic stand and the supernatant was removed for analysis. The entire volume of each extracted sample (50 μl) was loaded into one well of a 5 well, 1 mm 4-20% Tris Glycine gel (Invitrogen) and run at 200 V for 1.5 hrs. The gel was stained with Simply Blue stain (Invitrogen) overnight and destained in deionized water for 4 hrs prior to visualization. 10 bands were excised from each gel containing sample from wt mice or *pml*$^{-/-}$ mice for in-gel digestion and analysis.

i. In-Gel digestion

Excised bands were placed into clean 1.5 mL microcentrifuge tubes (Eppendorf North America, Inc., Westbury, NY), washed with 200 μl of 50mM NH_4HCO_3/ 50% ACN and rehydrated with 200 μl of 50mM NH_4HCO_3. This step was repeated until all gel slices were fully destained. Bands were then dehydrated by washing 2X with 200 μl of 50mM NH_4HCO_3/ 50% ACN, sliced into 2mm X 2mm

cubes and then vacuum concentrated to dryness (Thermo-Fisher, San Jose, CA). Samples were reduced by reconstituting the dehydrated bands with 200 μl of 10mM DTT in 50mM NH_4HCO_3 and incubating at 55C for 1hr. The supernatant was removed and the gel bands washed 1X with 50mM NH_4HCO_3. Samples were then resuspended in 60mM IAM in 25mM NH_4HCO_3 and incubated at RT in the dark for 40min to alkylate all the reduced cysteines. Bands were then completely dehydrated by washing 2X with 200 μl of 50mM NH_4HCO_3/ 50% CAN and then vacuum concentrated to dryness. Tryptic digestion was performed by rehydrating the bands in 200 μl of 50mM NH_4HCO_3, 10% ACN, and 1.0 μg of trypsin followed by incubation of the samples at 37°C for 12hrs. Following the incubation the supernatant of the digestion was removed to a clean 0.6mL microcentrifuge tube. The excised bands were further dehydrated with 2 washes of 50% ACN/ 0.1% Formic (150 μl), with all supernatants combined and vacuum concentrated to dryness. The final samples were reconstituted in 10μl of 0.1% Formic Acid for analysis by LC-MS/MS.

ii. LC-MS/MS

Qualitative analysis of extracted PML bodies from 1-D gel analysis was performed by NanoLC-MS/MS using a direct flow Nano HPLC system (NanoLC-2D, Eksigent, Palo Alto, CA) coupled to a LTQ-FT mass spectrometer (Thermo-Fisher, San Jose, CA). Samples were loaded at 2 μl/ minute onto a pre-equilibrated 100 micron (I.D.) x 200 mm C18 reverse-phase column constructed and packed (Magic C18 resin, Michrom Biosystems, Auburn, CA) by a high pressure capillary column packer (Nanobaume, Western Fluids Engineering & Mfg. LLC, Lake Elsinore, CA) at 5000psi. A dual analytical column system was used for analysis of the extracted samples. Two columns were situated onto a 10-port valve (VICI, Houston, TX) such that one analytical column could be loaded at higher flow and then brought in-line with the analytical, nano flow, pump for MS analysis. Upon completion of the loading phase, the column was developed using a linear gradient from 2 to 42% buffer B over 60 minutes (Buffer A, 0.1% aqueous FA; Buffer B, 90% ACN in 0.1% FA, v/v) at a reduced flow rate of 0.6 μl/ minute followed by a high organic washout at 90% B prior to a 5 minute re-equilibration. Sample introduction to the mass spectrometer was achieved using a resin-packed 100 μm of nanoelectrospray emitter interfaced with a nanoelectrospray source (New Objective, Woburn, MA) similar to that described

by McGinley (McGinley *et al.*, 2000). The off-analysis column on the 10-port valve was subjected to 3 gradients from 0-90% buffer B over the analysis time with a final equilibration of 15min in 98% buffer A.

iii. Data analysis

All LC-MS/MS experiments were analyzed using an integrated qualitative analysis platform developed in-house (SPECTRE, Amgen, Inc., Thousand Oaks, CA) using the IPI mouse and human reference databases and precursor and fragment ion tolerances of 0.05 and 0.5 Daltons, respectively. Full tryptic constraints (X/K, X/R, but not X = P) and a single static modification (carboxyamidomethylation, +57.0215 da) were employed for all analyses. The combined outputs from 6 search engines were used to gauge the relative "accuracy" of the hits. MatchMaker (Amgen, Thousand Oaks, CA), OMSSA (NCBI, Bethesda, MD), X!Tandem (GPM, www.thegpm.org), Mascot (Matrix Science, Boston, MA), Bequest (Immunex Corp.), and Lutefisk (Immunex Corp.) were used to score the results. A false positive rate of <5% was used as a first-pass validation filter with "identification" required by at least 2 search engines. Singleton matches were manually verified prior to inclusion in data set. Manual validation involved the correlation of all major fragment ions (e.g., > 20% relative intensity) with the predicted N and C-terminal fragments (b and y-type ions, respectively) or their expected neutral loss or internal cleavage products.

XI. Live Cell Imaging

Cells were seeded onto MatTek glass bottom microwells and grown for 2 days before imaging. Chromatin was visualized either by transient transfection of mCherry-H2A or by 5 min Hoechst 33324 staining at the final concentration of 0.2 μg/ ml. Before imaging began, cells were changed into Leibovitz's L-15 medium (Gibco) supplemented with 30% FBS before being mounted onto the stage of a DeltaVision RT microscope (Applied Precision) with a PlanApo 60x 1.40 n.a. objective lens (Olympus America, Inc., Center Valley, PA). The images were collected in different channels with 35 msec to 50 msec exposure time and deconvolved by using SoftWoRx software, during which the temperature was maintained at 37°C by an environmental chamber.

XII. Tracking and Image Analysis

The 4D live cell images were processed by 3 steps: registration, segmentation and tracking. Registration transformed each image in the series to match the position and orientation of the first one. A rigid registration was performed by using the TurboReg plugin of ImageJ freeware. The “rigid” mode in TurboReg compensated both translational and rotational movement of the cells. (http://bigwww.epfl.ch/thevenaz/turboreg/).

Image segmentation using a series of processing steps further defined and outlined the particles in each image. 6 steps were used for segmentation: 1. background subtraction. 2. normalization. 3. anisotropic diffusion filtering. 4. structure tensor calculation. 5. logarithm transformation. 6. automatic maximum entropy thresholding. All these steps were performed in ImageJ using standard ImageJ functions (step 1, 2, and 5) or the freeware plugins, including the edge preserving anisotropic diffusion (step 3), the FeatureJ (step 4), and the Multi-thresholder (step 6).

The tracking was performed by TIKAL. All tracks were manually corrected in TIKAL's interactive 4D viewer. The length of each track and possible fusion events were counted and recorded. The 3D trajectories were exported in ASCII format into MATLAB program (The Mathworks, Inc.) for data fitting and classification of the movement types. The mean square displacement was calculated for each track in each phase. The anomalous diffusion equation was then used to fit the MSD plot, and diffusion constant (D) and anomalous diffusion coefficient (α) were calculated from the curve fitting. The α values were then used for classification of the movement types. 3 types of movement were distinguished based on the α value: α = 0.40 to 0.75, constrained motion. α = 0.75 to 1.25, diffusive motion. α = 1.25 to 2.00, directed motion. Tracks exhibiting a specific movement type in an image set was counted and divided by the total number of tracks to obtain a percentage. The distribution of different movement types from all of the image sets was summarized using a box plot.

List of References

Afzelius, B.A. (1955). The ultrastructure of the nuclear membrane of the sea urchin oocyte as studied with the electron microscope. Exp Cell Res *8*, 147-158.

Andersen, J.S., Lyon, C.E., Fox, A.H., Leung, A.K., Lam, Y.W., Steen, H., Mann, M., and Lamond, A.I. (2002). Directed proteomic analysis of the human nucleolus. Curr Biol *12*, 1-11.

Andrade, L.E., Chan, E.K., Raska, I., Peebles, C.L., Roos, G., and Tan, E.M. (1991). Human autoantibody to a novel protein of the nuclear coiled body: immunological characterization and cDNA cloning of p80-coilin. J Exp Med *173*, 1407-1419.

Asakawa, Y., and Gotoh, E. (1997). A method for detecting sister chromatid exchanges using prematurely condensed chromosomes and immunogold-silver staining. Mutagenesis *12*, 175-177.

Ascoli, C.A., and Maul, G.G. (1991). Identification of a novel nuclear domain. J Cell Biol *112*, 785-795.

Bassermann, F., Peschel, C., and Duyster, J. (2005). Mitotic entry: a matter of oscillating destruction. Cell Cycle *4*, 1515-1517.

Beck, J.S. (1961). Variations in the morphological patterns of "autoimmune" nuclear fluorescence. Lancet *1*, 1203-1205.

Belmont, A.S. (2006). Mitotic chromosome structure and condensation. Curr Opin Cell Biol *18*, 632-638.

Berezney, R., and Coffey, D.S. (1974). Identification of a nuclear protein matrix. Biochem Biophys Res Commun *60*, 1410-1417.

Bernhard, W., Hauenau, F., and Oberling, C. (1952). [The ultrastructure of the nucleolus of some animal cells as revealed by the electron microscope.]. Experientia *8*, 58-59.

Bernstein, R.M., Bunn, C.C., Hughes, G.R., Francoeur, A.M., and Mathews, M.B. (1984). Cellular protein and RNA antigens in autoimmune disease. Mol Biol Med *2*, 105-120.

Biessmann, H., Prasad, S., Walter, M.F., and Mason, J.M. (2005). Euchromatic and heterochromatic domains at Drosophila telomeres. Biochem Cell Biol *83*, 477-485.

Bischof, O., Kirsh, O., Pearson, M., Itahana, K., Pelicci, P.G., and Dejean, A. (2002). Deconstructing PML-induced premature senescence. Embo J *21*, 3358-3369.

Bischof, O., Schwamborn, K., Martin, N., Werner, A., Sustmann, C., Grosschedl, R., and Dejean, A. (2006). The E3 SUMO ligase PIASy is a regulator of cellular senescence and apoptosis. Mol Cell *22*, 783-794.

Bishop, C.L., Ramalho, M., Nadkarni, N., May Kong, W., Higgins, C.F., and Krauzewicz, N. (2006). Role for centromeric heterochromatin and PML nuclear bodies in the cellular response to foreign DNA. Mol Cell Biol *26*, 2583-2594.

Borden, K.L. (2002). Pondering the promyelocytic leukemia protein (PML) puzzle: possible functions for PML nuclear bodies. Mol Cell Biol *22*, 5259-5269.

Bouteille, M., Kalifat, S.R., and Delarue, J. (1967). Ultrastructural variations of nuclear bodies in human diseases. J Ultrastruct Res *19*, 474-486.

Brown, M.J., Hallam, J.A., Colucci-Guyon, E., and Shaw, S. (2001). Rigidity of circulating lymphocytes is primarily conferred by vimentin intermediate filaments. J Immunol *166*, 6640-6646.

Bubulya, P.A., Prasanth, K.V., Deerinck, T.J., Gerlich, D., Beaudouin, J., Ellisman, M.H., Ellenberg, J., and Spector, D.L. (2004). Hypophosphorylated SR splicing factors transiently localize around active nucleolar organizing regions in telophase daughter nuclei. J Cell Biol *167*, 51-63.

Busch, H. (1974). The Cell Nucleus. New York, Academic Press

Busch, H., and Daskal, Y. (1977). Methods for isolation of nuclei and nucleoli. Methods Cell Biol *16*, 1-43.

Carmo-Fonseca, M., Mendes-Soares, L., and Campos, I. (2000). To be or not to be in the nucleolus. Nat Cell Biol *2*, E107-112.

Carvalho, T., Seeler, J.S., Ohman, K., Jordan, P., Pettersson, U., Akusjarvi, G., Carmo-Fonseca, M., and Dejean, A. (1995). Targeting of adenovirus E1A and

E4-ORF3 proteins to nuclear matrix-associated PML bodies. J Cell Biol *131*, 45-56.

Chalfie, M., Tu, Y., Euskirchen, G., Ward, W.W., and Prasher, D.C. (1994). Green fluorescent protein as a marker for gene expression. Science *263*, 802-805.

Chattopadhyay, S., and Pavithra, L. (2007). MARs and MARBPs: key modulators of gene regulation and disease manifestation. Subcell Biochem *41*, 213-230.

Chelbi-Alix, M.K., Pelicano, L., Quignon, F., Koken, M.H., Venturini, L., Stadler, M., Pavlovic, J., Degos, L., and de The, H. (1995). Induction of the PML protein by interferons in normal and APL cells. Leukemia *9*, 2027-2033.

Chen, D., Dundr, M., Wang, C., Leung, A., Lamond, A., Misteli, T., and Huang, S. (2005). Condensed mitotic chromatin is accessible to transcription factors and chromatin structural proteins. J Cell Biol *168*, 41-54.

Cohen, N., Sharma, M., Kentsis, A., Perez, J.M., Strudwick, S., and Borden, K.L. (2001). PML RING suppresses oncogenic transformation by reducing the affinity of eIF4E for mRNA. Embo J *20*, 4547-4559.

Condemine, W., Takahashi, Y., Zhu, J., Puvion-Dutilleul, F., Guegan, S., Janin, A., and de The, H. (2006). Characterization of endogenous human promyelocytic leukemia isoforms. Cancer Res *66*, 6192-6198.

Cremer, T., Cremer, M., Dietzel, S., Muller, S., Solovei, I., and Fakan, S. (2006). Chromosome territories--a functional nuclear landscape. Curr Opin Cell Biol *18*, 307-316.

Croft, J.A., Bridger, J.M., Boyle, S., Perry, P., Teague, P., and Bickmore, W.A. (1999). Differences in the localization and morphology of chromosomes in the human nucleus. J Cell Biol *145*, 1119-1131.

Cronshaw, J.M., Krutchinsky, A.N., Zhang, W., Chait, B.T., and Matunis, M.J. (2002). Proteomic analysis of the mammalian nuclear pore complex. J Cell Biol *158*, 915-927.

Csink, A.K., Linsk, R., and Birchler, J.A. (1994). The Lighten up (Lip) gene of Drosophila melanogaster, a modifier of retroelement expression, position effect variegation and white locus insertion alleles. Genetics *138*, 153-163.

Daniel, M.T., Koken, M., Romagne, O., Barbey, S., Bazarbachi, A., Stadler, M., Guillemin, M.C., Degos, L., Chomienne, C., and de The, H. (1993). PML protein expression in hematopoietic and acute promyelocytic leukemia cells. Blood *82*, 1858-1867.

De, D.N. (1957). Ultrastructure of nuclear membrane of plant cells. Exp Cell Res *12*, 181-184.

de The, H., Chomienne, C., Lanotte, M., Degos, L., and Dejean, A. (1990). The t(15;17) translocation of acute promyelocytic leukaemia fuses the retinoic acid receptor alpha gene to a novel transcribed locus. Nature *347*, 558-561.

de The, H., Lavau, C., Marchio, A., Chomienne, C., Degos, L., and Dejean, A. (1991). The PML-RAR alpha fusion mRNA generated by the t(15;17) translocation in acute promyelocytic leukemia encodes a functionally altered RAR. Cell *66*, 675-684.

de, T.H.E., Riviere, M., and Bernhard, W. (1960). [Examination by electron microscope of the VX2 tumor of the domestic rabbit derived from the Shope papilloma.]. Bull Assoc Fr Etud Cancer *47*, 570-584.

Dellaire, G., and Bazett-Jones, D.P. (2004). PML nuclear bodies: dynamic sensors of DNA damage and cellular stress. Bioessays *26*, 963-977.

Dellaire, G., Eskiw, C.H., Dehghani, H., Ching, R.W., and Bazett-Jones, D.P. (2006). Mitotic accumulations of PML protein contribute to the re-establishment of PML nuclear bodies in G1. J Cell Sci *119*, 1034-1042.

Dernburg, A.F., Broman, K.W., Fung, J.C., Marshall, W.F., Philips, J., Agard, D.A., and Sedat, J.W. (1996). Perturbation of nuclear architecture by long-distance chromosome interactions. Cell *85*, 745-759.

Dunleavy, E., Pidoux, A., and Allshire, R. (2005). Centromeric chromatin makes its mark. Trends Biochem Sci *30*, 172-175.

Durante, M., Furusawa, Y., and Gotoh, E. (1998). A simple method for simultaneous interphase-metaphase chromosome analysis in biodosimetry. Int J Radiat Biol *74*, 457-462.

Dyck, J.A., Maul, G.G., Miller, W.H., Jr., Chen, J.D., Kakizuka, A., and Evans, R.M. (1994). A novel macromolecular structure is a target of the promyelocyte-retinoic

acid receptor oncoprotein. Cell *76*, 333-343.

Eskiw, C.H., Dellaire, G., Mymryk, J.S., and Bazett-Jones, D.P. (2003). Size, position and dynamic behavior of PML nuclear bodies following cell stress as a paradigm for supramolecular trafficking and assembly. J Cell Sci *116*, 4455-4466.

Estey, E., Thall, P., Kantarjian, H., Pierce, S., Kornblau, S., and Keating, M. (1997). Association between increased body mass index and a diagnosis of acute promyelocytic leukemia in patients with acute myeloid leukemia. Leukemia *11*, 1661-1664.

Everett, R.D. (2001). DNA viruses and viral proteins that interact with PML nuclear bodies. Oncogene *20*, 7266-7273.

Everett, R.D., Earnshaw, W.C., Pluta, A.F., Sternsdorf, T., Ainsztein, A.M., Carmena, M., Ruchaud, S., Hsu, W.L., and Orr, A. (1999a). A dynamic connection between centromeres and ND10 proteins. J Cell Sci *112 (Pt 20)*, 3443-3454.

Everett, R.D., Freemont, P., Saitoh, H., Dasso, M., Orr, A., Kathoria, M., and Parkinson, J. (1998). The disruption of ND10 during herpes simplex virus infection correlates with the Vmw110- and proteasome-dependent loss of several PML isoforms. J Virol *72*, 6581-6591.

Everett, R.D., Lomonte, P., Sternsdorf, T., van Driel, R., and Orr, A. (1999b). Cell cycle regulation of PML modification and ND10 composition. J Cell Sci *112 (Pt 24)*, 4581-4588.

Everett, R.D., Meredith, M., Orr, A., Cross, A., Kathoria, M., and Parkinson, J. (1997). A novel ubiquitin-specific protease is dynamically associated with the PML nuclear domain and binds to a herpesvirus regulatory protein. Embo J *16*, 1519-1530.

Fakan, S., and Nobis, P. (1978). Ultrastructural localization of transcription sites and of RNA distribution during the cell cycle of synchronized CHO cells. Exp Cell Res *113*, 327-337.

Ferreira, J.A., Carmo-Fonseca, M., and Lamond, A.I. (1994). Differential interaction of splicing snRNPs with coiled bodies and interchromatin granules during mitosis and assembly of daughter cell nuclei. J Cell Biol *126*, 11-23.

Filipowicz, W., and Pogacic, V. (2002). Biogenesis of small nucleolar

ribonucleoproteins. Curr Opin Cell Biol *14*, 319-327.

Fogal, V., Gostissa, M., Sandy, P., Zacchi, P., Sternsdorf, T., Jensen, K., Pandolfi, P.P., Will, H., Schneider, C., and Del Sal, G. (2000). Regulation of p53 activity in nuclear bodies by a specific PML isoform. Embo J *19*, 6185-6195.

Frey, M.R., and Matera, A.G. (2001). RNA-mediated interaction of Cajal bodies and U2 snRNA genes. J Cell Biol *154*, 499-509.

Furuno, N., den Elzen, N., and Pines, J. (1999). Human cyclin A is required for mitosis until mid prophase. J Cell Biol *147*, 295-306.

Gall, J.G. (2000). Cajal bodies: the first 100 years. Annu Rev Cell Dev Biol *16*, 273-300.

Goldman, R.D., Gruenbaum, Y., Moir, R.D., Shumaker, D.K., and Spann, T.P. (2002). Nuclear lamins: building blocks of nuclear architecture. Genes Dev *16*, 533-547.

Gorisch, S.M., Wachsmuth, M., Ittrich, C., Bacher, C.P., Rippe, K., and Lichter, P. (2004). Nuclear body movement is determined by chromatin accessibility and dynamics. Proc Natl Acad Sci U S A *101*, 13221-13226.

Grasse, P.P., Carasso, N., and Favard, P. (1956). [Ultrastructure of chromosomes and their evolution during the spermiogenesis of the snail Helix pomatia. I. The spermatid; new concept of the chromosome structure.]. C R Hebd Seances Acad Sci *242*, 971-975.

Guccione, E., Lethbridge, K.J., Killick, N., Leppard, K.N., and Banks, L. (2004). HPV E6 proteins interact with specific PML isoforms and allow distinctions to be made between different POD structures. Oncogene *23*, 4662-4672.

Guldner, H.H., Szostecki, C., Schroder, P., Matschl, U., Jensen, K., Luders, C., Will, H., and Sternsdorf, T. (1999). Splice variants of the nuclear dot-associated Sp100 protein contain homologies to HMG-1 and a human nuclear phosphoprotein-box motif. J Cell Sci *112 (Pt 5)*, 733-747.

Gunn, S.R., Robetorye, R.S., and Mohammed, M.S. (2007). Comparative genomic hybridization arrays in clinical pathology: progress and challenges. Mol Diagn Ther *11*, 73-77.

Hagting, A., Jackman, M., Simpson, K., and Pines, J. (1999). Translocation of cyclin B1 to the nucleus at prophase requires a phosphorylation-dependent nuclear import signal. Curr Biol *9*, 680-689.

Hagting, A., Karlsson, C., Clute, P., Jackman, M., and Pines, J. (1998). MPF localization is controlled by nuclear export. Embo J *17*, 4127-4138.

Hancock, R. (2000). A new look at the nuclear matrix. Chromosoma *109*, 219-225.

Hancock, R. (2004). A role for macromolecular crowding effects in the assembly and function of compartments in the nucleus. J Struct Biol *146*, 281-290.

Harmon, B., and Sedat, J. (2005). Cell-by-cell dissection of gene expression and chromosomal interactions reveals consequences of nuclear reorganization. PLoS Biol *3*, e67.

Hernandez-Verdun, D. (2006). The nucleolus: a model for the organization of nuclear functions. Histochem Cell Biol *126*, 135-148.

Hernandez-Verdun, D., Roussel, P., and Gebrane-Younes, J. (2002). Emerging concepts of nucleolar assembly. J Cell Sci *115*, 2265-2270.

Hibino, Y., Usui, T., Morita, Y., Hirose, N., Okazaki, M., Sugano, N., and Hiraga, K. (2006). Molecular properties and intracellular localization of rat liver nuclear scaffold protein P130. Biochim Biophys Acta *1759*, 195-207.

Hofmann, T.G., and Will, H. (2003). Body language: the function of PML nuclear bodies in apoptosis regulation. Cell Death Differ *10*, 1290-1299.

Hoppe, A., Beech, S.J., Dimmock, J., and Leppard, K.N. (2006). Interaction of the adenovirus type 5 E4 Orf3 protein with promyelocytic leukemia protein isoform II is required for ND10 disruption. J Virol *80*, 3042-3049.

Hsu, J.Y., Sun, Z.W., Li, X., Reuben, M., Tatchell, K., Bishop, D.K., Grushcow, J.M., Brame, C.J., Caldwell, J.A., Hunt, D.F., Lin, R., Smith, M.M., and Allis, C.D. (2000). Mitotic phosphorylation of histone H3 is governed by Ipl1/aurora kinase and Glc7/PP1 phosphatase in budding yeast and nematodes. Cell *102*, 279-291.

Hunt, T., Luca, F.C., and Ruderman, J.V. (1992). The requirements for protein synthesis and degradation, and the control of destruction of cyclins A and B in the meiotic and mitotic cell cycles of the clam embryo. J Cell Biol *116*, 707-724.

Ishov, A.M., Sotnikov, A.G., Negorev, D., Vladimirova, O.V., Neff, N., Kamitani, T., Yeh, E.T., Strauss, J.F., 3rd, and Maul, G.G. (1999). PML is critical for ND10 formation and recruits the PML-interacting protein daxx to this nuclear structure when modified by SUMO-1. J Cell Biol *147*, 221-234.

Ishov, A.M., Vladimirova, O.V., and Maul, G.G. (2004). Heterochromatin and ND10 are cell-cycle regulated and phosphorylation-dependent alternate nuclear sites of the transcription repressor Daxx and SWI/SNF protein ATRX. J Cell Sci *117*, 3807-3820.

Jackman, M., Lindon, C., Nigg, E.A., and Pines, J. (2003). Active cyclin B1-Cdk1 first appears on centrosomes in prophase. Nat Cell Biol *5*, 143-148.

Jagatheesan, G., Thanumalayan, S., Muralikrishna, B., Rangaraj, N., Karande, A.A., and Parnaik, V.K. (1999). Colocalization of intranuclear lamin foci with RNA splicing factors. J Cell Sci *112 (Pt 24)*, 4651-4661.

James, T.C., Eissenberg, J.C., Craig, C., Dietrich, V., Hobson, A., and Elgin, S.C. (1989). Distribution patterns of HP1, a heterochromatin-associated nonhistone chromosomal protein of Drosophila. Eur J Cell Biol *50*, 170-180.

Janderova-Rossmeislova, L., Novakova, Z., Vlasakova, J., Philimonenko, V., Hozak, P., and Hodny, Z. (2007). PML protein association with specific nucleolar structures differs in normal, tumor and senescent human cells. J Struct Biol.

Janicki, S.M., Tsukamoto, T., Salghetti, S.E., Tansey, W.P., Sachidanandam, R., Prasanth, K.V., Ried, T., Shav-Tal, Y., Bertrand, E., Singer, R.H., and Spector, D.L. (2004). From silencing to gene expression: real-time analysis in single cells. Cell *116*, 683-698.

Jensen, K., Shiels, C., and Freemont, P.S. (2001). PML protein isoforms and the RBCC/TRIM motif. Oncogene *20*, 7223-7233.

Jenuwein, T., and Allis, C.D. (2001). Translating the histone code. Science *293*, 1074-1080.

Johnson, R.T., and Rao, P.N. (1970). Mammalian cell fusion: induction of premature chromosome condensation in interphase nuclei. Nature *226*, 717-722.

Kawai, T., Akira, S., and Reed, J.C. (2003). ZIP kinase triggers apoptosis from nuclear PML oncogenic domains. Mol Cell Biol *23*, 6174-6186.

Kentsis, A., and Borden, K.L. (2004). Physical mechanisms and biological significance of supramolecular protein self-assembly. Curr Protein Pept Sci *5*, 125-134.

Kentsis, A., Gordon, R.E., and Borden, K.L. (2002). Control of biochemical reactions through supramolecular RING domain self-assembly. Proc Natl Acad Sci U S A *99*, 15404-15409.

Khan, M.M., Nomura, T., Kim, H., Kaul, S.C., Wadhwa, R., Shinagawa, T., Ichikawa-Iwata, E., Zhong, S., Pandolfi, P.P., and Ishii, S. (2001). Role of PML and PML-RARalpha in Mad-mediated transcriptional repression. Mol Cell *7*, 1233-1243.

Koken, M.H., Puvion-Dutilleul, F., Guillemin, M.C., Viron, A., Linares-Cruz, G., Stuurman, N., de Jong, L., Szostecki, C., Calvo, F., Chomienne, C., and et al. (1994). The t(15;17) translocation alters a nuclear body in a retinoic acid-reversible fashion. Embo J *13*, 1073-1083.

Krishan, A., Uzman, B.G., and Hedley-Whyte, E.T. (1967). Nuclear bodies: a component of cell nuclei in hamster tissues and human tumors. J Ultrastruct Res *19*, 563-572.

Kumar, P.P., Bischof, O., Purbey, P.K., Notani, D., Urlaub, H., Dejean, A., and Galande, S. (2007). Functional interaction between PML and SATB1 regulates chromatin-loop architecture and transcription of the MHC class I locus. Nat Cell Biol *9*, 45-56.

Kurz, A., Lampel, S., Nickolenko, J.E., Bradl, J., Benner, A., Zirbel, R.M., Cremer, T., and Lichter, P. (1996). Active and inactive genes localize preferentially in the periphery of chromosome territories. J Cell Biol *135*, 1195-1205.

Lallemand-Breitenbach, V., Zhu, J., Puvion, F., Koken, M., Honore, N., Doubeikovsky, A., Duprez, E., Pandolfi, P.P., Puvion, E., Freemont, P., and de The, H. (2001). Role of promyelocytic leukemia (PML) sumolation in nuclear body formation, 11S proteasome recruitment, and As2O3-induced PML or PML/retinoic acid receptor alpha degradation. J Exp Med *193*, 1361-1371.

Lam, Y.W., Lyon, C.E., and Lamond, A.I. (2002). Large-scale isolation of Cajal bodies from HeLa cells. Mol Biol Cell *13*, 2461-2473.

Lam, Y.W., Trinkle-Mulcahy, L., and Lamond, A.I. (2005). The nucleolus. J Cell Sci *118*, 1335-1337.

Lamond, A.I., and Spector, D.L. (2003). Nuclear speckles: a model for nuclear organelles. Nat Rev Mol Cell Biol *4*, 605-612.

Lane, H.A., and Nigg, E.A. (1996). Antibody microinjection reveals an essential role for human polo-like kinase 1 (Plk1) in the functional maturation of mitotic centrosomes. J Cell Biol *135*, 1701-1713.

Langer, P.R., Waldrop, A.A., and Ward, D.C. (1981). Enzymatic synthesis of biotin-labeled polynucleotides: novel nucleic acid affinity probes. Proc Natl Acad Sci U S A *78*, 6633-6637.

Langley, E., Pearson, M., Faretta, M., Bauer, U.M., Frye, R.A., Minucci, S., Pelicci, P.G., and Kouzarides, T. (2002). Human SIR2 deacetylates p53 and antagonizes PML/p53-induced cellular senescence. Embo J *21*, 2383-2396.

Lawrence, J.B., Singer, R.H., and Marselle, L.M. (1989). Highly localized tracks of specific transcripts within interphase nuclei visualized by in situ hybridization. Cell *57*, 493-502.

Leung, A.K., Gerlich, D., Miller, G., Lyon, C., Lam, Y.W., Lleres, D., Daigle, N., Zomerdijk, J., Ellenberg, J., and Lamond, A.I. (2004). Quantitative kinetic analysis of nucleolar breakdown and reassembly during mitosis in live human cells. J Cell Biol *166*, 787-800.

Leung, A.K., Trinkle-Mulcahy, L., Lam, Y.W., Andersen, J.S., Mann, M., and Lamond, A.I. (2006). NOPdb: Nucleolar Proteome Database. Nucleic Acids Res *34*, D218-220.

Li, M., Chen, D., Shiloh, A., Luo, J., Nikolaev, A.Y., Qin, J., and Gu, W. (2002). Deubiquitination of p53 by HAUSP is an important pathway for p53 stabilization. Nature *416*, 648-653.

Lichter, P., Cremer, T., Borden, J., Manuelidis, L., and Ward, D.C. (1988). Delineation of individual human chromosomes in metaphase and interphase cells by in situ suppression hybridization using recombinant DNA libraries. Hum Genet *80*, 224-234.

Lin, D.Y., Huang, Y.S., Jeng, J.C., Kuo, H.Y., Chang, C.C., Chao, T.T., Ho, C.C.,

Chen, Y.C., Lin, T.P., Fang, H.I., Hung, C.C., Suen, C.S., Hwang, M.J., Chang, K.S., Maul, G.G., and Shih, H.M. (2006). Role of SUMO-interacting motif in Daxx SUMO modification, subnuclear localization, and repression of sumoylated transcription factors. Mol Cell *24*, 341-354.

Lin, H.K., Bergmann, S., and Pandolfi, P.P. (2004). Cytoplasmic PML function in TGF-beta signalling. Nature *431*, 205-211.

Lippincott-Schwartz, J., and Patterson, G.H. (2003). Development and use of fluorescent protein markers in living cells. Science *300*, 87-91.

Luciani, J.J., Depetris, D., Usson, Y., Metzler-Guillemain, C., Mignon-Ravix, C., Mitchell, M.J., Megarbane, A., Sarda, P., Sirma, H., Moncla, A., Feunteun, J., and Mattei, M.G. (2006). PML nuclear bodies are highly organised DNA-protein structures with a function in heterochromatin remodelling at the G2 phase. J Cell Sci *119*, 2518-2531.

Luderus, M.E., den Blaauwen, J.L., de Smit, O.J., Compton, D.A., and van Driel, R. (1994). Binding of matrix attachment regions to lamin polymers involves single-stranded regions and the minor groove. Mol Cell Biol *14*, 6297-6305.

Manuelidis, L., Langer-Safer, P.R., and Ward, D.C. (1982). High-resolution mapping of satellite DNA using biotin-labeled DNA probes. J Cell Biol *95*, 619-625.

Marcello, A., Ferrari, A., Pellegrini, V., Pegoraro, G., Lusic, M., Beltram, F., and Giacca, M. (2003). Recruitment of human cyclin T1 to nuclear bodies through direct interaction with the PML protein. Embo J *22*, 2156-2166.

Margalit, A., Vlcek, S., Gruenbaum, Y., and Foisner, R. (2005). Breaking and making of the nuclear envelope. J Cell Biochem *95*, 454-465.

Maul, G.G. (1998). Nuclear domain 10, the site of DNA virus transcription and replication. Bioessays *20*, 660-667.

Maul, G.G., Guldner, H.H., and Spivack, J.G. (1993). Modification of discrete nuclear domains induced by herpes simplex virus type 1 immediate early gene 1 product (ICP0). J Gen Virol *74 (Pt 12)*, 2679-2690.

McGinley, M.D., Davis, M.T., Robinson, J.H., Spahr, C.S., Bures, E.J., Beierle, J., Mort, J., and Patterson, S.D. (2000). A simplified device for protein identification

by microcapillary gradient liquid chromatography-tandem mass spectrometry. Electrophoresis *21*, 1678-1684.

Melnick, A., and Licht, J.D. (1999). Deconstructing a disease: RARalpha, its fusion partners, and their roles in the pathogenesis of acute promyelocytic leukemia. Blood *93*, 3167-3215.

Minton, A.P. (1993). Macromolecular crowding and molecular recognition. J Mol Recognit *6*, 211-214.

Mintz, P.J., Patterson, S.D., Neuwald, A.F., Spahr, C.S., and Spector, D.L. (1999). Purification and biochemical characterization of interchromatin granule clusters. Embo J *18*, 4308-4320.

Misteli, T., Caceres, J.F., and Spector, D.L. (1997). The dynamics of a pre-mRNA splicing factor in living cells. Nature *387*, 523-527.

Moir, R.D., Montag-Lowy, M., and Goldman, R.D. (1994). Dynamic properties of nuclear lamins: lamin B is associated with sites of DNA replication. J Cell Biol *125*, 1201-1212.

Monneron, A., and Bernhard, W. (1969). Fine structural organization of the interphase nucleus in some mammalian cells. J Ultrastruct Res *27*, 266-288.

Morgan, D.O. (1999). Regulation of the APC and the exit from mitosis. Nat Cell Biol *1*, E47-53.

Muller, S., Matunis, M.J., and Dejean, A. (1998). Conjugation with the ubiquitin-related modifier SUMO-1 regulates the partitioning of PML within the nucleus. Embo J *17*, 61-70.

Mura, C.V., Becker, M.I., Orellana, A., and Wolff, D. (2002). Immunopurification of Golgi vesicles by magnetic sorting. J Immunol Methods *260*, 263-271.

Muralikrishna, B., Dhawan, J., Rangaraj, N., and Parnaik, V.K. (2001). Distinct changes in intranuclear lamin A/C organization during myoblast differentiation. J Cell Sci *114*, 4001-4011.

Muratani, M., Gerlich, D., Janicki, S.M., Gebhard, M., Eils, R., and Spector, D.L. (2002). Metabolic-energy-dependent movement of PML bodies within the mammalian cell nucleus. Nat Cell Biol *4*, 106-110.

Nasmyth, K., Peters, J.M., and Uhlmann, F. (2000). Splitting the chromosome: cutting the ties that bind sister chromatids. Science *288*, 1379-1385.

Nathanson, L., Xia, T., and Deutscher, M.P. (2003). Nuclear protein synthesis: a re-evaluation. Rna *9*, 9-13.

Nayler, O., Stratling, W., Bourquin, J.P., Stagljar, I., Lindemann, L., Jasper, H., Hartmann, A.M., Fackelmayer, F.O., Ullrich, A., and Stamm, S. (1998). SAF-B protein couples transcription and pre-mRNA splicing to SAR/MAR elements. Nucleic Acids Res *26*, 3542-3549.

Nefkens, I., Negorev, D.G., Ishov, A.M., Michaelson, J.S., Yeh, E.T., Tanguay, R.M., Muller, W.E., and Maul, G.G. (2003). Heat shock and Cd2+ exposure regulate PML and Daxx release from ND10 by independent mechanisms that modify the induction of heat-shock proteins 70 and 25 differently. J Cell Sci *116*, 513-524.

Negorev, D.G., Vladimirova, O.V., Ivanov, A., Rauscher, F., 3rd, and Maul, G.G. (2006). Differential role of Sp100 isoforms in interferon-mediated repression of herpes simplex virus type 1 immediate-early protein expression. J Virol *80*, 8019-8029.

Nervi, C., Ferrara, F.F., Fanelli, M., Rippo, M.R., Tomassini, B., Ferrucci, P.F., Ruthardt, M., Gelmetti, V., Gambacorti-Passerini, C., Diverio, D., Grignani, F., Pelicci, P.G., and Testi, R. (1998). Caspases mediate retinoic acid-induced degradation of the acute promyelocytic leukemia PML/RARalpha fusion protein. Blood *92*, 2244-2251.

Nicklas, R.B., and Arana, P. (1992). Evolution and the meaning of metaphase. J Cell Sci *102 (Pt 4)*, 681-690.

Pandolfi, P.P. (2001). In vivo analysis of the molecular genetics of acute promyelocytic leukemia. Oncogene *20*, 5726-5735.

Pantelias, G.E., and Maillie, H.D. (1983). A simple method for premature chromosome condensation induction in primary human and rodent cells using polyethylene glycol. Somatic Cell Genet *9*, 533-547.

Pearson, M., Carbone, R., Sebastiani, C., Cioce, M., Fagioli, M., Saito, S., Higashimoto, Y., Appella, E., Minucci, S., Pandolfi, P.P., and Pelicci, P.G. (2000).

PML regulates p53 acetylation and premature senescence induced by oncogenic Ras. Nature *406*, 207-210.

Pederson, T. (2000). Half a century of "the nuclear matrix". Mol Biol Cell *11*, 799-805.

Perrin-Cocon, L.A., Marche, P.N., and Villiers, C.L. (1999). Purification of intracellular compartments involved in antigen processing: a new method based on magnetic sorting. Biochem J *338 (Pt 1)*, 123-130.

Pfleger, C.M., and Kirschner, M.W. (2000). The KEN box: an APC recognition signal distinct from the D box targeted by Cdh1. Genes Dev *14*, 655-665.

Pines, J., and Rieder, C.L. (2001). Re-staging mitosis: a contemporary view of mitotic progression. Nat Cell Biol *3*, E3-6.

Platani, M., Goldberg, I., Lamond, A.I., and Swedlow, J.R. (2002). Cajal body dynamics and association with chromatin are ATP-dependent. Nat Cell Biol *4*, 502-508.

Platani, M., Goldberg, I., Swedlow, J.R., and Lamond, A.I. (2000). In vivo analysis of Cajal body movement, separation, and joining in live human cells. J Cell Biol *151*, 1561-1574.

Prasanth, K.V., Sacco-Bubulya, P.A., Prasanth, S.G., and Spector, D.L. (2003). Sequential entry of components of the gene expression machinery into daughter nuclei. Mol Biol Cell *14*, 1043-1057.

Rieder, C.L., and Cole, R.W. (1998). Entry into mitosis in vertebrate somatic cells is guarded by a chromosome damage checkpoint that reverses the cell cycle when triggered during early but not late prophase. J Cell Biol *142*, 1013-1022.

Rivera, O.J., Song, C.S., Centonze, V.E., Lechleiter, J.D., Chatterjee, B., and Roy, A.K. (2003). Role of the promyelocytic leukemia body in the dynamic interaction between the androgen receptor and steroid receptor coactivator-1 in living cells. Mol Endocrinol *17*, 128-140.

Saitoh, N., Spahr, C.S., Patterson, S.D., Bubulya, P., Neuwald, A.F., and Spector, D.L. (2004). Proteomic analysis of interchromatin granule clusters. Mol Biol Cell *15*, 3876-3890.

Scaglioni, P.P., Yung, T.M., Cai, L.F., Erdjument-Bromage, H., Kaufman, A.J., Singh, B., Teruya-Feldstein, J., Tempst, P., and Pandolfi, P.P. (2006). A CK2-dependent mechanism for degradation of the PML tumor suppressor. Cell *126*, 269-283.

Scheer, U., and Hock, R. (1999). Structure and function of the nucleolus. Curr Opin Cell Biol *11*, 385-390.

Seeler, J.S., Marchio, A., Losson, R., Desterro, J.M., Hay, R.T., Chambon, P., and Dejean, A. (2001). Common properties of nuclear body protein SP100 and TIF1alpha chromatin factor: role of SUMO modification. Mol Cell Biol *21*, 3314-3324.

Seeler, J.S., Marchio, A., Sitterlin, D., Transy, C., and Dejean, A. (1998). Interaction of SP100 with HP1 proteins: a link between the promyelocytic leukemia-associated nuclear bodies and the chromatin compartment. Proc Natl Acad Sci U S A *95*, 7316-7321.

Shen, T.H., Lin, H.K., Scaglioni, P.P., Yung, T.M., and Pandolfi, P.P. (2006). The mechanisms of PML-nuclear body formation. Mol Cell *24*, 331-339.

Shiels, C., Islam, S.A., Vatcheva, R., Sasieni, P., Sternberg, M.J., Freemont, P.S., and Sheer, D. (2001). PML bodies associate specifically with the MHC gene cluster in interphase nuclei. J Cell Sci *114*, 3705-3716.

Shopland, L.S., Byron, M., Stein, J.L., Lian, J.B., Stein, G.S., and Lawrence, J.B. (2001). Replication-dependent histone gene expression is related to Cajal body (CB) association but does not require sustained CB contact. Mol Biol Cell *12*, 565-576.

Shu, X., Shaner, N.C., Yarbrough, C.A., Tsien, R.Y., and Remington, S.J. (2006). Novel chromophores and buried charges control color in mFruits. Biochemistry *45*, 9639-9647.

Singer, R.H., and Ward, D.C. (1982). Actin gene expression visualized in chicken muscle tissue culture by using in situ hybridization with a biotinated nucleotide analog. Proc Natl Acad Sci U S A *79*, 7331-7335.

Sleeman, J.E., Trinkle-Mulcahy, L., Prescott, A.R., Ogg, S.C., and Lamond, A.I. (2003). Cajal body proteins SMN and Coilin show differential dynamic behaviour

in vivo. J Cell Sci *116*, 2039-2050.

Smith, K.P., and Lawrence, J.B. (2000). Interactions of U2 gene loci and their nuclear transcripts with Cajal (coiled) bodies: evidence for PreU2 within Cajal bodies. Mol Biol Cell *11*, 2987-2998.

Soignet, S.L., Maslak, P., Wang, Z.G., Jhanwar, S., Calleja, E., Dardashti, L.J., Corso, D., DeBlasio, A., Gabrilove, J., Scheinberg, D.A., Pandolfi, P.P., and Warrell, R.P., Jr. (1998). Complete remission after treatment of acute promyelocytic leukemia with arsenic trioxide. N Engl J Med *339*, 1341-1348.

Song, J., Durrin, L.K., Wilkinson, T.A., Krontiris, T.G., and Chen, Y. (2004). Identification of a SUMO-binding motif that recognizes SUMO-modified proteins. Proc Natl Acad Sci U S A *101*, 14373-14378.

Spector, D.L. (2001). Nuclear domains. J Cell Sci *114*, 2891-2893.

Spector, D.L. (2003). The dynamics of chromosome organization and gene regulation. Annu Rev Biochem *72*, 573-608.

Spector, D.L., Goldman, R. D., and Leinwand, L. A. (1998). Cells: a laboratory manual. Cold Spring Harbor, NY, Cold Spring Harbor Laboratory Press

Spector, D.L., Schrier, W.H., and Busch, H. (1983). Immunoelectron microscopic localization of snRNPs. Biol Cell *49*, 1-10.

Sternsdorf, T., Jensen, K., Reich, B., and Will, H. (1999). The nuclear dot protein sp100, characterization of domains necessary for dimerization, subcellular localization, and modification by small ubiquitin-like modifiers. J Biol Chem *274*, 12555-12566.

Sternsdorf, T., Jensen, K., and Will, H. (1997). Evidence for covalent modification of the nuclear dot-associated proteins PML and Sp100 by PIC1/SUMO-1. J Cell Biol *139*, 1621-1634.

Strudwick, S., and Borden, K.L. (2002). Finding a role for PML in APL pathogenesis: a critical assessment of potential PML activities. Leukemia *16*, 1906-1917.

Stuurman, N., de Graaf, A., Floore, A., Josso, A., Humbel, B., de Jong, L., and van Driel, R. (1992). A monoclonal antibody recognizing nuclear matrix-associated

nuclear bodies. J Cell Sci *101 (Pt 4)*, 773-784.

Suzuki, T., Ichiyama, A., Saitoh, H., Kawakami, T., Omata, M., Chung, C.H., Kimura, M., Shimbara, N., and Tanaka, K. (1999). A new 30-kDa ubiquitin-related SUMO-1 hydrolase from bovine brain. J Biol Chem *274*, 31131-31134.

Swift, H. (1959). Studies on nuclear fine structure. Brookhaven Symp Biol *12*, 134-152.

Szostecki, C., Guldner, H.H., Netter, H.J., and Will, H. (1990). Isolation and characterization of cDNA encoding a human nuclear antigen predominantly recognized by autoantibodies from patients with primary biliary cirrhosis. J Immunol *145*, 4338-4347.

Takizawa, C.G., and Morgan, D.O. (2000). Control of mitosis by changes in the subcellular location of cyclin-B1-Cdk1 and Cdc25C. Curr Opin Cell Biol *12*, 658-665.

Tan, J.H., Wooley, J.C., and LeStourgeon, W.M. (2000). Nuclear matrix-like filaments and fibrogranular complexes form through the rearrangement of specific nuclear ribonucleoproteins. Mol Biol Cell *11*, 1547-1554.

Tolstonog, G.V., Sabasch, M., and Traub, P. (2002). Cytoplasmic intermediate filaments are stably associated with nuclear matrices and potentially modulate their DNA-binding function. DNA Cell Biol *21*, 213-239.

Topisirovic, I., Capili, A.D., and Borden, K.L. (2002). Gamma interferon and cadmium treatments modulate eukaryotic initiation factor 4E-dependent mRNA transport of cyclin D1 in a PML-dependent manner. Mol Cell Biol *22*, 6183-6198.

Trask, B.J. (2002). Human cytogenetics: 46 chromosomes, 46 years and counting. Nat Rev Genet *3*, 769-778.

Tsukamoto, T., Hashiguchi, N., Janicki, S.M., Tumbar, T., Belmont, A.S., and Spector, D.L. (2000). Visualization of gene activity in living cells. Nat Cell Biol *2*, 871-878.

Visintin, R., Prinz, S., and Amon, A. (1997). CDC20 and CDH1: a family of substrate-specific activators of APC-dependent proteolysis. Science *278*, 460-463.

Wang, J., Shiels, C., Sasieni, P., Wu, P.J., Islam, S.A., Freemont, P.S., and Sheer, D. (2004). Promyelocytic leukemia nuclear bodies associate with transcriptionally active genomic regions. J Cell Biol *164*, 515-526.

Wang, Z.G., Rivi, R., Delva, L., Konig, A., Scheinberg, D.A., Gambacorti-Passerini, C., Gabrilove, J.L., Warrell, R.P., Jr., and Pandolfi, P.P. (1998a). Arsenic trioxide and melarsoprol induce programmed cell death in myeloid leukemia cell lines and function in a PML and PML-RARalpha independent manner. Blood *92*, 1497-1504.

Wang, Z.G., Ruggero, D., Ronchetti, S., Zhong, S., Gaboli, M., Rivi, R., and Pandolfi, P.P. (1998b). PML is essential for multiple apoptotic pathways. Nat Genet *20*, 266-272.

Warrell, R.P., Jr., de The, H., Wang, Z.Y., and Degos, L. (1993). Acute promyelocytic leukemia. N Engl J Med *329*, 177-189.

Wasylyk, C., Schlumberger, S.E., Criqui-Filipe, P., and Wasylyk, B. (2002). Sp100 interacts with ETS-1 and stimulates its transcriptional activity. Mol Cell Biol *22*, 2687-2702.

Weis, K., Rambaud, S., Lavau, C., Jansen, J., Carvalho, T., Carmo-Fonseca, M., Lamond, A., and Dejean, A. (1994). Retinoic acid regulates aberrant nuclear localization of PML-RAR alpha in acute promyelocytic leukemia cells. Cell *76*, 345-356.

Wiesmeijer, K., Molenaar, C., Bekeer, I.M., Tanke, H.J., and Dirks, R.W. (2002). Mobile foci of Sp100 do not contain PML: PML bodies are immobile but PML and Sp100 proteins are not. J Struct Biol *140*, 180-188.

Xirodimas, D.P., Chisholm, J., Desterro, J.M., Lane, D.P., and Hay, R.T. (2002). P14ARF promotes accumulation of SUMO-1 conjugated (H)Mdm2. FEBS Lett *528*, 207-211.

Yang, X., Khosravi-Far, R., Chang, H.Y., and Baltimore, D. (1997). Daxx, a novel Fas-binding protein that activates JNK and apoptosis. Cell *89*, 1067-1076.

Yeager, T.R., Neumann, A.A., Englezou, A., Huschtscha, L.I., Noble, J.R., and Reddel, R.R. (1999). Telomerase-negative immortalized human cells contain a novel type of promyelocytic leukemia (PML) body. Cancer Res *59*, 4175-4179.

Zbarskii, I.B. (1948). Property of nonhistone proteins of the cell nucleus to form non-chromatin structural carcass (nuclear matrix). State Committee of the USSR on Inventions and Discoveries, No. 348, Moscow, August 27.

Zhong, S., Muller, S., Ronchetti, S., Freemont, P.S., Dejean, A., and Pandolfi, P.P. (2000). Role of SUMO-1-modified PML in nuclear body formation. Blood *95*, 2748-2752.

Zhou, Z., Licklider, L.J., Gygi, S.P., and Reed, R. (2002). Comprehensive proteomic analysis of the human spliceosome. Nature *419*, 182-185.

Zhu, J., Gianni, M., Kopf, E., Honore, N., Chelbi-Alix, M., Koken, M., Quignon, F., Rochette-Egly, C., and de The, H. (1999). Retinoic acid induces proteasome-dependent degradation of retinoic acid receptor alpha (RARalpha) and oncogenic RARalpha fusion proteins. Proc Natl Acad Sci U S A *96*, 14807-14812.

Zhu, J., Lallemand-Breitenbach, V., and de The, H. (2001). Pathways of retinoic acid- or arsenic trioxide-induced PML/RARalpha catabolism, role of oncogene degradation in disease remission. Oncogene *20*, 7257-7265.

Zimmerman, S.B. (1993). Macromolecular crowding effects on macromolecular interactions: some implications for genome structure and function. Biochim Biophys Acta *1216*, 175-185.